Effects of Surface Contamination and Water Chemistry on the Behaviors of Illite, Kaolinite and Montmorillonite in Organic and Aqueous Media

by

Amin Pourmohammadbagher

A thesis submitted in partial fulfillment of the requirements for the degree of

Doctor of Philosophy

in

Chemical and Materials Engineering

Department of Chemical and Materials Engineering
University of Alberta

Abstract:

Clays, due to their specific surface area and electrical charge density, are among the most active minerals in aquifers, oil and gas reservoirs, and tailings ponds. Clays, in tailings, are a significant ongoing environmental concern in the mining and oil sands production industries and clay rehabilitation following contamination poses challenges episodically. Important problems, such as limited oil recovery during petroleum exploration, involve the interaction of process fluids with minerals, which constitute reservoir pore walls. Detailed understanding of the fundamentals of clay behaviors contributes to better environmental impact mitigation strategies, to the development of production processes for heavy oils and bitumen with lower environmental impacts, to the treatment of tailings from mined bitumen, and to the mitigation of impacts from oil spills in natural environments.

Probes, such as solution calorimetry are sensitive to species transfer to and from clay surfaces. Outcomes can be interpreted unambiguously, when these data are supplemented with TGA and SEM measurements. Systematic calorimetric measurements provide a framework for parsing the synergistic and antagonistic impacts of trace (i.e., ppm level) components on the surface compositions of clays in diverse natural and process environments.

In this study, the effects of clay surface contamination, solvent contamination, and the effects of water chemistry (temperature, pH, salinity) on the enthalpy of solution of kaolinite, illite and montmorillonite clays in toluene, n-heptane, pyridine and deionized water were investigated. Clay contamination included pre-saturation of clays with water, organic liquids, and asphaltenes. Solvent contamination included addition of trace water to organic liquids and trace organic liquids to water. A quantitative mass and energy balance modeling framework was developed for

interpreting the enthalpy of solution outcomes that isolates terms for solvents and trace contaminant sorption/desorption and surface energy effects. Mechanistic and quantitative insights underlying the surface properties of clay dispersions in tailings ponds, and the behaviors of these clays in diverse industrial and natural environments are discussed.

Preface:

Chapter 2 of this thesis has been published as A. Pourmohammadbagher and J.M. Shaw, "Excess enthalpy and excess volume for pyridine + methyldiethanolamine and pyridine + ethanolamine mixtures" at the Journal of Chemical & Engineering Data.

Chapter 3 has been published as A. Pourmohammadbagher and J.M. Shaw, "Probing Contaminant Transport to and from Clay Surfaces in Organic Solvents and Water Using Solution Calorimetry" at the Journal of Environmental Science & Technology.

Chapter 4 has been submitted to Energy & Fuels as A. Pourmohammadbagher and J.M. Shaw, "Probing asphaltene contamination of kaolinite and illite clays: A calorimetric study".

Chapter 5 has been submitted to Energy & Fuels as A. Pourmohammadbagher and J.M. Shaw, "Probing the role of water chemistry on the behavior of clays using solution calorimetry".

I was responsible for experimental measurements, modeling and analysis as well as the manuscript composition. It is noteworthy to mention that none of these journal papers and chapters would have been possible without J.M. Shaw's assistance.

Dedication

To my beloved wife, my parents and my brother

Acknowledgements

I owe every single achievement of my life to my parents who have always been there for me regardless of the circumstances. I am also extremely thankful to my wife for her unlimited and wholehearted support, her patience, and unconditional love.

I would like to express my deep sense of thanks and gratitude to my supervisor, Professor Shaw. His dedication and keen interest above all his overwhelming attitude to help his students played the main role in completing my work. His timely advice and meticulous scrutiny have helped me to a great extent to accomplish this task. I also thank profusely for the time and the effort the members of the supervisory and examining committees have spent on reviewing this thesis.

I really appreciate the assistance and support from Mildred Becerra. She is one of the greatest lab managers I've ever seen. I am thankful that I had the pleasure of working with and using her help. I also appreciate the assistance and support from Linda Kaert who has been most kind to me. I want to extend my appreciation to Gayle Hatchard from the Nanofabrication and Characterization Facility (nanoFab) of the University of Alberta; my co-op students (Michelle Liu, Gabriel Wong, Jordon French); my WISEST student (Abigayle Peterson); Jeoffrey Ollinger and Jun Zhao.

I gratefully acknowledge financial support from the sponsors of the NSERC Industrial Research Chair in Petroleum Thermodynamics: the Natural Sciences and Engineering Research Council of Canada (NSERC), Alberta Innovates Energy and Environment Solutions, BP Canada, ConocoPhillips Canada Resources Corp., Nexen Energy ULC, Shell Canada Ltd., Total E&P Canada Ltd., Virtual Materials Group.

Table of Contents

List of Tables

List of Figures

CHAPTER 1: INTRODUCTION

1.1 TAILINGS

Mines and mineral processing plants produce valuable products and byproducts, as well as waste, typically in the form of tailings. Tailings, consist of process water, clays, process by-products, minerals and metals, inorganic and organic chemicals.[1] Tailings are generally discharged into and contained in large above ground structures - tailings ponds - (Figure 1.1) where they await reclamation.[2] Large sand/mineral particles in tailings settle quickly to form stable deposits. Finer clay particles, known as mature fine tailings (MFT), remain suspended in the form of sludge and take years or centuries to settle and solidify.[3] This has led to the accumulation of millions of cubic meters of MFT, in the Fort McMurray region of Alberta alone as a consequence of bitumen mining operations.[4] Attempts have been made to increase the settling rate of the tailings for efficient water recycling and to compact the tailings sediment, thus reducing volume of tailings ponds and speeding land reclamation efforts. However, increasing the settling rate of tailings is still one of the main challenges in tailings management in the Fort McMurray region and around the world.[5]

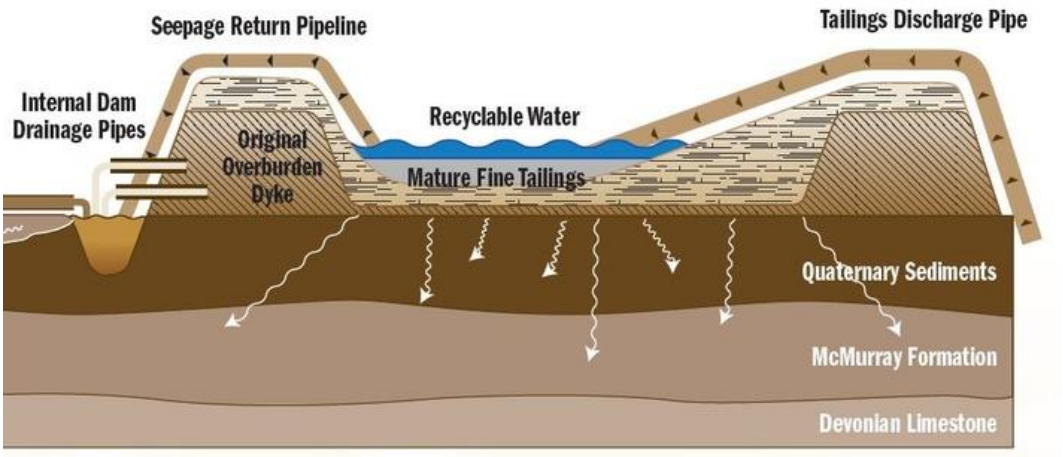

Figure 1.1 *Schematic of a tailings pond.*[6]

1.1.1 Challenges and Environmental Concerns

Tailings production results in large environmental footprints for individual sites because of the large storage volumes[3] and the long time-scales over which tailings must be managed and rehabilitated.[7] Environmental challenges include tailings pond integrity and management and mitigation of impacts from inorganic and organic contaminants present (petroleum hydrocarbons,[4] salts,[8] metals,[9,10] naphthenic acids,[11] etc.) and emission of biogenic greenhouse gases (CH_4 and CO_2).[12]

Failure to manage tailings can result in severe and sometimes catastrophic consequences with large human and environmental costs. The severe and sometimes irreversible economic, social and environmental consequences of poor tailings management, underscore the need for considered and careful tailings management of the environmental, economic, and social challenges listed in Table 1.1.

Table 1.1 *The environmental, economic, and social challenges in tailings management*[7]

Environmental	Economic	Social
Air and water pollution	Capital expenditure	Health issues
Water resources depletion	Operating expenditure	Safety issues for public (during operation and after closure)
Ecosystem destruction	Reagent loss	
Ecosystem alteration	Energy cost	
Land footprint	Closure cost	
Emissions		
Flooding		

1.1.2 Tailings Water

Tailings water chemistry (e.g., ionic strength and pH) is critical for the settlement of fine clays. Residual organic matter present during mineral processing adsorb onto clay particle surfaces, producing biwettable characteristics[13] that cause clay particles to exhibit some degree of hydrophobicity.[14] Chemical aids such as sodium hydroxide (NaOH) are often added to control the pH during mineral processing. Alkalinity also alters the wettability of clays.[15] Soluble salts extracted from ores or present in the process water are released into tailings and interact with clays. These interactions have also been found to influence the settling and flocculation behavior of fine clays.[16,17] Sodium and calcium are major electrolyte components found in processing water. From mean particle size and zeta potential measurements, monovalent ions enhance clay particle dispersion. Particles become less dispersed as the valency of the cations is increased.[17–19]

1.1.3 Tailings Solids

The grain size of tailings ranges from clays ~ 2 μm to sand ~ 2 mm. Dry tailings typically consist of 70–80 wt.% sand-sized particles and 20–30 wt.% finer clay-sized particles.[20–22] The grain size depends on the liberation characteristics of the ore and the crushing and grinding processes applied. The grain size influences the behavior and settling characteristics of particles in tailings ponds. The mineralogical and geochemical composition of tailings solids is site specific, and such variations impose site-specific challenges. In addition, some tailings solids and liquids are reactive, with one another and with species in the environment[23].

1.1.4 Treatment Technologies

Possible tailings treatment technologies are constrained by (i) the operation and maintenance costs the tailings ponds impose due to the amount of tailings produced from mining processes every day and by (ii) the need to minimize impacts on the surrounding natural environments and local ecology. Fresh water intake is typically limited by legislation. Tailings treatment includes land reclamation, but tailings water must also be recovered for reuse within mining processes. To accelerate the settling process, additional physical and chemical treatments are also needed. The treatment technologies available for dewatering tailings can be categorized as:[5]

- Physical/Mechanical Processes

  Physical/mechanical processes include the use of different technologies to separate tailings water without using any chemicals (e.g., filtration, centrifuging, heating, and electrical treatments).

- Natural Processes

  Natural processes consist of using environmental or geophysical processes for water separation (e.g., sedimentation and consolidation, evaporation, and plant dewatering).

- Chemical/Biological Processes

  Chemical/biological processing includes changing the properties of the tailings to make the water/solid separation easier (e.g., thickening, using flocculants, and biodrying).

- Permanent Storage

  Most of the tailings mass produced worldwide is pumped into tailings storage facilities, including tailings ponds (Figure 1.1). Because of their size, they leave the largest footprint of any mining activity in the landscape.

1.2 OIL SANDS: A SPECIAL CASE

There are approximately 2.5 trillion barrels of bitumen entrained in a mineral matrix of sand and clay in Alberta.[24] The Clark hot water extraction (CHWE) process is commonly used to produce bitumen from surface minable oil sands ore.[25] The waste effluent is transferred to a tailings pond where the coarse sands settle rapidly, the fine material stay in the middle and the low solid content water supernatant stays on the top layer.[26] Other than the general components that can be fined in tailings, oil sands tailings also contain a residual amount of un-extracted bitumen which impacts the characteristics and behavior of the tailings, and introduces operational complexities.[5] Aqueous organic matter and bitumen are usually attached to the fine particles[27] and this alters their hydrophilic/ hydrophobic balance through surface composition changes that impact surface wettability, surface energy, and surface charge.[28–33] Many methods have been proposed,

investigated or implemented in laboratory and in field studies to expedite the consolidation of MFT and the subsequent reclamation of tailings ponds.[34–37] None the less, oil sands tailings ponds pose threats to local wildlife and local ecosystems and have become one of the most critical challenges for the oil sands industry, and for mining based bitumen production in particular.

1.3 COLLOIDAL AND SURFACE CHEMISTRY BASICS

1.3.1 Clay Minerals

Clay particles are composed of sheets of silicon-oxygen tetrahedrons and sheets of aluminum-oxygen octahedrons. Different types of clays have different arrangements of these sheets as their unit layer. A perfect clay crystal is built by laying these unit layers on top of one another. Two-layered clay particles, such as kaolinite, have a tetrahedral silicon-oxygen sheet attached to an octahedral aluminum-oxide sheet. These layers are held together partly by van der Waals forces and partly by hydrogen bonds from the hydroxyl groups of the octahedral sheet. Three-layered clay particles, such as illite or montmorillonite, comprise an octahedral aluminum-oxide sheet in between two tetrahedral silicon-oxygen sheets. Clay particles obtain electric charge by substitution of cations in the unit layers. A negative charge occurs when a tetravalent silicon ion is replaced by a trivalent aluminum ion because of the similar morphology of the ions. This charging mechanism is known as isomorphous substitution of ions. The charges on basal planes are considered permanent charges, independent of pH while primary alumina and silica bonds broken along particle edges lead to pH dependent charges.[38]

1.3.2. Electrical Double Layer

In tailings, charged clay particles are surrounded by water with an inhomogeneous distribution of ions. Co-ions, bearing the same charge as clays, are depleted from clay surfaces and counter-ions, bearing opposite charge as clays, adsorb at the surface of clays. Far from the clay surfaces the concentrations of co-ions and counter-ions attain a constant value. The inhomogeneous layer around clays is called the double layer. The double layer includes the surface charge, the Stern layer, and the diffuse layer, as illustrated in Figure 1.2.[39] The Stern layer is the space between the charged particle surface and the Stern plane. The ions in the stern layer are believed to be bonded to the particle surface.[40] The slip plane is deemed to contain ions and solution that move around the particle surface. The potential at the slip plane is known as the zeta potential.[41] Zeta potential is an important parameter for colloidal particles. Charged colloids repel each other upon approach due to double layer repulsion. Adding counter-ions to the medium can result in weaker repulsion.[39]

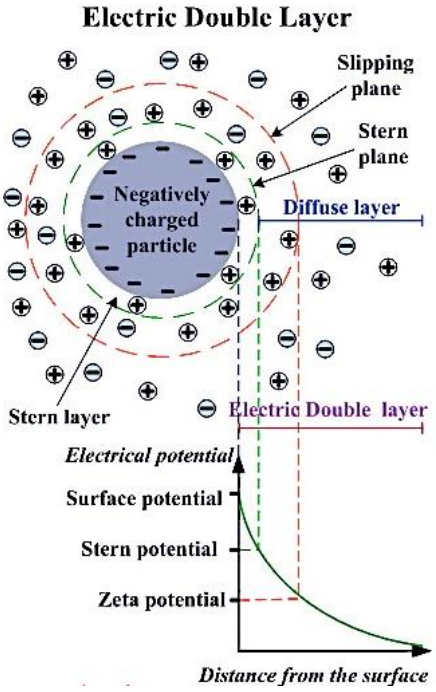

Figure 1.2 *Colloidal particle electrical double layer*.[39]

1.3.3 Mechanisms Leading to Particle Aggregation

1.3.3.1 Coagulation

In the process of coagulation, the charges on clay particles (Figure 1.3a) are neutralized or reduced by adding multivalent organic cations or inorganic salts such as aluminum sulphate, potassium alum, gypsum, etc. known as coagulants. Therefore particles can be brought together and form aggregates.[42]

1.3.3.1.1 Double Layer Compression

Double layer compression involves adding salts like KCl, NaCl, etc. to the suspension. When enough counter ions are added to the suspension, the double layer is compressed until there is no

longer an energy barrier. At this time, van der Waals attractive forces dominate and the particles are able to form aggregates (Figure 1.3b).[43]

1.3.3.1.2 Surface Charge Neutralization

Charge neutralization involves reduction of the net surface charge (zeta potential) of the particles in the suspension. As the net surface charge diminishes, the diffuse layer thickness surrounding the particles is reduced and the energy required to move the particles into contact is minimized (Figure 1.3c). Charge neutralization is accomplished by addition of coagulants such as $CaCO_3$. Coagulants adsorb onto the particle surface. The tendency of the coagulants to adsorb is usually attributed to both poor coagulant-solvent interaction and a chemical affinity of the coagulant for the particle surface.[43]

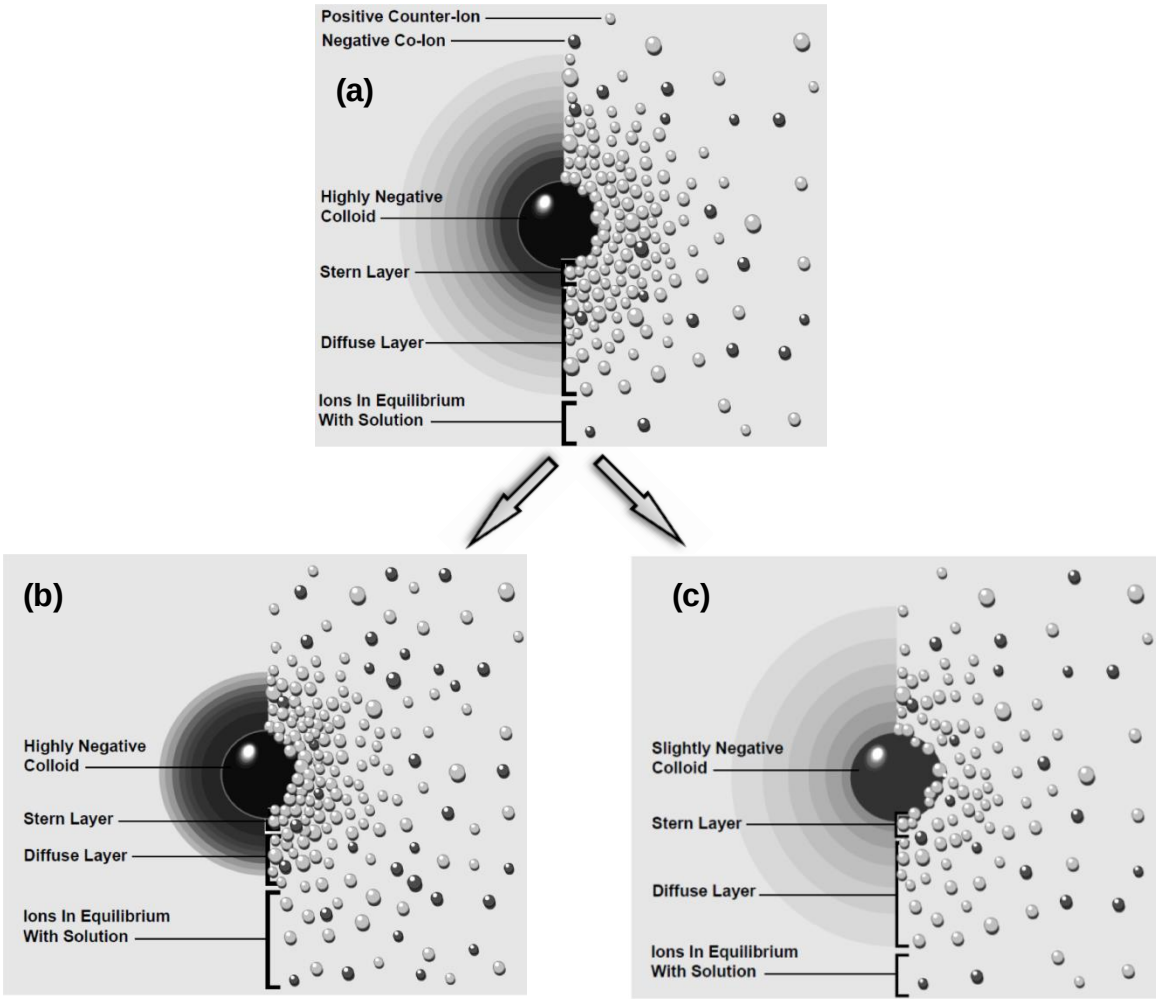

Figure 1.3 *A schematic of (a) charged colloid particle double layer (b) double layer compression by addition of indifferent electrolyte (the electrolyte retains its identity and does not adsorb on the surface of colloid) and (c) charge neutralization by adsorption of counter ions on the surface of colloid.*[46]

1.3.3.2 Flocculation

Flocculation refers to the aggregation of colloidal particles into packed flocs by addition of polymeric flocculant.[39,44] Long-chain polymers adsorb on multiple particles simultaneously thus bridging particles together (Figure 1.4).[45]

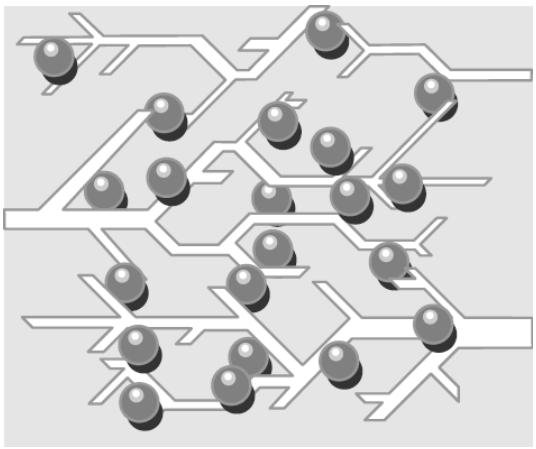

Figure 1.4 *Flocculation of colloids using polymer chains.*[46]

1.4 OBJECTIVES

Gibbs free energy, a thermodynamic criterion for predicting the directions of processes, is the most useful parameter for investigating the behaviors of clays in diverse environments. For example, quantitative displacement of water from clay surfaces by ppm concentrations of organic compounds in water is driven by the free energy difference between the compound in the water and on the surface. Clays with positive Gibbs free energies of solution are more readily aggregated than ones with negative values. Change in the Gibbs free energy of a mixture at temperature T (k) can be evaluated using equation 1.1:

$$\Delta G = \Delta H - T\Delta S \qquad (1.1)$$

where ΔH is the change in the enthalpy of the mixture (enthalpy of solution) and ΔS is the change in the enthropy of the mixture (enthropy of solution). The Gibbs free energy can be modeled by constructing modelling frameworks for enthalpy and enthropy of solution.

The objectives of this thesis are to investigate the surface properties of clays in water and organic liquids and to develop a solution enthalpy modeling framework to improve the understanding of

clay behaviors in diverse environments. The enthalpy framework can be used to develop a general Gibbs free energy model for predicting the settling of clays in different environment.

Roles played by solvent contamination, clay surface contamination, solvent sorption/desorption on/from the surface of clays, trace impurities sorption/desorption on/from the surface of clays, asphaltene contamination of clay surfaces, and water chemistry (pH, Temperature, and salinity) are evaluated systematically. For example, in Chapter 2 the experimental procedure is validated and experimental data for uncommon combinations of compounds (e.g., Pyridine + monoethanolamine) are reported. These new data targeted additions to the Dortmund Data base that are particularly important for the ongoing development of group-contribution based thermodynamic models. The impact of trace impurities, in the solvent and on the surface of clays, is presented in Chapter 3 along with a preliminary enthalpy + mass balance model. Since oil contamination of clays is one of the main problems in tailing ponds, in chapter 4, the effects of asphaltene coating on the behavior of clays is investigated and the model is extended to include these effects. The impacts of water chemistry (temperature, pH, and salinity) on the solution behavior of clays in water are investigated in Chapter 5 and the model is further extended to include these effects.

1.5 THESIS OUTLINE

A series of chapters follow the general introduction (Chapter 1) and they address specific topics. The experimental methods and procedures, data processing methods, and the repeatability and reliability of data are validated using the heptane + toluene binary mixture, where it is possible to compare experimental results obtained with literature values (Chapter 2). Experimental excess

enthalpy, excess volume, and density data for two binary liquid mixtures that are not currently available in the literature are also reported which are particularly important for the ongoing development of group-contribution based thermodynamic models linked to the impact of specific molecular features on molecular interactions in mixtures and improving the parametrization of equation of state models. The results of this chapter have been published as A. Pourmohammadbagher and J.M. Shaw, "Excess enthalpy and excess volume for pyridine + methyldiethanolamine and pyridine + ethanolamine mixtures" at Journal of Chemical & Engineering Data. Chapter 3 examines the effect of trace, i.e., parts per million (ppm) level by mass, compounds on the enthalpy of solution of kaolinite and illite clays in toluene, n- heptane, pyridine, and water with a focus on impacts that alter the surface composition of the clays. An experimental and theoretical interpretative frame-work for performing and parsing enthalpy of solution measurements and for determining and validating the signs and magnitudes of the energetics of specific clay surface−liquid interactions is presented. The outcomes of this chapter have been published as A. Pourmohammadbagher and J.M. Shaw, "Probing Contaminant Transport to and from Clay Surfaces in Organic Solvents and Water Using Solution Calorimetry" at Journal of Environmental Science & Technology. In chapter 4, the effects of asphaltene coating on the enthalpy of solution of kaolinite and illite clays in toluene, n-heptane, and water are investigated. Experimental outcomes are interpreted using a quantitative mass and energy balance model framework. Mechanistic and quantitative insights underlying the stability of asphaltene coated clay dispersions in tailings ponds, and the behaviors of these clays in diverse industrial and natural environments are discussed. The results of this chapter have been submitted as A. Pourmohammadbagher and J.M. Shaw, "Probing asphaltene contamination of kaolinite and illite clays: A calorimetric study" at Energy and Fuels. Chapter 5 focuses on the

impacts of water chemistry (temperature, pH, and salinity) on the solution behavior of kaolinite, illite, and montmorillonite clays in water. The outcomes of this chapter have been submitted as A. Pourmohammadbagher and J.M. Shaw, "Probing the role of water chemistry on the behavior of clays using solution calorimetry" at Energy and Fuels. Finally, conclusions and future work are presented in Chapter 6.

REFERENCES

(1) What are tailings? Their nature and production http://www.tailings.info/basics/tailings.htm (accessed Jan 1, 2016).

(2) Madden, P. B.; Morawski, J. D. The future of the Canadian Oil Stands: Engineering and project management advances. Energy Environ. **2011**, 22 (5), 579–596.

(3) Beier, N.; Wilson, W.; Dunmola, A.; Sego, D. Impact of flocculation-based dewatering on the shear strength of oil sands fine tailings. Can. Geotech. J. **2013**, 50, 1001–1007.

(4) Siddique, T.; Fedorak, P. M.; Foght, J. M. Biodegradation of short-chain n-alkanes in oil sands tailings under methanogenic conditions. Environ. Sci. Technol. **2006**, 40 (17), 5459–5464.

(5) BGC Engineering Inc. Oil Sands Tailings Technology Review. Oil Sands Res. Inf. Network, Univ. Alberta, Sch. Energy Environ. Edmonton, Alberta. **2010**, OSRIN Report No. TR – 1. 136 pp.

(6) http://tarsands.weebly.com/environmental-issues.html.

(7) Adiansyah, J. S.; Rosano, M.; Vink, S.; Keir, G. A framework for a sustainable approach to mine tailings management: disposal strategies. J. Clean. Prod. **2015**, 108, 1050–1062.

(8) Sun, D.; Zhou, X.; Luo, W.; Liu, Z.; Shi, Z.; Zhang, X. Study on the settlement experiment of iron tailings. Appl. Mech. Mater. **2013**, 281, 511–516.

(9) Ostergren, J. D.; Brown, G. E.; Parks, G. A.; Tingle, T. N. Quantitative speciation of lead in selected mine tailings from Leadville, CO. Environ. Sci. Technol. **1999**, 33 (10), 1627–1636.

(10) Macur, R. E.; Wheeler, J. T.; Mcdermott, T. R.; Inskeep, W. P. Microbial populations associated with the reduction and enhanced mobilization of arsenic in mine tailings. Environ. Sci. Technol. **2001**, 35 (18), 3676–3682.

(11) Scott, A. C.; MacKinnon, M. D.; Fedorak, P. M. Naphthenic acids in athabasca oil sands tailings waters are less biodegradable than commercial naphthenic acids. Environ. Sci. Technol. **2005**, 39 (21), 8388–8394.

(12) Siddique, T.; Penner, T.; Klassen, J.; Nesbø, C.; Foght, J. M. Microbial communities involved in methane production from hydrocarbons in oil sands tailings. Environ. Sci. Technol. **2012**, 46, 9802–9810.

(13) Dongbao, F.; Woods, J. R.; Kung, J.; Kingston, D. M.; Kotlyar, L. S.; Sparks, B. D.; Mercier, P. H. J.; McCracken, T.; Ng, S. Residual Organic Matter Associated with Toluene-Extracted Oil Sands Solids and Its Potential Role in Bitumen Recovery via Adsorption onto Clay Minerals. Energy & Fuels **2010**, 24 (4), 2249–2256.

(14) Liu, J.; Xu, Z.; Masliyah, J. Interaction between Bitumen and Fines in Oil Sands Extraction System. Can. J. Chem. Eng. **2004**, 82, 655–666.

(15) Jiang, T.; Hirasaki, G. J.; Miller, C. A.; Ng, S. Wettability alteration of clay in solid-stabilized emulsions. Energy and Fuels **2011**, 25 (6), 2551–2558.

(16) Nasser, M. S.; James, A. E. The effect of electrolyte concentration and ph on the flocculation and rheological behaviour of kaolinite suspensions. J. Eng. Sci. Technol. **2009**, 4 (4), 430–446.

(17) Chorom, M.; Rengasamy, P. Dispersion and zeta potential of pure clays as related to net particle charge under varying pH, electrolyte concentration and cation type. Eur. J. Soil Sci. **1995**, 46, 657–665.

(18) Yukselen, Y.; Kaya, A. Zeta potential of kaolinite in the presence of alkali, alkaline earth and hydrolyzable metal ions. Water. Air. Soil Pollut. **2003**, 145, 155–168.

(19) Marchuk, A.; Rengasamy, P. Clay behaviour in suspension is related to the ionicity of clay-cation bonds. Appl. Clay Sci. **2011**, 53 (4), 754–759.

(20) Bobos, I.; Duraes, N.; Noronha, F. Mineralogy and geochemistry of mill tailings impoundments from Algares (Aljustrel), Portugal: Implications for acid sulfate mine

waters formation. J. Geochemical Explor. **2006**, 88, 1–5.

(21) Craw, D. Geochemical changes in mine tailings during a transition to pressure–oxidation process discharge, Macraes mine, New Zealand. J. Geochemical Explor. **2003**, 80 (1), 81–94.

(22) Sidenko, N. V.; Sherriff, B. L. The attenuation of Ni, Zn and Cu, by secondary Fe phases of different crystallinity from surface and ground water of two sulfide mine tailings in Manitoba, Canada. Appl. Geochemistry **2005**, 20, 1180–1194.

(23) Praharaj, T.; Fortin, D. Seasonal variations of microbial sulfate and iron reduction in alkaline Pb-Zn mine tailings (Ontario, Canada). Appl. Geochemistry **2008**, 23 (12), 3728–3740.

(24) Penner, T. J.; Foght, J. M. Mature fine tailings from oil sands processing harbour diverse methanogenic communities. Can. J. Microbiol. **2010**, 56 (6), 459–470.

(25) Clark, K. A.; Pasternack, D. S. Hot water separation of bitumen from Alberta bituminous sand. Ind. Eng. Chem. **1932**, 24 (12), 1410–1416.

(26) Long, J.; Xu, Z.; Masliyah, J. H. Role of illite – illite interactions in oil sands processing. Colloids Surfaces A Physicochem. Eng. Asp. **2006**, 281, 202–214.

(27) Adegoroye, A.; Wang, L.; Omotoso, O.; Xu, Z.; Masliyah, J. Characterization of organic-coated solids isolated from different oil sands. Can. J. Chem. Eng. **2010**, 88 (3), 462–470.

(28) Lebedeva, E. V.; Fogden, A. Wettability alteration of kaolinite exposed to crude oil in salt solutions. Colloids Surfaces A Physicochem. Eng. Asp. **2011**, 377 (1-3), 115–122.

(29) Lebedeva, E. V.; Fogden, A. Nano-scale structure of crude oil deposits on water-wet substrates: Dependence on aqueous phase and organic solvents. Colloids Surfaces A Physicochem. Eng. Asp. **2011**, 380 (1-3), 280–291.

(30) Lebedeva, E. V.; Fogden, A. Adhesion of oil to kaolinite in water. Environ. Sci. Technol. **2010**, 44 (24), 9470–9475.

(31) Dudášová, D.; Simon, S.; Hemmingsen, P. V.; Sjöblom, J. Study of asphaltenes adsorption onto different minerals and clays Part 1. Experimental adsorption with UV depletion detection. Colloids Surfaces A Physicochem. Eng. Asp. **2008**, 317, 1–9.

(32) Kumar, M.; Fogden, A. Patterned wettability of oil and water in porous media. Langmuir **2010**, 26 (6), 4036–4047.

(33) Jada, A.; Debih, H. Hydrophobation of clay particles by asphaltenes adsorption. Compos. Interfaces **2009**, 16 (2-3), 219–235.

(34) Matthews, J. G.; Shaw, W. H.; MacKinnon, M. D.; Cuddy, R. G. Development of composite tailings technology at syncrude. Int. J. Surf. Mining, Reclam. Environ. **2002**, 16 (1), 24–39.

(35) Redfield, E.; Croser, C.; Zwiazek, J. J.; MacKinnon, M. D.; Qualizza, C. Responses of red-osier dogwood to oil sands tailings treated with gypsum or alum. J. Environ. Qual. **2003**, 32 (3), 1008–1014.

(36) Zhu, R.; Liu, Q.; Xu, Z.; Masliyah, J. H.; Khan, A. Role of dissolving carbon dioxide in densification of oil sands tailings. Energy & Fuels **2011**, 25 (5), 2049–2057.

(37) Liang, J.; Tumpa, F.; Pérez Estrada, L.; Gamal El-Din, M.; Liu, Y. Impact of ozonation on particle aggregation in mature fine tailings. J. Environ. Manage. **2014**, 146, 535–542.

(38) Chan, M. C. W. A novel flocculant for enhanced dewatering of oil sands tailings, University of Alberta, **2011**.

(39) Pouralhosseini, S. S. Extending depletion flocculation phase behavior models to partially soluble and aggregating colloids - asphaltenes, Ph.D. Thesis, University of Alberta, **2014**.

(40) Henderson, D. Recent progress in the theory of the electric double layer. Prog. Surf. Sci. **1983**, 13 (3), 197–224.

(41) Masliyah, J. H.; Bhattacharjee, S. Electrokinetic and colloid transport phenomena; John Wiley & Sons, **2006**.

(42) Aseyev, V. O.; Tenhu, H.; Winnik, F. M. Temperature dependence of the colloidal stability of neutral amphiphilic polymers in water. Adv. Polym. Sci. **2006**, 196, 1–85.

(43) Kaura, A. Understanding and developing new methods for treating oil sands tailings, MS.c. Thesis, University of Alberta, 2014.

(44) Gregory, J.; O'Melia, C. R. Fundamentals of flocculation. Crit. Rev. Environ. Control **1989**, 19 (3), 185–230.

(45) Bolto, B.; Gregory, J. Organic polyelectrolytes in water treatment. Water Res. **2007**, 41, 2301–2324.

(46) Ravina, L.; Moramarco, N. Everything you want to know about Coagulation & Flocculation; Zeta-Meter, Inc, **1993**.

CHAPTER 2: EXCESS ENTHALPY AND EXCESS VOLUME FOR PYRIDINE + METHYLDIETHANOLAMINE AND PYRIDINE + ETHANOLAMINE MIXTURES

This chapter has been published as Pourmohammadbagher, A.; Shaw, J. M. Excess enthalpy and excess volume for pyridine + methyldiethanolamine and pyridine + ethanolamine mixtures. J. Chem. Eng. Data 2013, 58 (8), 2202–2209

ABSTRACT: Experimental excess enthalpy, excess volume and density data for the binary liquid mixtures: pyridine + n-methyldiethanolamine (MDEA), and pyridine + monoethanolamine (MEA) are reported at atmospheric pressure and 15, 25, and 80 °C. Experimental data are not currently available for these mixtures and the reported values are particularly important for ongoing development of group-contribution based thermodynamic models linked to the impact of specific molecular features on molecular interactions in mixtures and improving the parameterization of Equation of State models. The experimental methods and procedures, and data processing methods were validated using the heptane + toluene binary mixture, where it was possible to compare experimental and computational results obtained with literature values. Mixture liquid density, excess volume and excess enthalpy data are also compared with values computed using the Peng-Robinson Equation of State.

Key words: measurement, excess, molar, enthalpy, volume, pyridine, methyldiethanolamine, ethanolamine.

2.1 INTRODUCTION

Enthalpies and volumes of mixing, and excess functions for mixtures more broadly are important both for designing chemical processes,[1] and for the development, elaboration and validation of thermodynamic models.[2–4] A survey of the literature showed very limited data concerning excess molar enthalpies of mixtures containing n-methyldiethanolamine (MDEA)[5–8] and monoethanolamine (MEA),[7–9] and no excess volume and excess enthalpy data are available for the mixtures pyridine + MEA and pyridine + MDEA. Aqueous solutions of amines have been

widely applied as an absorbent in natural gas scrubbing processes and pyridine has been used as a diluent in the oil industry as well as kinetic enhancer to promote carbon dioxide absorption in MDEA aqueous solutions. Data for uncommon combinations of compounds such as these provide needed data sets for group contribution models for chemical equilibrium of mixtures such as the UNIFAC and UNIQUAC models. Relevant experimental data improve the reliability of group contribution models and can also be used to validate equation of state based thermodynamic models. In this work, excess enthalpies and volumes were determined using an isothermal titration calorimeter and a density meter, respectively. These techniques are well established and are both known for their high accuracy and precision.

2.2 EXPERIMENTAL SECTION

2.2.1 Materials

N-methyldiethanolamine (also known as 2,2-methyliminodiethanol or MDEA, 99.8 %), and monoethanolamine (also known as ethanolamine or MEA, 99.9 %) were purchased from SIGMA-ALDRICH and pyridine (99.9 %), toluene (99.9 %) and heptane (99.4 %) were purchased from Fisher Scientific.

2.2.2 Apparatus and Procedure

2.2.2.1 Calorimetry Measurements

Calorimetry measurements were performed using an isothermal titration calorimetry module (ITC) and precision solution calorimetry module (SolCal) from TA Instruments inserted in a

TAM III thermostat with an uncertainty of 1μ°C. SolCal is a semi-adiabatic system with a short-term noise of <10 μ°C /5 min.[10] The ITC consists of a nanocalorimeter, 1 and 4 mL removable titration ampoule with mixers and a precision syringe pump with the resolution of 1 nL. The ITC can detect heat flow in micro joule level with a noise of <50 nW/hr. The repeatability and the reliability of excess enthalpy and partial molar excess enthalpy at infinite dilution values obtained were validated using heptane + toluene binary mixtures.

The experimental excess molar enthalpy (H^E) values obtained for the heptane + toluene binary, as a function of heptane mole fraction (x_1) at 25 °C and atmospheric pressure are reported in Table 2.1 and are shown in Figure 2.1 where they are also compared with literature data[11–14]. The uncertainties for data reported in this work are estimated to be less than 1 J/mole. The uncertainties for the literature data are not available. While the primary role of these data is to illustrate the accuracy of the experimental method, the composition range for this binary mixture is also extended beyond that available in the literature. The repeatability of the excess molar enthalpy measurements was within ± 0.2%.

Excess molar enthalpies were correlated using the Redlich–Kister equation:

$$H^E = x_2(1-x_2)\,\Sigma\, A_n (1-2x_2)^{n-1} \qquad (2.1)$$

A_n values and the standard deviations for all three binary mixtures are given in Table 2.2. The standard deviations were obtained using $\sigma=\{\Sigma(H^{Ecalc} - H^E)^2 / (N-n)\}^{0.5}$, where H^{Ecalc} and H^E are the calculated and experimental excess molar enthalpies, respectively. N is the number of the experimental points, and n is number of the fitting coefficients A_i. The significance of terms appearing in equation (2.1) was evaluated using the F-test[15,16]. Partial molar enthalpies were obtained by differentiating equation (2.1):

$$H_1 = x_2^2 \Sigma A_n (1 - 2x_2)^{n-1} + 2x_2^2 (1 - x_2) \Sigma A_n (n - 1) (1 - 2x_2)^{n-2} \quad (2.2)$$

and

$$H_2 = (1 - x_2)^2 \Sigma A_n (1 - 2x_2)^{n-1} - 2x_2 (1 - x_2)^2 \Sigma A_n (n - 1) (1 - 2x_2)^{n-2} \quad (2.3)$$

At infinite dilution (x_1 = 0, and x_2 = 0), the partial molar enthalpies of component 1 in component 2 (H_1^{∞}), and component 2 in component 1 (H_2^{∞}) are:

$$H_1^{\infty} = \Sigma A_n (-1)^{n-1} \quad (2.4)$$

and

$$H_2^{\infty} = \Sigma A_n \quad (2.5)$$

The experimental data using the precision solution calorimetry module (SolCal) at x_1= 0.005 for partial molar enthalpies at infinite dilution (H^{∞}) for the heptane + toluene binary mixture are reported in Table 2.3 where they are compared with results from the Redlich–Kister coefficients, Table 2.3, fit to the H^E data as a whole and values reported by Schnaible[17] and values calculated from reported excess molar enthalpies of Lundberg[14] using the Redlich–Kister equation. In this work each measurement was performed with three samples, and the values obtained for the partial molar enthalpies at infinite dilution are reproducible to within ± 5% as shown in Table 2.3. Measurement errors are not mentioned in the prior work. While there is a good agreement between this work and Lundberg[14], Schnaible[17] appears to underestimate values.

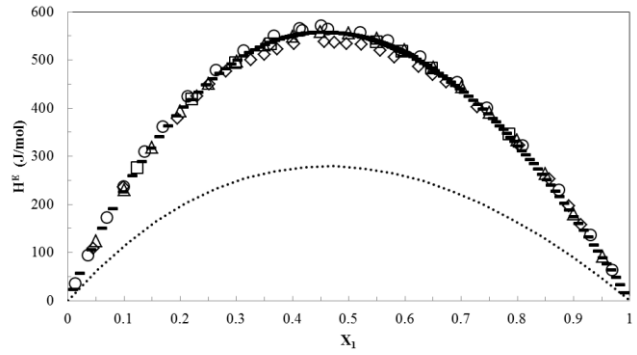

Figure 2.1 *Excess enthalpy for heptane (x_1) + toluene mixtures at 25 °C and atmospheric pressure: data (◇Kuchenbecker[11], △Segovia et al.[12], ○Tamura et al.[13], □Lundberg[14], ▁ this work) and (.....) the Peng-Robinson equation of state.*

Table 2.1 *Experimental values of excess enthalpy H^E at mole fraction x, 25 °C and atmospheric pressure for the liquid mixture heptane (1) + toluene (2)*[a]

x_1	H^E (J/mol)	x_1	H^E (J/mol)	x_1	H^E (J/mol)	x_1	H^E (J/mol)	x_1	H^E (J/mol)
0.00901	23	0.41122	554	0.52667	547	0.61478	507	0.90016	175
0.02172	57	0.41366	554	0.52986	546	0.62089	502	0.90881	161
0.04198	106	0.41609	554	0.53301	545	0.62712	498	0.91763	147
0.06142	150	0.41849	555	0.53612	544	0.63348	493	0.92662	132
0.08009	191	0.42087	555	0.53919	543	0.63997	488	0.93580	116
0.09803	226	0.42324	556	0.54222	542	0.64659	484	0.94337	103
0.11529	260	0.42558	556	0.54521	541	0.65336	478	0.95106	90
0.13189	289	0.42791	556	0.54816	540	0.66026	473	0.95888	77
0.14789	317	0.43022	557	0.55107	539	0.66731	467	0.96683	63
0.16330	341	0.43251	557	0.55394	538	0.67452	461	0.97492	48
0.17817	364	0.43478	557	0.55678	537	0.68188	454	0.98314	33
0.19252	384	0.43818	557	0.55887	536	0.68941	447	0.99150	16
0.20638	402	0.44154	558	0.56095	535	0.69710	440		
0.21977	418	0.44487	558	0.56300	534	0.70497	433		
0.23271	433	0.44815	558	0.56504	533	0.71301	424		
0.24523	448	0.45139	558	0.56706	532	0.72125	416		
0.25735	461	0.45460	558	0.56906	531	0.72967	408		
0.26909	472	0.45777	558	0.57104	530	0.73830	398		
0.28046	483	0.46090	558	0.57300	529	0.74713	388		
0.29148	492	0.46400	558	0.57495	528	0.75617	378		
0.30217	501	0.46706	558	0.57687	527	0.76227	371		
0.31255	508	0.47008	557	0.57878	527	0.76846	364		
0.32261	516	0.47308	557	0.58068	526	0.77476	356		
0.33239	522	0.47604	557	0.58255	525	0.78116	348		
0.34189	527	0.47896	557	0.58441	524	0.78767	340		
0.35113	532	0.48185	556	0.58625	523	0.79428	330		
0.36010	536	0.48471	556	0.58808	522	0.80101	322		
0.36884	540	0.48754	556	0.58989	521	0.80786	312		
0.37733	544	0.49034	555	0.59168	520	0.81482	303		
0.38561	547	0.49311	555	0.59346	519	0.82190	294		
0.38827	548	0.49585	554	0.59523	518	0.82911	284		
0.39091	548	0.49947	553	0.59697	517	0.83645	274		
0.39352	549	0.50304	553	0.59871	516	0.84391	263		
0.39611	550	0.50656	552	0.60043	515	0.85151	252		
0.39868	551	0.51003	552	0.60213	514	0.85925	240		
0.40123	551	0.51345	551	0.60382	513	0.86713	228		
0.40376	552	0.51682	550	0.60549	512	0.87516	216		
0.40627	552	0.52015	549	0.60715	511	0.88334	203		
0.40875	553	0.52343	548	0.60880	510	0.89167	189		

[a]Standard uncertainties u are $u(x_1)$ = 0.00001, $u(T)$ = 0.01°C, and the combined expanded uncertainty U_c is $U_c(H^E)$ = 2 J/mol with 0.95 level of confidence ($k \approx 2$).

Table 2.2 *Redlich–Kister coefficients, for equations 2.1-2.5, and the standard deviations for (heptane + toluene), (pyridine + MDEA), and (pyridine + MEA) mixtures at 25°C*

A_1 (J/mol)	A_2 (J/mol)	A_3 (J/mol)	A_4 (J/mol)	A_5 (J/mol)	A_6 (J/mol)	σ (J/mol)
Heptane + Toluene						
2215.3	-373.81	86.467				0.73
MDEA + Pyridine						
-394.06	421.44	-82.105	-156.55	125.44	490.05	6.01
MEA + Pyridine						
3433	1004.6	1139.9	-541.25	15.796	880.51	2.44

Table 2.3 *H^{∞} values for the liquid mixture heptane (1) + toluene (2) at 25 °C and atmospheric pressure*

H^{∞} (J/mol)	This work		Lundberg[14] + Eq.(2.1-2.5)	Schnaible[17]
	Measurement	Eq. (2.1-2.5)		
H_1^{∞}	2670± 70	2675	2668	2414.8
H_2^{∞}	1900± 100	1927	1974	1788.8

2.2.2.2 Density Measurements

Density measurements were performed using an Anton Paar DMA 5000 density meter with an uncertainty of 0.1 kg/m^3. The instrument records the temperature with an uncertainty of 0.001°C[18]. The repeatability of the density measurements was ± 0.2 kg/m^3. Experimental excess molar volume (V^E) values obtained for the heptane + toluene binary mixture were used to validate the measurement method and procedures employed in this work. V^E values as a function

of heptane mole fraction (x_1) at 25 °C and atmospheric pressure are reported in Table 2.4, and are compared with literature data[19–21] in Figure 2.2. The uncertainty for this work, ± 0.0001 m^3/mol is smaller than the points shown in the figure. The uncertainties for the literature data are not available. Again, while the primary role of these data is to illustrate the accuracy of the V^E experimental method, the composition range is also extended beyond the range available in the literature.

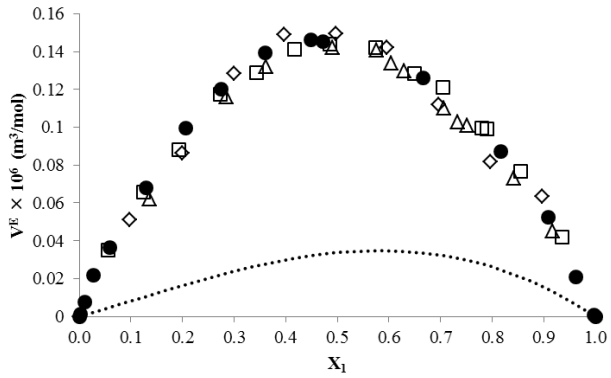

Figure 2.2 *Excess volume for heptane + toluene as a function of heptane mole fraction (x_1) at 25 °C and atmospheric pressure, data (◇Gonzalez et al.[19], □Bravo et al.[20], △ Letcher[21], ● this work) and (.....) the Peng-Robinson equation of state.*

Table 2.4 *Experimental values of density ρ and excess volume V^E at mole fraction x, 25 °C and atmospheric pressure for the liquid mixture heptane (1)+ toluene (2)*[a]

x_1	ρ (kg/m^3)	$V^E \times 10^6$ (m^3/mol)
0	862.222	
0.00177	861.767	0.0013
0.01118	859.353	0.0076
0.02670	855.387	0.0216
0.05849	847.515	0.0363
0.12966	830.567	0.0678
0.20595	813.369	0.0994
0.27522	798.596	0.1200
0.36045	781.402	0.1394
0.44943	764.554	0.1461
0.47181	760.485	0.1452
0.66591	727.559	0.1263
0.81665	704.661	0.0871
0.90938	691.588	0.0525
0.96238	684.471	0.0210
0.99682	679.955	0.0008
1	679.537	

[a]Standard uncertainties u are $u(x_1) = 0.00001$, $u(T) = 0.001$°C, and the combined expanded uncertainty U_c is $U_c(\rho) = 0.2$ kg/m^3 with 0.95 level of confidence ($k \approx 2$).

2.3 RESULTS AND DISCUSSION

2.3.1 Excess Enthalpy

The excess enthalpies for pyridine + MEA and MDEA as functions of pyridine mole fraction (x_1) at 25 °C and atmospheric pressure are presented in Figure 2.3 and listed in Tables 2.5 and 2.6 respectively. There is a weak endothermic interaction between pyridine and MDEA at x_1>0.8855 and an exothermic interaction at x_1<0.8855. For pyridine + MEA the interactions lead to an

endothermic H^E with a maximum of 881.32 J.mol^{-1} at x_1= 0.5786. H^∞ values for (pyridine + MDEA), and (pyridine + MEA) mixtures were measured in this work using the precision solution calorimetry module (SolCal) at x_1= 0.005 and these values are compared with results from the Redlich–Kister coefficients, Table 2.3, fit to the H^E data as a whole. The regressed values are in good agreement with experimental measurements, ± 1%, as shown in Table 2.7. Thus, H^∞ values obtained from individual, high-quality direct measurements, at near infinite dilution, provide values of equivalent quality to those obtained by regressing large numbers of H^E measurements over a broad range of compositions. Further, the impact of amine hygroscopicity on H^∞ measurement outcomes was minimal. Intentional contamination of two samples, exposed to air in open vials for 24 hours, agreed to within ± 50 J/mole, of equivalent unexposed samples.

Equations of state are frequently employed to interpolate and extrapolate sparse data sets. In this work, the Peng-Robinson (PR), available in VMGSim (v7.0.46) was used to simulate mixture excess enthalpy. The interaction parameters appearing in the PR equation of state are 0.00028 for toluene + heptane and zero for the other binaries. The critical constants for components are presented in Table 2.8. The PR model provides values in qualitative agreement with the experimental excess enthalpy of toluene + heptane mixtures, Figure 2.1, and for pyridine + MEA mixtures, Figure 2.3, and in qualitative disagreement with experimental values for enthalpy of pyridine + MDEA mixtures also shown in Figure 2.3.

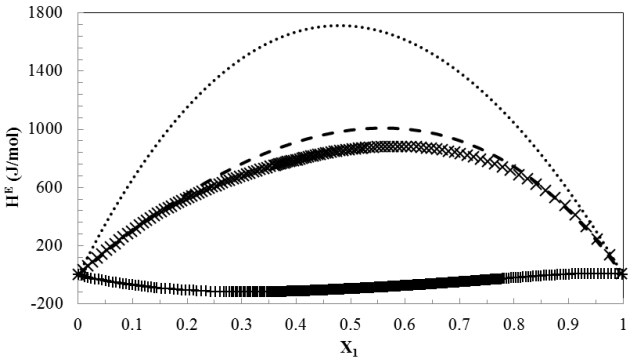

Figure 2.3 *Excess enthalpy for pyridine (x_1) + MDEA (data: +; Peng-Robinson equation of state: .....) and MEA (data: ×; Peng-Robinson equation of state: ----) mixtures at 25 °C and atmospheric pressure.*

Table 2.5 *Experimental values of excess enthalpy H^E at mole fraction x, 25 °C and atmospheric pressure for the liquid mixture pyridine (1)+ MEA (2)*[a]

x_1	H^E (J/mol)	x_1	H^E (J/mol)	x_1	H^E (J/mol)	x_1	H^E (J/mol)
0.00998	32	0.27822	649	0.45963	838	0.77935	739
0.01870	60	0.28447	657	0.46464	841	0.79385	715
0.02728	88	0.29072	666	0.46975	845	0.80890	687
0.03570	114	0.29697	674	0.47498	848	0.82453	656
0.04398	140	0.30322	682	0.48033	851	0.84078	620
0.05212	165	0.30947	690	0.48580	855	0.85768	576
0.06012	189	0.31573	698	0.49139	858	0.87527	529
0.06798	213	0.32198	706	0.49712	860	0.89361	472
0.07572	235	0.32823	713	0.50298	863	0.91272	407
0.08333	257	0.33448	721	0.50898	866	0.93268	331
0.09081	279	0.34073	728	0.51513	868	0.95352	240
0.09818	299	0.34698	735	0.52142	870	0.97532	135
0.10542	319	0.35323	742	0.52193	871	0.99814	5
0.11255	338	0.35948	749	0.52839	873		
0.11957	356	0.36211	752	0.53502	875		
0.12648	374	0.36521	755	0.54181	877		
0.13327	389	0.36836	758	0.54878	878		
0.13997	404	0.37157	762	0.55593	880		
0.14656	419	0.37483	765	0.56327	880		
0.15305	433	0.37815	768	0.57081	881		
0.15944	446	0.38154	772	0.57855	881		
0.16574	459	0.38498	775	0.58650	881		
0.17195	471	0.38848	778	0.59468	881		
0.17821	483	0.39205	781	0.60308	880		
0.18446	495	0.39569	782	0.61173	879		
0.19071	507	0.39939	786	0.62063	877		
0.19696	519	0.40317	790	0.62979	874		
0.20321	530	0.40701	794	0.63923	871		
0.20946	541	0.41093	797	0.64895	867		
0.21572	552	0.41493	801	0.65897	862		
0.22197	562	0.41901	805	0.66931	856		
0.22822	573	0.42316	809	0.67998	849		
0.23447	583	0.42740	813	0.69099	841		
0.24072	593	0.43173	816	0.70237	832		
0.24697	602	0.43614	820	0.71412	822		
0.25322	612	0.44064	824	0.72628	809		
0.25947	621	0.44524	827	0.73886	796		
0.26572	631	0.44994	831	0.75188	779		
0.27197	640	0.45473	834	0.76536	761		

[a]Standard uncertainties u are $u(x_1) = 0.00001$, $u(T) = 0.01°C$, and the combined expanded uncertainty U_c is $U_c(H^E) = 2$ J/mol with 0.95 level of confidence ($k \approx 2$).

Table 2.6 *Experimental values of excess enthalpy H^E at mole fraction x, 25 °C and atmospheric pressure for the liquid mixture pyridine (1)+ MDEA (2)*[a]

x_1	H^E (J/mol)	x_1	H^E (J/mol)	x_1	H^E (J/mol)	x_1	H^E (J/mol)	x_1	H^E (J/mol)	x_1	H^E (J/mol)	x_1	H^E (J/mol)	x_1	H^E (J/mol)
0.00136	-2	0.26045	-118	0.39222	-115	0.48495	-101	0.57441	-82	0.66387	-61	0.75334	-36	0.90712	3
0.00718	-8	0.26838	-119	0.39488	-115	0.48724	-100	0.57670	-82	0.66617	-60	0.75563	-36	0.91270	4
0.01292	-14	0.27223	-120	0.39752	-114	0.48953	-100	0.57900	-81	0.66846	-60	0.75792	-35	0.91835	5
0.01860	-19	0.27798	-120	0.40013	-114	0.49183	-99	0.58129	-81	0.67075	-59	0.76022	-34	0.92407	6
0.02422	-25	0.28173	-121	0.40272	-114	0.49412	-99	0.58358	-80	0.67305	-58	0.76251	-34	0.92985	6
0.03106	-30	0.28545	-120	0.40529	-113	0.49642	-98	0.58588	-80	0.67534	-58	0.76481	-33	0.93572	7
0.03780	-35	0.28912	-120	0.40784	-113	0.49871	-98	0.58817	-79	0.67764	-57	0.76710	-32	0.94165	7
0.04445	-40	0.29275	-121	0.41036	-113	0.50100	-98	0.59047	-79	0.67993	-57	0.76939	-32	0.94767	7
0.05100	-44	0.29635	-121	0.41287	-112	0.50330	-97	0.59276	-78	0.68222	-56	0.77169	-31	0.95376	8
0.05747	-48	0.29992	-121	0.41535	-112	0.50559	-97	0.59505	-78	0.68452	-55	0.77398	-30	0.95992	7
0.06385	-52	0.30344	-121	0.41781	-112	0.50788	-96	0.59735	-77	0.68681	-55	0.77628	-30	0.96617	7
0.07015	-56	0.30693	-121	0.42025	-111	0.51018	-96	0.59964	-76	0.68911	-54	0.77857	-29	0.97250	7
0.07636	-60	0.31039	-121	0.42267	-111	0.51247	-95	0.60194	-76	0.69140	-53	0.78086	-28	0.97892	6
0.08249	-63	0.31381	-121	0.42507	-111	0.51477	-95	0.60423	-75	0.69369	-53	0.78274	-28	0.98542	5
0.08853	-66	0.31720	-120	0.42745	-110	0.51706	-94	0.60652	-75	0.69599	-52	0.78689	-27	0.99200	3
0.09450	-69	0.32055	-120	0.42981	-110	0.51935	-94	0.60882	-74	0.69828	-52	0.79108	-25	0.99868	1
0.10039	-72	0.32388	-120	0.43215	-110	0.52165	-93	0.61111	-74	0.70058	-51	0.79532	-24		
0.10621	-75	0.32717	-120	0.43448	-109	0.52394	-93	0.61341	-73	0.70287	-50	0.79961	-23		
0.11195	-78	0.33042	-120	0.43678	-109	0.52624	-93	0.61570	-73	0.70516	-50	0.80394	-22		
0.11761	-80	0.33365	-120	0.43906	-108	0.52853	-92	0.61799	-72	0.70746	-49	0.80832	-21		
0.12321	-83	0.33684	-120	0.44136	-108	0.53082	-92	0.62029	-72	0.70975	-48	0.81274	-19		
0.12873	-85	0.34001	-120	0.44365	-108	0.53312	-91	0.62258	-71	0.71205	-48	0.81722	-18		
0.13419	-87	0.34314	-119	0.44595	-107	0.53541	-91	0.62488	-70	0.71434	-47	0.82174	-17		
0.13957	-90	0.34625	-119	0.44824	-107	0.53771	-90	0.62717	-70	0.71663	-47	0.82632	-15		
0.14489	-92	0.34933	-119	0.45054	-107	0.54000	-90	0.62946	-69	0.71893	-46	0.83094	-14		
0.15282	-94	0.35237	-119	0.45283	-106	0.54229	-89	0.63176	-69	0.72122	-45	0.83562	-13		

0.16061	-97	0.35539	-119	0.45512	-106	0.54459	-89	0.63405	-68	0.72352	-45	0.84035	-12
0.16825	-100	0.35838	-118	0.45742	-105	0.54688	-88	0.63635	-68	0.72581	-44	0.84514	-10
0.17575	-102	0.36135	-118	0.45971	-105	0.54918	-88	0.63864	-67	0.72810	-43	0.84998	-9
0.18312	-104	0.36428	-118	0.46201	-105	0.55147	-87	0.64093	-67	0.73040	-43	0.85487	-8
0.19036	-105	0.36719	-118	0.46430	-104	0.55376	-87	0.64323	-66	0.73269	-42	0.85983	-7
0.19747	-107	0.37007	-117	0.46659	-104	0.55606	-86	0.64552	-65	0.73498	-41	0.86484	-5
0.20446	-109	0.37293	-117	0.46889	-103	0.55835	-86	0.64782	-65	0.73728	-41	0.86991	-4
0.21132	-110	0.37576	-117	0.47118	-103	0.56065	-85	0.65011	-64	0.73957	-40	0.87503	-3
0.21807	-112	0.37857	-116	0.47348	-103	0.56294	-85	0.65240	-64	0.74187	-40	0.88022	-2
0.22693	-113	0.38135	-116	0.47577	-102	0.56523	-84	0.65470	-63	0.74416	-39	0.88548	-1
0.23559	-115	0.38410	-116	0.47806	-102	0.56753	-84	0.65699	-62	0.74645	-38	0.89079	0
0.24406	-116	0.38683	-116	0.48036	-101	0.56982	-83	0.65928	-62	0.74875	-38	0.89617	1
0.25235	-117	0.38954	-115	0.48265	-101	0.57212	-83	0.66158	-61	0.75104	-37	0.90161	2

[a]Standard uncertainties u are $u(x_1) = 0.00001$, $u(T) = 0.01$°C, and the combined expanded uncertainty U_c is $U_c(H^E) = 2$ J/mol with 0.95 level of confidence ($k \approx 2$).

Table 2.7 *H^{∞} values for the liquid mixtures pyridine (1) + MDEA (2) and pyridine (1) + MEA (2) at 25 °C and atmospheric pressure*

H^{∞} (J/mol)	Pyridine + MDEA		Pyridine + MEA	
	Measurement	Eq. (2.1-2.5)	Measurement	Eq. (2.1-2.5)
H_1^{∞}	-1100 ± 50	-1105	3250 ± 50	3245
H_2^{∞}	400 ± 20	404	5980 ± 40	5933

Table 2.8 *Critical constants for components.*

Critical property	Heptane	Toluene	Pyridine	MDEA	MEA
Pressure (kPa)	2736	4109	5634	3880	6870
Volume (m^3/mol)	0.4264	0.316	0.254	0.401	0.225
Temperature (°C)	267.11	318.6	346.8	404.9	364.9
Compressibility	0.263	0.264	0.278	0.276	0.291

2.3.2 Excess Volume

Experimental excess molar volume values for pyridine + MDEA and pyridine + MEA mixtures are depicted in Figures 2.4 a and b, and presented in Tables 2.9 and 2.10 respectively as functions of pyridine mole fraction (x_1) at atmospheric pressure and 15, 25 and 80°C. Both mixtures have small and positive excess molar volumes that increase with temperature. The excess molar volumes are larger in the pyridine + MDEA mixture than in the pyridine + MEA mixture, while the values in the pyridine + MEA mixture are more asymmetric. Again the measurement uncertainty, ± 0.0001 m^3/mol, is smaller than the size of the data markers. Density and excess volume data for the toluene + heptane, pyridine + MDEA and MEA binaries are presented in Tables 2.4, 2.9 and 2.10 respectively.

The Peng-Robinson (PR) model, available in VMGSim (v7.0.46) was used to simulate mixture density and excess volume. The volumes obtained are corrected by adding a constant fit to experimental pure-component liquid molar volumes at 25°C. The results obtained are illustrative and highlight the computational challenges and limitations. As correlations for component densities diverge from measurements remote from benchmark data, systematic displacement of

simulated vs. experimental density values for mixtures can be anticipated. This effect is not evident for toluene + heptane mixtures at 25°C, Figure 2.5, as benchmark density data are available at 25°C, but systematic displacement is evident for pyridine + MDEA and MEA mixtures, Figures 2.6a and 6b, particularly at 80°C. For excess volume calculations, Figures 2.7a and 7b, the impact of systematic displacement of component densities is reduced, but it is clear that the Peng-Robinson equation of state does not approximate the excess volumes of pyridine + MDEA and MEA mixtures. However, results obtained with the Peng-Robinson equation of state results for the heptane + toluene mixture are in qualitative agreement with the experimental excess volume values, Figure 2.2.

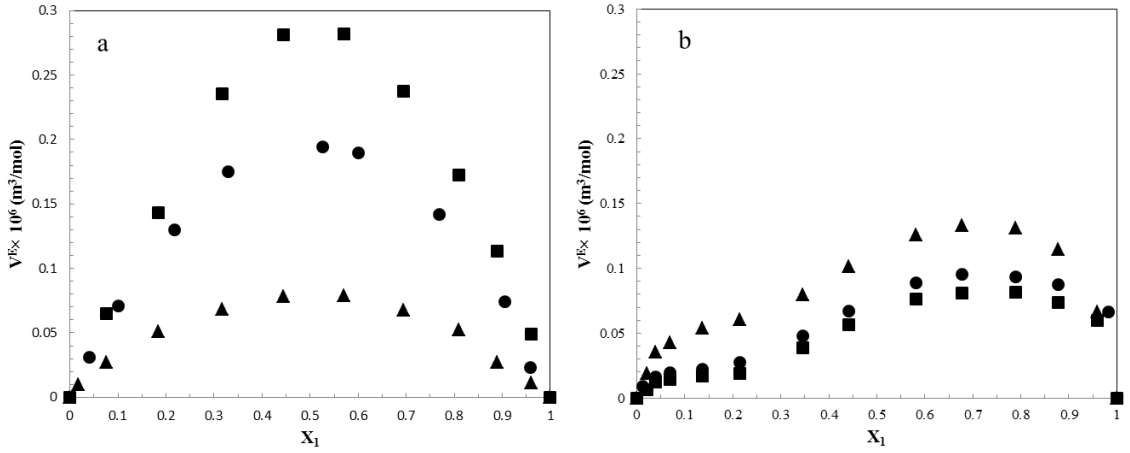

Figure 2.4 *Excess volume for pyridine (x_1) + (a) MDEA and (b) MEA binary mixtures at atmospheric pressure: ■15 °C, ●25 °C ▲80 °C.*

Table 2.9 *Experimental values of density ρ and excess volume V^E at mole fraction x, 15, 25 and 80 °C and atmospheric pressure for the liquid mixture pyridine (1)+ MDEA (2)*[a].

15°C			25°C			80°C		
x_1	ρ (kg/m^3)	$V^E\times10^6$ (m^3/mol)	x_1	ρ (kg/m^3)	$V^E\times10^6$ (m^3/mol)	x_1	ρ (kg/m^3)	$V^E\times10^6$ (m^3/mol)
0	1046.362		0	1036.805		0	994.015	
0.07502	1041.454	0.0652	0.04000	1034.218	0.0309	0.01699	992.733	0.0099
0.18439	1034.444	0.1429	0.10000	1030.395	0.0708	0.07502	988.525	0.0272
0.31777	1025.814	0.2352	0.21829	1023.026	0.1297	0.18439	980.64	0.0508
0.44466	1017.998	0.2815	0.33000	1016.102	0.1752	0.31777	971.05	0.0684
0.57077	1010.676	0.2817	0.52647	1004.445	0.1943	0.44466	961.905	0.0778
0.69449	1003.925	0.2375	0.60000	1000.154	0.1896	0.57077	952.805	0.0791
0.80950	997.843	0.1723	0.76874	990.603	0.1418	0.69449	943.917	0.0675
0.88861	993.774	0.1135	0.90585	983.032	0.0742	0.80950	935.616	0.0520
0.95968	990.221	0.0491	0.95816	980.414	0.0229	0.88861	930.006	0.0272
1	988.343		1	978.086		0.95968	924.867	0.0109
						1	921.952	

[a]Standard uncertainties u are $u(x_1) = 0.00001$, $u(T) = 0.001$°C, and the combined expanded uncertainty U_c is $U_c(\rho) = 0.2$ kg/m^3 with 0.95 level of confidence ($k \approx 2$).

Table 2.10 *Experimental values of density ρ and excess volume V^E at mole fraction x, 15, 25 and 80 °C and atmospheric pressure for the liquid mixture pyridine (1)+ MEA (2)*[a]

15°C			25°C			80°C		
x_1	ρ (kg/m^3)	$V^E\times10^6$ (m^3/mol)	x_1	ρ (kg/m^3)	$V^E\times10^6$ (m^3/mol)	x_1	ρ (kg/m^3)	$V^E\times10^6$ (m^3/mol)
0	1019.872		0	1012.123		0	968.332	
0.02208	1018.828	0.0066	0.01329	1011.365	0.0093	0.02208	966.667	0.0189
0.03932	1018.014	0.0123	0.03932	1010.085	0.0164	0.03932	965.353	0.0353
0.06973	1016.732	0.0145	0.06973	1008.705	0.0194	0.06973	963.408	0.0425
0.13692	1014.029	0.0169	0.13692	1005.81	0.0224	0.13692	959.323	0.0537
0.21465	1011.06	0.0187	0.21465	1002.592	0.0273	0.21465	954.908	0.0609
0.34549	1006.116	0.0390	0.34549	997.334	0.0481	0.34549	947.883	0.0798
0.44136	1002.696	0.0567	0.44136	993.687	0.0672	0.44136	943.004	0.1011
0.58186	998.105	0.0764	0.58186	988.794	0.0886	0.58186	936.439	0.1260
0.67671	995.328	0.0808	0.67671	985.804	0.0957	0.67671	932.426	0.1332
0.78999	992.252	0.0817	0.78999	982.566	0.0938	0.78999	928.035	0.1310
0.87805	990.097	0.0737	0.87805	980.237	0.0879	0.87805	924.973	0.1146
0.96000	988.258	0.0598	0.98169	977.805	0.0664	0.96000	922.401	0.0667
1	988.041		1	978.145		1	921.953	

[a]Standard uncertainties u are $u(x_1) = 0.00001$, $u(T) = 0.001$°C, and the combined expanded uncertainty U_c is $U_c(\rho) = 0.2$ kg/m^3 with 0.95 level of confidence ($k \approx 2$).

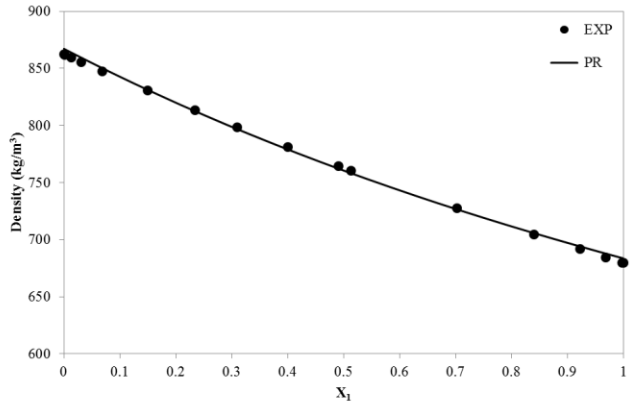

Figure 2.5 *Comparison between the heptane + toluene experimental density data with the Peng-Robinson equation of state (PR) as a function of heptane mole fraction (x_1) at 25 °C and atmospheric pressure.*

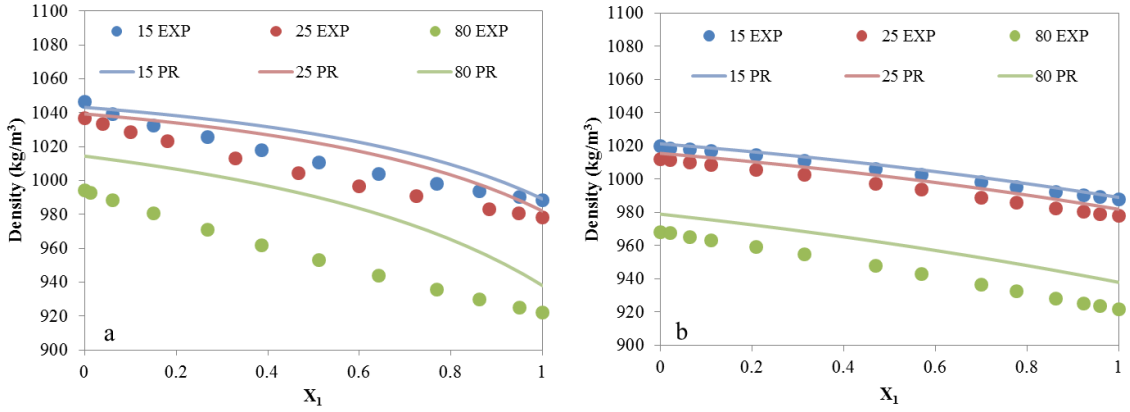

Figure 2.6 *Comparison of experimental density data with Peng-Robinson equation of state (PR) for pyridine (x_1) + (a) MDEA and (b) MEA at 15, 25 and 80 °C and atmospheric pressure*

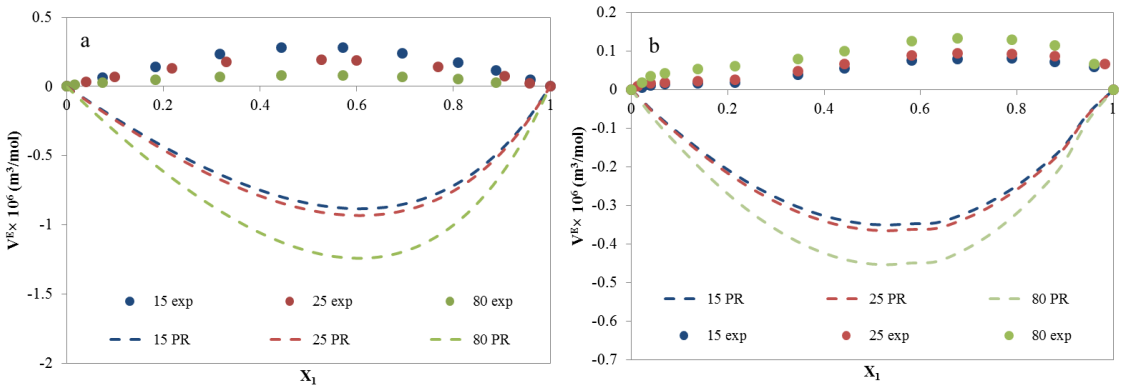

Figure 2.7 *Comparison of experimental excess volume data with the Peng-Robinson equation of state (PR) model for pyridine (x_1) + (a) MDEA and (b) MEA at 15, 25 and 80 °C and atmospheric pressure*

2.4 CONCLUSIONS

Atmospheric excess enthalpy (25°C) and excess volume (15, 25 and 80°C) data for pyridine + MDEA and pyridine + MEA binary mixtures are reported along with the corresponding partial molar enthalpies at infinite dilution (25 °C). The quality of the data acquisition and data processing methods were validated using the heptane + toluene binary mixture. Data obtained for this mixture were compared with data available in the literature and data points at near infinite dilution were added to the database for this benchmark mixture. The excess enthalpy and excess volume data for the heptane + toluene mixture are in good agreement with the data in the literature. Illustrative calculations based on the Peng-Robinson Equation of State, underscore the role of such data in improving the parameterization of thermodynamic property models.

ACKNOWLEDGEMENTS

The authors thank Ms. M. Becerra and Dr. K. Nikooyeh for their assistance in the laboratory and Dr. Y. Maham and Mr. W. Cordes for their support in literature studies and gratefully acknowledge funding from Alberta Innovates Energy and Environment Solutions, British Petroleum, ConocoPhillips Inc., Imperial Oil Resources, Halliburton Energy Services Ltd., Kellogg Brown and Root, NEXEN Inc., Shell Canada, Total E & P Canada, VMG Inc., and the Natural Sciences and Engineering Research Council of Canada (NSERC).

REFERENCES

(1) Kojima, K. Thermodynamic Analysis of Chemical Processes: ASOG-Based Methods for the Prediction of Excess Enthalpy and Excess Entropy. J. Chem. Eng. Jpn. **1994**, 27, 143–151.

(2) Tamilarasan, R.; Prabu, A. A.; Kim, K. J.; Kumar, M. D. Effect of Dissolved Inorganic Salts on the Enthalpy of Mixing of the Ethanol + Pyridine System at 303 . 15 K. J. Chem. Eng. Data **2010**, 55, 3567–3571.

(3) Dong, H.; Li, S.; Yan, W. Excess Molar Enthalpies of N,N-Dimethylethanolamine with (Methanol, Ethanol, 1-Propanol, and 2-Propanol) at T) (298.2, 313.2, and 328.2) K and p) (0.1 and 10.0) MPa. J. Chem. Eng. Data **2008**, 53, 1927–1931.

(4) Clara, A. R.; Marigliano, A. C. G.; Morales, D.; Solimo, H. N. Density , Viscosity , Vapor-Liquid Equilibrium , and Excess Molar Enthalpy of [Chloroform + Methyl tert-Butyl Ether]. J. Chem. Eng. Data **2010**, 55, 5862–5867.

(5) Arcis, H.; Rodier, L.; Ballerat-Busserolles, K.; Coxam, J.-Y. Modeling of (vapor+liquid) equilibrium and enthalpy of solution of carbon dioxide (CO2) in aqueous methyldiethanolamine (MDEA) solutions. J. Chem. Thermodynamics **2009**, 41, 783–789.

(6) Maham, Y.; Mather, A. E.; Mathonat, C. Excess properties of (alkyldiethanolamine + H2O) mixtures at temperatures from (298.15 to 338.15) K. J. Chem. Thermodynamics **2000**, 32, 229–236.

(7) Maham, Y.; Mather, A. E.; Hepler, L. G. Excess Molar Enthalpies of (Water + Alkanolamine) Systems and Some Thermodynamic Calculations. J. Chem. Eng. Data **1997**, 42, 988–992.

(8) Mathonat, C.; Maham, Y.; Mather, A. E.; Hepler, L. G. Excess Molar Enthalpies of (Water + Monoalkanolamine) Mixtures at 298 . 15 K and 308 . 15 K. J. Chem. Eng. Data 1997, 42, 993–995.

(9) Maham, Y.; Liew, C. N.; Mather, A. E. Viscosities and Excess Properties of Aqueous Solutions of Ethanolamines from 25 to 80 ◦C. J. Solution Chem. **2002**, 31, 743–756.

(10) Nikooyeh, K.; Bagheri, S. R.; Shaw, J. M. Interactions Between Athabasca Pentane Asphaltenes and n-Alkanes at Low Concentrations. Energy & Fuels **2012**, 26, 1756 – 1766.

(11) Kuchenbecker, D. Rationelle Ermittlung kalorischer Exzeßfunktionen von n-Alkylamin/n-Alkan- und Aromat/n-Alkan-Systemen, Universität Leipzig, **1976**.

(12) Segovia, J. J.; Martín, C. M.; Vega-Maza, D.; Chamorro, C. R.; Villamañán, M. a. Thermodynamics of biofuels: Excess enthalpies for binary mixtures involving ethyl 1,1-dimethylethyl ether and hydrocarbons at different temperatures using a new flow calorimeter. J. Chem. Thermodynamics **2009**, 41, 759–763.

(13) Tamura, K.; Murakami, S.; Fujishiro, R. Excess enthalpies of binary mixtures of aromatic hydrocarbons and aliphatic ketones at 298.15 K. J. Chem. Thermodynamics **1975**, 7, 1089–1095.

(14) Lundberg, G. W. Thermodynamics of solutions XI. heats of mixing of hedrocarbons. J. Chem. Eng. Data **1964**, 9, 193–198.

(15) Bevington, P. R. Data Reduction and Error Analysis for the Physical Sciences; McGraw-Hill: New York, **1969**.

(16) Shoemaker, D. P.; Garland, C. W.; Nibler, J. W. Experimental Physical Chemistry; 5th ed.; McGraw-Hill: New York, **1989**.

(17) Schnaible, H. W.; Van Ness, H. C.; Smith, J. M. Heats of mixing of liquids. AIChE Journal **1957**, 3, 147–152.

(18) Nikooyeh, K.; Shaw, J. M. On the Applicability of the Regular Solution Theory to Asphaltene + Diluent Mixtures. Energy & Fuels **2012**, 26, 576–585.

(19) González, E. J.; Calvar, N.; González, B.; Domínguez, Á. Separation of toluene from alkanes using 1-ethyl-3-methylpyridinium ethylsulfate ionic liquid at T=298.15K and atmospheric pressure. J. Chem. Thermodyn. **2010**, 42, 752–757.

(20) Bravo, R.; Pintos, M.; Amigo, A. Excess molar volumes of (o-xylene + n-heptane + toluene or n-hex-1-ene) at the temperature 298.15 K. J. Chem. Thermodyn. **1991**, 23, 905–910.

(21) Letcher, T. M. Thermodynamics of aliphatic amine mixtures I . The excess volumes of mixing for primary , secondary , and tertiary aliphatic amines with benzene and substituted benzene compounds. J. Chem. Thermodyn. **1972**, 4, 159–173.

CHAPTER 3: PROBING CONTAMINANT TRANSPORT TO AND FROM CLAY SURFACES IN ORGANIC SOLVENTS AND WATER USING SOLUTION CALORIMETRY

This chapter has been published as Pourmohammadbagher, A.; Shaw, J. M. Probing contaminant transport to and from clay surfaces in organic solvents and water using solution calorimetry. Environ. Sci. Technol. 2015, 49, 10841–10849.

ABSTRACT: Clays, in tailings, are a significant ongoing environmental concern in the mining and oil sands production industries and clay rehabilitation following contamination poses challenges episodically. Understanding the fundamentals of clays behavior can lead to better environmental impact mitigation strategies. Systematic calorimetric measurements are shown to provide a framework for parsing the synergistic and antagonistic impacts of trace (i.e., ppm level) components on the surface compositions of clays. The enthalpy of solution of as-received and "contaminated" clays, in as-received and "contaminated" organic solvents and water, at 60 °C and atmospheric pressure, provide important illustrative examples. Clay contamination included presaturation of clays with water and organic liquids. Solvent contamination included addition of trace water to organic solvents and trace organic liquids to water. Enthalpy of solution outcomes are interpreted using a quantitative mass and energy balance modeling framework that isolates terms for solvent and trace contaminant sorption/desorption and surface energy effects. Underlying surface energies are shown to dominate the energetics of solvent-clay interaction, and organic liquids as solvents or as trace contaminants are shown to displace water from as-received clay surfaces. This approach can be readily extended to include pH, salts or other effects and is expected to provide mechanistic and quantitative insights underlying the stability of clays in tailings ponds and the behaviors of clays in diverse industrial and natural environments.

Key words: Clays, surface contamination, tailings, calorimetry, thermodynamic model

3.1 INTRODUCTION

Tailings management is a significant environmental concern facing mining industries around the world and it poses challenges for oil sands production in particular.[1] These latter tailings comprise sand, silt, clay, water and soluble organic liquids that are present initially or added during separation processes, and remain in post process streams.[2] The tailings bottom layer, a mixture of clay, water and soluble organic liquids called mature fine tailings (MFT), takes a long time (in some cases up to 30 years) to settle and solidify.[3] This has led to the accumulation of millions of cubic meters of MFT[4] requiring long-term storage in fluid containment structures[3] which present numerous environmental risks that require management and mitigation. Environmental challenges include tailings pond integrity, and management and mitigation of impacts from inorganic and organic contaminants present (petroleum hydrocarbons[4], salts[5], metals[6,7], naphthenic acids[8], etc.) and emission of biogenic greenhouse gases (CH_4 and CO_2)[9]. It is critical to understand the fundamentals of clay behavior in tailings environments so that the need for long-term storage contaminant structures covering hundreds of square kilometers of landscape can be reduced or eliminated. More broadly, clays, such as kaolinite and illite, are known to possess a strong affinity for the adsorption of organic liquids on their surfaces due to their structure, surface acid-base character and cation exchange capacity.[10] Adsorption of organic liquids on clay surfaces alters their hydrophilic/hydrophobic balance through surface composition changes that impact surface wettability, surface energy, and surface charge.[10–15] This clay property poses challenges in diverse industries[11,13,16–20] during normal operation and during site remediation following chemical spills. Kaolinite is a 1:1 layered alumino-silicate with one tetrahedral sheet linked to one octahedral sheet with hydrogen bonds in interlayer space. It is a non-expanding clay and has a low cation exchange capacity (CEC) (1-15 meq/100g). Illite is a

2:1 layered alumino-silicate with an octahedral sheet linked to two tetradedral sheets (TOT). The cation exchange capacity (CEC) of illite is higher than that of kaolinite, typically around 20-30 meq/100g.[21]

Solution calorimetry measures the amount of heat that is exchanged during chemical, physical or biological processes. It is sensitive to particle surface properties and to the variation in surface properties of particles arising from changes in the surrounding medium. This study examines the effect of trace, i.e., ppm level by mass, compounds on the enthalpy of solution of kaolinite and illite clays in toluene, n-heptane, pyridine, and water, that are the main solvents being used in different parts of oil sands production and can be in tailings environments, with a focus on impacts that alter the surface composition of the clays. Clay hydration state is sensitive to the relative humidity of the environment and other external parameters[22,23] and must be controlled in order to avoid measurement artifacts. To eliminate bias as to the state of hydration of both the clays and the organic liquids, which can act as hidden and uncontrolled variables, the behaviors of dry and water-saturated solvents are included in the experimental matrix. An experimental and theoretical interpretative framework for performing and parsing enthalpy of solution measurements, and for determining and validating the signs and magnitudes of the energetics of specific clay surface - liquid interactions is presented. The power of the framework is illustrated by showing that water is displaced from clay surfaces by trace n-heptane and toluene dissolved in the surrounding water.

3.2 EXPERIMENTAL

3.2.1 Materials

HPLC grade toluene (99.9 %, 20 ppm water), n-heptane (99.4 %, 10 ppm water), and pyridine (99.9 %, 200 ppm water) were purchased from Fisher Scientific and used as-received . Clay samples, provided by Prof. Murray Gray at the University of Alberta and described in detail previously,[24] were purchased from Ward's Natural Science (Rochester, NY) and used as-received . Table 3.1 shows the properties of clay samples as stated by the supplier. Clays are well known to possess both hydrophilic and hydrophobic surfaces. However, kaolinite is primarily hydrophobic, and illite is primarily hydrophilic.[25] Pre-saturation of clays with organic liquids, water or water + organic liquids was performed by exposing particles to saturated solvent/water vapor for 24 hours at 60 °C.

Table 3.1 *Kaolinite and illite properties*

Clay	CEC (meq/100g)	Surface area (m^2/g)
Kaolinite	3 ± 1	20 ± 5
Illite	25 ± 2	83 ± 5

3.2.2 Thermogravimetric Analysis (TGA)

Thermogravimetric analysis was performed using a TG-DSC 111 thermoanalyzer (Setaram, France). The crucibles were subject to a 20 mL/min stream of dry nitrogen, and were heated from 20 to 150 °C at 5 °C/min. Baseline measurements were performed using empty crucibles prior to each experiment so that mass loss measurements could be corrected for the temperature dependent impact of buoyancy.

3.2.3 Solution Calorimetry

The solution calorimetry measurements were performed using a precision solution calorimetry module (SolCal) from TA Instruments at 60 °C to simulate this industrial environment.[26] The module was inserted into a TAM III thermostat with a temperature uncertainty of 1 μ°C. The repeatability and reliability of data obtained with this equipment was validated in the second chapter. The measurements in the present work followed the same procedure. For each measurement a 30 mg sample was placed in an ampule that was then sealed and placed in 25 mL of a solvent. This assembly was then placed in a TAM III thermostat at 60 °C. Once the short-term noise of the system dropped below 10 μ°C / 5 min the experiment was started. One calibration was performed prior to breaking the ampule. During the experiment the sample was mixed at 500 rpm using a gold impeller. Following ampule breakage, the heat flow data was recorded for 5 min to capture the energy generated or sorbed. After 5 min another calibration was performed. The amount of energy released or sorbed during the mixing period, on a unit mass of solute basis, was then calculated relative to the two calibrations. Positive enthalpy of

solution values indicate net endothermic behaviors while negative values indicate net exothermic behaviors. Identification of specific phenomena requires careful parsing of detailed measurements, and a value of zero may mean no interaction or a balance of concurrent exothermic and endothermic interactions. All of the data are reported and computations performed on a mass basis because many organic liquids and organic solvents of environmental interest, such as "black oils", comprise complex mixtures that do not have specific molar masses or even well-defined mean molar masses.

3.2.4 Interpretative Framework for Calorimetric and Thermogravimetric Data

The interactions between clays and organic solvents or water are complex and variable. Clays possess an underlying surface energy that can be altered by the presence of trace contaminants on their surfaces. When immersed in a solvent, species initially present on clay surfaces or in the solvent transfer from one to the other as equilibrium is established. Naturally species such as trace contaminants with large chemical potential differences in the two states are most prone to transfer. A cartoon illustrating these processes is presented as Figure 3.1. The interpretive framework for the calorimetric and thermogravimetric data is rooted in a linear energy balance model for enthalpy of solution of clays in solvents comprising organic liquids and water:

$$\Delta h_s = \Delta h_s^0 + \Delta h_{solvent\ sorption/desorption} + \Delta h_{TC\ sorption/desorption} + \Delta h_{surface,TC} \qquad (3.1)$$

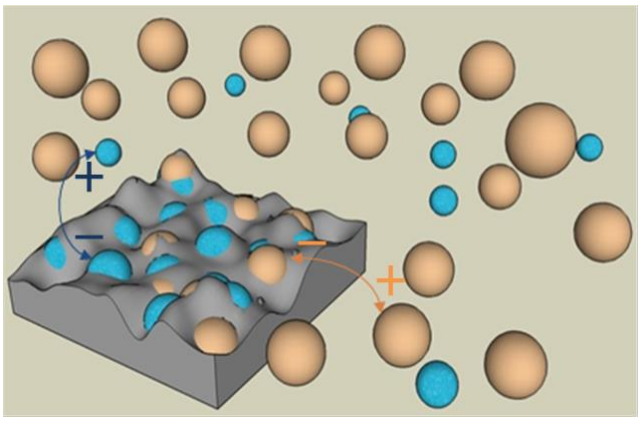

Figure 3.1 *Cartoon showing processes occurring when clays interact with solvents. Clay surface (gray), trace contaminant (blue), solvent (brown). Arrows show directions for processes that sorb (+) or release (-) energy.*

The experiment matrix for calorimetric and thermogravimetric experiments is potentially large as it includes assessment of clay type (kaolinite, illite), contamination of clays (none, water, organic liquid (3), water + organic liquid (3)), contamination of solvents (a minimum of 10 variants). There are 16 combinations for each clay + solvent pair, as illustrated in Figure 3.2a. Since the objective is to isolate impacts of individual terms appearing in the energy balance model (equation 3.1) based on one measurement, with an uncertainty of ± 1 J/g, or by the difference of two measurements, with an uncertainty of ± 2 J/g, only a small subset of the experimental matrix must be performed – six experiments per clay + solvent pair. For example, the two experiments marked only with red dots, Figure 3.2b, permit direct evaluation of Δh_s^0 because there are no trace contaminants present, and there are no solvent sorption/desorption effects. $\Delta h_{solvent\ sorption/desorption}$ values are isolated as a difference between enthalpy of solution measurements marked with red and blue dots and those with only red dots because while solvent sorption occurs, trace contaminants are not present. The combined impacts of

$\Delta h_{TC\ sorption/desorption} + \Delta h_{surface,TC}$ are obtained similarly as a difference measurement between experiments denoted with red and green dots and those denoted with only red dots.

3.3 RESULTS AND DISCUSSION

3.3.1 Thermogravimetric Analysis

These measurements were carried out to determine the amount of water sorbed on as-received and water-saturated clays, and the amount of solvent sorbed on solvent-saturated clays. The mass losses, in mass fraction, arising when the temperature is increased from 20 °C to 150 °C at the rate of 5 °C/min are reported in Table 3.2.

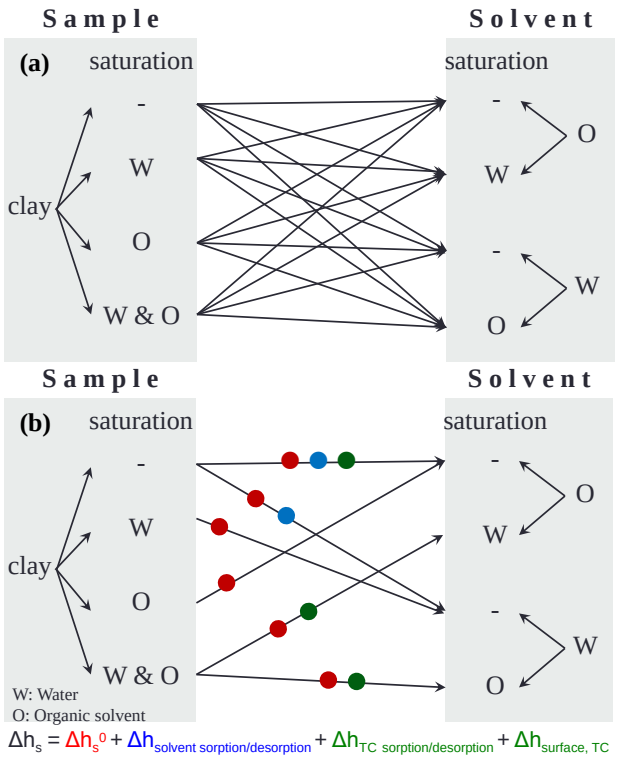

Figure 3.2 *The enthalpy of solution experimental matrix for clay + solvent pairs: (a) full matrix, (b) measurements required to isolate specific contributions. The dots are colour coded to terms in the enthalpy of solution model (inset).*

As-received kaolinite and illite have similar water contents. While the water fraction of illite increases a little following saturation, the water content of the kaolinite increases significantly. Clearly, the as-received kaolinite sorbs more water in absolute terms than as-received illite, and is relatively under saturated. Organic liquid pre-saturation of clays displaces water, as discussed below, and the sorption capacity for both water and organic liquids is comparable.

Table 3.2 *Mass loss (mass fraction) for as-received clays and clays saturated at 60 °C on heating from 20 to 150 °C at 5 °C/min*

Kaolinite	Mass loss (± 0.001)	Illite	Mass loss (± 0.001)
As-received kaolinite	0.005	As-received illite	0.003
Water-saturated kaolinite	0.01	Water-saturated illite	0.005
Toluene-saturated kaolinite	0.009	Toluene-saturated illite	0.005
n-Heptane-saturated kaolinite	0.007	n-Heptane-saturated illite	0.004
Pyridine-saturated kaolinite	0.01	Pyridine-saturated illite	0.005

3.3.2 Enthalpy of Solution of Clays in Organic Solvents

3.3.2.1 Impact of Clay Contamination

Enthalpies of solution of as-received and pre-saturated clays in as-received toluene, n-heptane, and pyridine at 60 °C and atmospheric pressure are shown in Figure 3.3a and b for kaolinite and illite respectively. For the cases surveyed, the range of values is broad, from 0 to more than +20 J/g of solute. The lowest values arise in pyridine and the highest values arise in n-heptane. Hydrogen bonding between pyridine and OH groups on the as-received clay particles appears to contribute a significant exothermic effect that is not observed in the other solvents. The strong endothermic interaction between the clays and n-heptane is orders of magnitude too large to be caused by disaggregation of particles[27]. These results underscore the significant variation in the nature and relative balance of the complex interactions that arise between clays and surrounding media.

A decrease in the enthalpy of solution can be observed by pre-saturation of clays with toluene and n-heptane. This outcome cannot be explained unless water present on the as-received particle surfaces is displaced during pre-saturation with solvent because in the absence of such a secondary effect, with the elimination of solvent sorption, the enthalpy of solution is expected to increase. With reference to equation 3.1, pre-saturation of particles with solvents would appear to eliminate the effect of water desorption and dissolution into the solvents during calorimetric measurements resulting in a net decrease in the enthalpy of solution. This observation was validated by measuring the enthalpy of solution of toluene pre-saturated kaolinite in water-saturated toluene. The enthalpy of solution decreased by 5.5 J/g compared to the case of toluene pre-saturated kaolinite in toluene, showing that water present in the solvent sorbs on clay surfaces. Clearly, differences in the chemical potential of trace and sparingly soluble species, such as water in toluene, drive mass transfer to or from particle surfaces, and must be accounted for explicitly in quantitative enthalpy of solution measurements and models for clays.

Pre-saturation of clays with water also decreases the enthalpy of solution. Since desorption of water from clay surfaces is endothermic, and the dissolution of water in toluene and n-heptane is also endothermic (see Table S2 in Appendix A), the impact of pre-saturation of clays with water cannot be attributed to water desorption from surfaces. Pre-saturation of clays with water also prevents trace water in the solvents from adsorbing and one would anticipate that the enthalpy of solution would therefore increase rather than decrease. Clearly, the surface energies between clay particles and the two organic solvents are reduced by water saturation of particle surfaces. In principle, aggregation can also contribute to the enthalpy of solution.[28] However, from an enthalpy perspective, this effect is negligible ($<<$ 0.1 J/g).[27] As as-received kaolinite sorbs more

water on saturation than illite, Table 3.2, it is under saturated at the outset. Thus water saturation impacts the enthalpy of solution of kaolinite more than illite.

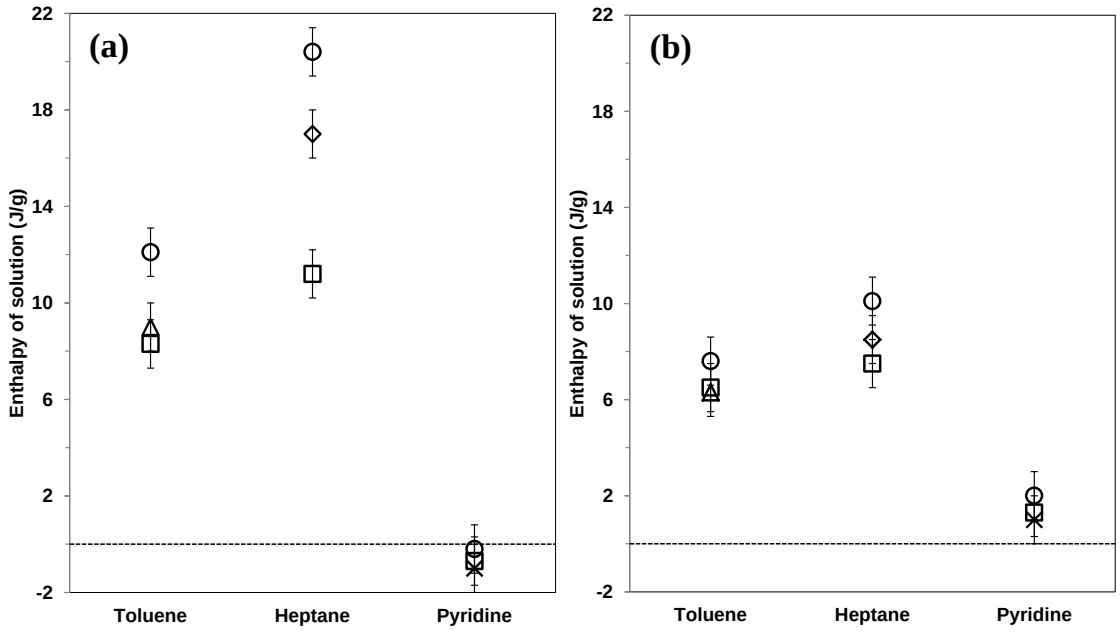

Figure 3.3 *Enthalpy of solution of as-received clays (○), water-saturated clays (□), toluene-saturated clays (△), n-heptane-saturated clays (◇), and pyridine saturated clays (×) for kaolinite (a) and illite (b) at 60 °C and atmospheric pressure.*

3.3.2.2 Impact of Organic Solvent Contamination with Water

The impact of trace water in toluene, n-heptane, and pyridine on the enthalpy of solution of clays was investigated systematically. For toluene and n-heptane, three water concentrations were employed. The as-received water content, water-saturated solvent at 25 °C, and water-saturated solvent at 60 °C. Since water and pyridine are miscible, 910, 2050, 5010 ppm water were

selected for this solvent. The mole fraction of water (1) in toluene and n-heptane at saturation have been estimated within ± 30% using equation 3.2[29] and are reported in ppm:

$$\ln x_1 = d_1 + d_2\left(\frac{1}{T_r} - 1\right) + d_3(1 - T_r)^{\frac{1}{3}} + d_4(1 - T_r) \quad (3.2)$$

where for toluene $d_1 = -0.495$, $d_2 = -3.700$, $d_3 = -0.102$, $d_4 = -4.641$, and $T_r = T/553.0$ and for n-heptane $d_1 = -0.633$, $d_2 = -6.177$, $d_3 = -0.846$, $d_4 = -3.372$, and $T_r = T/524.2$. The accuracy of equation 3.2 is comparable to measurement error. Computed concentrations of water at saturation in toluene (547 ppm and 1525 ppm) and in n-heptane (110 ppm and 450 ppm) at 25 °C and 60 °C respectively are in agreement with available experimental data (543 ppm and 1540 ppm for water in toluene at 25 °C[30] and 60 °C[31], and 91 ppm for water in n-heptane at 25 °C[32]). The enthalpy of solution decreases systematically with trace water addition to these solvents, as shown in Figure 3.4a-c, and is linear within experimental error. The impact is greatest in toluene (Figure 3.4a), followed by n-heptane (Figure 3.4b), and is least for pyridine (Figure 3.4c). Since pyridine has the ability to interact with both Bronsted and Lewis acid sites, acid-base reaction between pyridine and the acid sites on the clay surfaces can explain the difference in behavior of clays in pyridine vis-a-vis toluene and n-heptane. The enthalpy of solution values for kaolinite are more affected by trace water addition than illite. Trace water addition to organic solvents with low water solubilities reduces water desorption from particle surfaces, an endothermic effect, leading to a decrease in the enthalpy of solution relative to as-received particles. The decrease in the enthalpy of solution can also be attributed, in part, to the impact of sorbed water on surface energy as the two impacts are not well parsed in the data sets.

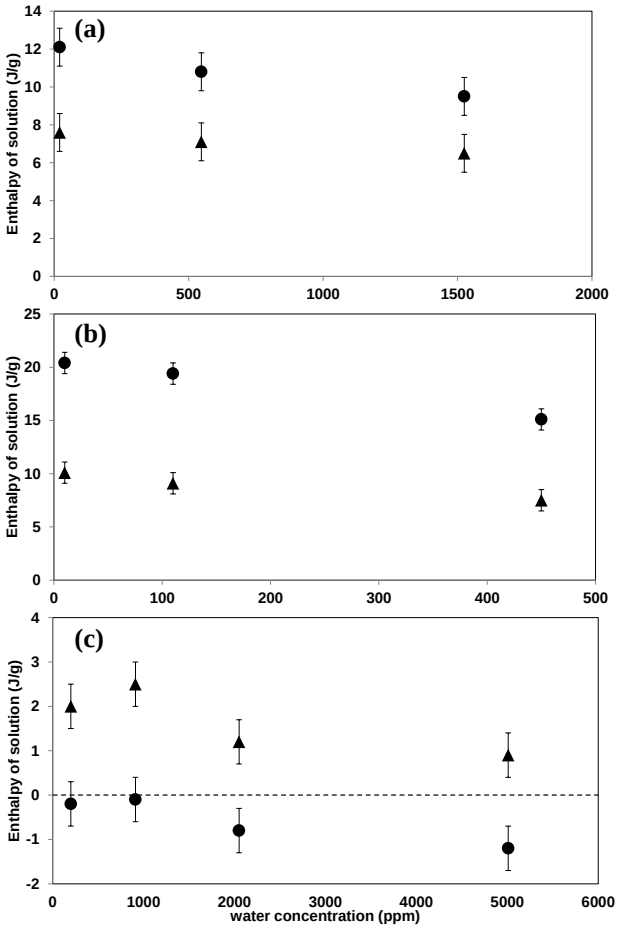

Figure 3.4 *Effect of trace water addition to organic solvents on the enthalpy of solution of as-received kaolinite (●) and as-received illite (▲) in toluene (a), n-heptane (b), and pyridine (c) at 60 °C and atmospheric pressure.*

3.3.3 Enthalpy of Solution of Clays in Water

As Figure 3.3 and 3.4 show, clay surface contamination by pyridine and also pyridine contamination as a solvent does not affect the enthalpy of solution given the experimental uncertainties. This is not the case for toluene and n-heptane. Hence, toluene and n-heptane contamination are the main focus of the following sections. Enthalpies of solution of as-received

and water pre-saturated kaolinite and illite in water, toluene-saturated water, and n-heptane-saturated water at 60 °C and atmospheric pressure are shown in Figure 3.5. This series of experiments parallels the survey with organic solvents. In water, the range of enthalpy of solution values is small. For as-received clays the enthalpies of solution are negative (-4.3 ± 1 J/g and -2.4 ± 1 J/g for kaolinite and illite respectively). By pre-saturating these particles with water, the enthalpy of solution values in water remain negative but increase toward zero, an expected outcome. Pre-saturation of water with toluene (toluene concentration: 740 ppm or Total Organic Carbon (TOC) of 675 ppm)[33] yields positive and similar enthalpies of solution values ~ +1.5 J/g, for all particles. Pre-saturation of water with n-heptane (n-heptane concentration: 3 ppm or Total Organic Carbon (TOC) of 2.5 ppm)[33] also raises the enthalpies of solution of as-received particles - to zero or greater, to a first approximation. Thus a key outcome from this survey is that if trace hydrocarbons are present in water the enthalpy of solution values change sign and an increase in the water TOC can cause an increase in the enthalpy change.

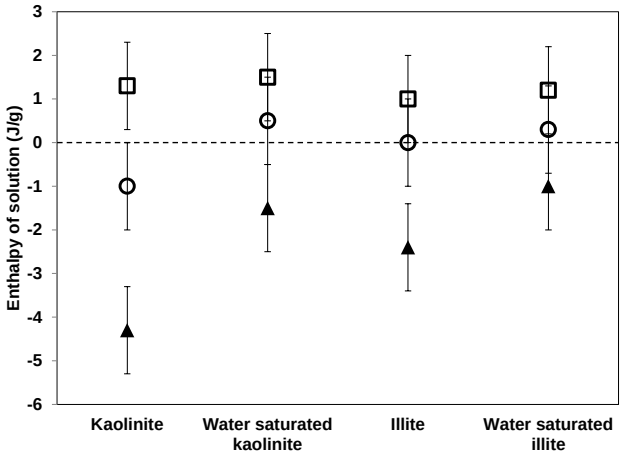

Figure 3.5 *Enthalpy of solution of clays and water-saturated clays in water (◢), toluene-saturated water (TOC: 675 ppm) (□), and n-heptane-saturated water (TOC: 2.5 ppm) (○) at 60 °C and atmospheric pressure.*

3.3.4 Effect of Trace Contamination on the Surface Energy of Clays

Pre-saturation of clays with both organic liquids and water, and pre-saturation of organic solvents with water, and water with organic liquids prevents both sorption and desorption of solvent and trace contaminants during enthalpy of solution measurements. This provides a focus on surface energies introduced by trace contaminants and permits indirect evaluation of this property. Figure 3.6 shows the enthalpy of solution of water + organic liquid-saturated clays in water-saturated organic solvents and organic liquid-saturated water at 60 °C and atmospheric pressure. Enthalpy of solution values for water + organic liquids pre-saturated clays in organic liquid-saturated water are all zero, within experimental uncertainty, while the enthalpy of solution values for these particles in water-saturated organic solvents are all large and positive. These results are parsed below in the context of the enthalpy of solution model, equation 3.1.

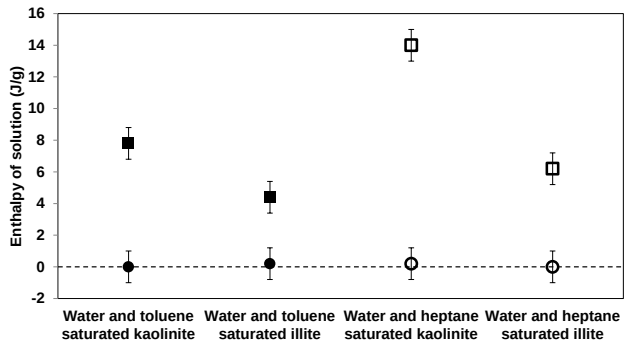

Figure 3.6 *Enthalpy of solution of water and organic liquid-saturated clays in toluene-saturated water (●) n-heptane-saturated water (○), water-saturated toluene (■), and water-saturated n-heptane (□) at 60 °C and atmospheric pressure.*

3.3.5 Enthalpy of Solution Evaluation Framework for Clays

By asserting that enthalpy of solution measurements reflect the establishment of equilibrium, and that the chemical potentials of surface sorbed and dissolved species, including trace species, are proportional to their local compositions, a linear enthalpy balance model for the enthalpy of solution of clays, which combines both TGA and calorimetric measurements and literature data for the solubility of trace contaminants in solvents, can be obtained from equation 3.1. The enthalpy of solvent sorption/desorption on/from the surface of particles is:

$$\Delta h_{solvent\ sorption/desorption} = (x_s^F - x_s^I)\left(-h_{f,s}\right) \tag{3.3}$$

where $(x_s^F - x_s^I)$ is the change in mass fraction of solvent on the surface of particles. The enthalpy of trace contaminant sorption/desorption on the surface is:

$$\Delta h_{TC\ sorption/desorption} = (x_{TC}^F - x_{TC}^I)[-\left(h_{s,TC} + h_{f,TC}\right)] \tag{3.4}$$

where $(x_{TC}^{F} - x_{TC}^{I})$ is the change in mass fraction of trace contaminant on the surface of particles. Also noting that surface contamination at saturation can change the enthalpy of solution by $\Delta h_{surface,TC}^{sat}$, the surface enthalpy change arising from trace contaminant sorption/desorption can be expressed as:

$$\Delta h_{surface,TC} = (x_{TC}^{F} - x_{TC}^{I})[\frac{\Delta h_{surface,TC}^{sat}}{x_{TC}^{sat}}] \quad (3.5)$$

The impact of trace contaminant sorption/desorption then becomes:

$$\Delta h_{TC\,sorption/desorption} + \Delta h_{surface,TC} = (x_{TC}^{F} - x_{TC}^{I})[\frac{\Delta h_{surface,TC}^{sat}}{x_{TC}^{sat}} - (h_{s,TC} + h_{f,TC})] \quad (3.6)$$

and the enthalpy of solution of clay particles in solvents becomes the sum of solvent and trace contaminant contributions:

$$\Delta h_s = \Delta h_s^0 - (x_s^F - x_s^I)(h_{f,s}) + (x_{TC}^{F} - x_{TC}^{I})[\frac{\Delta h_{surface,TC}^{sat}}{x_{TC}^{sat}} - (h_{s,TC} + h_{f,TC})] \quad (3.7)$$

3.3.5.1 Evaluation of Generalizable Parameters

Pre-saturation of particles with a solvent and then measuring the enthalpy of solution in the same solvent eliminates the solvent sorption and trace contaminant desorption terms from the enthalpy of solution, equation 3.7, and the measured enthalpy of solution equals the reference enthalpy:

$$\Delta h_s = \Delta h_s^0 \quad (3.8)$$

Measured Δh_s^0 values are reported in Table 3.3. For clays in water, the Δh_s^0 values agree with one another within experimental uncertainty with the average value of -1 J/g, while Δh_s^0 values in toluene and n-heptane are large, positive and variable. By pre-saturating clays with both water and organic liquids, the measured enthalpies of solution in organic liquid-saturated water or water-saturated organic solvents becomes:

$$\Delta h_s = \Delta h_s^0 + \Delta h_{surface,TC}^{sat} \tag{3.9}$$

As Δh_s and Δh_s^0 are measured, the surface energy changes introduced by contaminants, $\Delta h_{surface,TC}^{sat}$ are obtained by difference. $\Delta h_{surface,TC}^{sat}$ values for water, toluene and n-heptane (reported in Table 3.3) are small and possess an uncertainty of ± 2 J/g. In water, all values are positive and agree within the experimental uncertainty with an average value of 1.5 J/g. For trace water contamination in toluene and n-heptane the values are uniformly negative and agree within the experimental uncertainty with an average value of -2 J/g. Since pyridine and water are miscible, $\Delta h_{surface,TC}^{sat}$ values for trace water in pyridine are negligible and are assumed to be zero.

Table 3.3 *Measured* Δh_s^0 *and* $\Delta h_{surface,TC}^{sat}$ *at 60 °C and atmospheric pressure*

Solvent	Contamination	Asphaltene coated Kaolinite		Asphaltene coated Illite	
		Δh_s^0 ± 1 J/g	$\Delta h_{surface,TC}^{sat}$ ± 2 J/g	Δh_s^0 ± 1 J/g	$\Delta h_{surface,TC}^{sat}$ ± 2 J/g
Toluene	none	7.8		6	
	Water		-1		-2
n-Heptane	none	14		9	
	Water		-2		-2
Water	none	0		-0.5	
	Toluene		1		1
	n-Heptane		1		1

On immersion in a liquid, the mass fraction of solvent plus contaminant on the surface of clays is expected to reach the saturation limit, γ:

$$x_s^F + x_{TC}^F = \gamma \tag{3.10}$$

Given the uncertainty of TGA measurements, Table 3.2, γ is well approximated as a clay dependent constant possessing the values 0.01 and 0.005 for kaolinite and illite respectively. By combining the energy balance (equation 3.7) with the mass balance (equation 3.10) and inputting the parameter values from Table 3.3, the surface coverage by solvents and residual water mass fraction on clays can be inferred. While the uncertainty of the calculated mass fractions reported in Table 3.4 is significant (± 0.1 for the fractional surface coverage by solvents and ± 0.001 for residual water mass fraction), it is clear that organic solvents such as toluene, n-heptane and pyridine displace water from as-received clays on immersion in them, and that the trace organic

contaminants, such as toluene and n-heptane, in water also displace water from clay surfaces. This finding has implications for proposed added organic solvent production processes for heavy oil production[34] where solvent trapping or loss within reservoirs can be expected to be significant in the presence of clays, and for the spreading of liquid organic contaminant plumes in water or soil based natural environments rich in clays[35].

Table 3.4. *Clay surface coverage by solvents and trace contaminants for kaolinite and illite clays following immersion at 60 °C and atmospheric pressure*

Solvent	Contaminant	Kaolinite			Illite		
		$\frac{x_s^F}{x_s^F + x_{TC}^F}$	$x_{H_2O}^F$	α	$\frac{x_s^F}{x_s^F + x_{TC}^F}$	$x_{H_2O}^F$	α
Toluene	–	1	0		0.7	0.002	
	Water*	0.5	0.005	-3	0.4	0.003	-0.9
n-Heptane	–	0.9	0.001		0.9	0.001	
	Water*	0.4	0.006	-11.8	0.3	0.004	-6.7
Pyridine	–	0.7	0.003		0.9	0.003	
	Water**	0.5	0.005	-0.32	0.6	0.002	-0.34
Water	–	1	0.01		1	0.005	
	Toluene*	0	0	-13.5	0	0	-6.8
	n-Heptane*	0.3	0.003	-2692	0.1	0.001	-1731

* at saturation in the solvent.
** at 5010 ppm.

3.3.5.2 Working Equations for the Enthalpy of Solution of Clays

Exploiting the linearity of the relationship between the enthalpy of solution and contaminant composition in a solvent (Figure 3.4) the mass fractions of solvents and contaminants on immersion can be related to the mass fraction of trace contaminant in the solvent (y_{TC}) and equation 3.7 then becomes:

$$\Delta h_s = \Delta h_s^0 - (\gamma + \alpha y_{TC} - x_s^I)\left(h_{f,s}\right) + (-\alpha y_{TC} - x_{TC}^I)[\frac{\Delta h_{surface,TC}^{sat}}{x_{TC}^{sat}} - \left(h_{s,TC} + h_{f,TC}\right)] \quad (3.11)$$

where α is an empirical coefficient, reported in Table 3.4, that is obtained by fitting the enthalpy of solution data for each combination of solvent contaminant and clay. In hydrocarbon liquids, the maximum surface energy change introduced by trace sorbed water on clays is constant, -1 J/g, and the simplest model for the enthalpy of solution of clays in organic solvents + trace water mixtures, that captures the relevant chemistry, is:

$$\Delta h_s = \Delta h_s^0 - (\gamma + \alpha y_{H_2O} - x_O^I)\left(h_{f,O}\right) + (-\alpha y_{H_2O} - x_{H_2O}^I)[\frac{-1\left(\frac{J}{g}\right)}{x_{H_2O}^{sat}} - \left(h_{s,H_2O} + h_{f,H_2O}\right)] \quad (3.12)$$

In water, where Δh_s^0, is -1 J/g and the maximum surface energy of trace sorbed organic liquid is 2 J/g, the simplest model for the enthalpy of solution of clays in water + trace organic contaminants that captures the relevant chemistry is:

$$\Delta h_s = -1\ (\frac{\mathrm{J}}{\mathrm{g}}) - (\gamma + \alpha y_O - x_{H_2O}^I)\left(h_{f,H_2O}\right) + (-\alpha y_O - x_O^I)[\frac{2(\frac{\mathrm{J}}{\mathrm{g}})}{x_O^{sat}} - \left(h_{s,O} + h_{f,O}\right)] \quad (3.13)$$

Equations 3.12 and 3.13, combined with a carefully posed experiment matrix provide a framework for interpreting enthalpy of solution measurements for kaolinite and illite clays at 60 °C that can be extended to include additional effects from the ionic strength or pH of water to inadvertent or intentionally introduced modifications that cause clay behaviors to differ from those arising in the natural or industrial environment from which they were originally obtained.[36,37]

3.4 ENVIRONMENTAL IMPLICATIONS

The surface properties of clays dictate their aggregation and sorption behaviors in industrial and natural environments. Detailed foreknowledge of surface properties permits the identification of potential risks and mitigation strategies. As these properties are linked to details of the surrounding media, probes such as solution calorimetry, that are sensitive to species transfer to and from clay surfaces can provide both quantitative data and mechanistic insights. Key findings of this work are that trace and sparingly soluble organic liquids in water can displace sorbed water from clay particle surfaces and that this process can lead to a change in the sign of the interactions between clay particles in contaminated water from net negative to net positive values. This one outcome impacts the development of predictive models for how oil spills or contaminated water plumes spread in clay rich environments; illustrates how easily surface properties of clays can be altered through handling or treatments intended to “clean” or “purify” samples; and how even the sign of the enthalpy term in the Gibbs Free energy equation can be changed by trace constituents. Clays with positive Gibbs free energies of solution are more

readily aggregated than ones with negative values. Careful experimental design permits reference enthalpies of solution and impacts of solvent and trace contaminant sorption on clays to be isolated. By parsing the roles of individual species and their interactions with other species present, a quantitative modeling framework for clay behaviors can be constructed. Quantitation of the impacts of temperature, water pH and sparingly soluble ionic species in water (both individually and jointly), and of sorbed tar or asphaltene-rich oil components on clay surfaces, are subjects of ongoing interest that are relevant to diverse industrial and natural environments.

ACKNOWLEDGEMENTS

The authors thank Mildred Becerra and Jordon French for their assistance in the laboratory, and Jun Zhao for supplying the clay samples. The authors gratefully acknowledge the sponsors of the NSERC Industrial Research Chair in Petroleum Thermodynamics for funding: Alberta Innovates Energy and Environment Solutions, British Petroleum, ConocoPhillips Inc., Nexen Energy ULC, Shell Canada, Total E & P Canada, VMG Inc., and the Natural Sciences and Engineering Research Council of Canada (NSERC).

NOMENCLATURE

Δh_s - enthalpy of solution (J/g)

Δh_s^0 - reference enthalpy of solution in the absence of sorption or desorption effects (J/g)

$\Delta h_{solvent\ sorption/desorption}$ - enthalpy of sorption/desorption of solvent on/from particles, for both organic liquids and water when they are used as a solvent (J/g)

$\Delta h_{TC\ sorption/desorption}$ - enthalpy of sorption/desorption of trace contaminant on/from particles, for both organic liquids and water when they are used as a contaminant (J/g)

$\Delta h_{surface,TC}$ - enthalpic effect of surface modification due to trace contaminant, for both organic liquids and water when they are used as a contaminant (J/g)

$\Delta h_{surface,TC}^{sat}$ - enthalpic effect of surface modification due to trace contaminant when the particles are saturated with the contaminant, for both organic liquids and water when they are used as a contaminant (J/g)

y_{TC} - composition of trace contaminant in the solvent, for both organic liquids and water when they are used as a contaminant (wt/wt)

y_{H_2O} - composition of water in organic solvent (wt/wt)

y_O - composition of organic liquids in water (wt/wt)

x_s^I and x_s^F - initial and final mass fraction of solvent on the surface of particles respectively, for both organic liquids and water when they are used as a solvent (wt/wt)

x_{TC}^I and x_{TC}^F - initial and final mass fraction of trace contaminant on the surface of particles respectively, for both organic liquids and water when they are used as a contaminant (wt/wt)

$x_{H_2O}^I$ and $x_{H_2O}^F$ - initial and final mass fraction of water on the surface of particles respectively (wt/wt)

x_O^I - initial mass fraction of organic liquids on the surface of particles (wt/wt)

x_{TC}^{sat} - saturation mass fraction of trace contaminant, for both organic liquids and water when they are used as a contaminant

$x_{H_2O}^{sat}$, x_O^{sat}- saturation mass fraction of water and organic liquids at the surface of clay particles (wt/wt)

$h_{s,TC}$ - enthalpy of solution of trace contaminant in the solvent, for both organic liquids and water when they are used as a contaminant (J/g)

h_{s,H_2O} - enthalpy of solution of water in the organic solvent (J/g)

$h_{s,o}$ - enthalpy of solution of organic liquids in the water (J/g)

$h_{f,s}$ - enthalpy of fusion of solvent, for both organic liquids and water when they are used as a solvent (J/g)

$h_{f,TC}$ - enthalpy of fusion of trace contaminant, for both organic liquids and water when they are used as a contaminant (J/g)

h_{f,H_2O}, $h_{f,O}$ - enthalpy of fusion of water and organic liquids (J/g)

α - an empirical coefficient, reported in Table 3.4, that is obtained by fitting the enthalpy of solution data for each combination of solvent contaminant and clay

γ - the saturation limit of the mass fraction of solvent plus contaminant on the surface of clays (wt/wt)

x_1 – mole fraction of water (1) in different solvents at saturation

T – temperature (K)

REFERENCES

(1) Chalaturnyk, R. J.; Don Scott, J.; Özüm, B. Management of oil sands tailings. Pet. Sci. Technol. **2002**, 20 (9-10), 1025–1046.

(2) An, D.; Brown, D.; Chatterjee, I.; Dong, X.; Ramos-Padron, E.; Wilson, S.; Bordenave, S.; Caffrey, S. M.; Gieg, L. M.; Sensen, C. W.; et al. Microbial Community and Potential Functional Gene Diversity Involved in Anaerobic Hydrocarbon Degradation and Methanogenesis in an Oil Sands Tailings Pond. Genome **2013**, 56, 612–618.

(3) Beier, N.; Wilson, W.; Dunmola, A.; Sego, D. Impact of Flocculation-Based Dewatering on the Shear Strength of Oil Sands Fine Tailings. Can. Geotech. J. **2013**, 50, 1001–1007.

(4) Siddique, T.; Fedorak, P. M.; Foght, J. M. Biodegradation of Short-Chain N-Alkanes in Oil Sands Tailings under Methanogenic Conditions. Environ. Sci. Technol. **2006**, 40, 5459–5464.

(5) Sun, D.; Zhou, X.; Luo, W.; Liu, Z.; Shi, Z.; Zhang, X. Study on the Settlement Experiment of Iron Tailings. Appl. Mech. Mater. **2013**, 281, 511–516.

(6) Ostergren, J. D.; Brown, G. E.; Parks, G. A.; Tingle, T. N. Quantitative Speciation of Lead in Selected Mine Tailings from Leadville, CO. Environ. Sci. Technol. **1999**, 33, 1627–1636.

(7) Macur, R. E.; Wheeler, J. T.; Mcdermott, T. R.; Inskeep, W. P. Microbial Populations Associated with the Reduction and Enhanced Mobilization of Arsenic in Mine Tailings. Environ. Sci. Technol. **2001**, 35, 3676–3682.

(8) Scott, A. C.; MacKinnon, M. D.; Fedorak, P. M. Naphthenic Acids in Athabasca Oil Sands Tailings Waters Are Less Biodegradable than Commercial Naphthenic Acids. Environ. Sci. Technol. **2005**, 39, 8388–8394.

(9) Siddique, T.; Penner, T.; Klassen, J.; Nesbø, C.; Foght, J. M. Microbial Communities Involved in Methane Production from Hydrocarbons in Oil Sands Tailings. Environ. Sci. Technol. **2012**, 46, 9802–9810.

(10) Lebedeva, E. V.; Fogden, A. Wettability Alteration of Kaolinite Exposed to Crude Oil in Salt Solutions. Colloids Surfaces A Physicochem. Eng. Asp. **2011**, 377, 115–122.

(11) Dudášová, D.; Simon, S.; Hemmingsen, P. V.; Sjöblom, J. Study of Asphaltenes Adsorption onto Different Minerals and Clays Part 1. Experimental Adsorption with UV Depletion Detection. Colloids Surfaces A Physicochem. Eng. Asp. **2008**, 317, 1–9.

(12) Lebedeva, E. V.; Fogden, A. Nano-Scale Structure of Crude Oil Deposits on Water-Wet Substrates: Dependence on Aqueous Phase and Organic Solvents. Colloids Surfaces A Physicochem. Eng. Asp. **2011**, 380, 280–291.

(13) Kumar, M.; Fogden, A. Patterned Wettability of Oil and Water in Porous Media. Langmuir **2010**, 26, 4036–4047.

(14) Lebedeva, E. V.; Fogden, A. Adhesion of Oil to Kaolinite in Water. Environ. Sci. Technol. **2010**, 44, 9470–9475.

(15) Jada, A.; Debih, H. Hydrophobation of Clay Particles by Asphaltenes Adsorption. Compos. Interfaces **2009**, 16, 219–235.

(16) Zornoza, R.; Faz, Á.; Carmona, D. M.; Acosta, J. A.; Martínez-Martínez, S.; De Vreng, A. Carbon Mineralization, Microbial Activity and Metal Dynamics in Tailing Ponds Amended with Pig Slurry and Marble Waste. Chemosphere **2013**, 90, 2606–2613.

(17) Wang, B.; Zhang, H.; Fan, Z.; Ju, Y. Compacted Sewage Sludge as a Barrier for Tailing Impoundment. Environ. Earth Sci. **2010**, 61, 931–937.

(18) Hur, M.; Kim, Y.; Song, H. R.; Kim, J. M.; Choi, Y. I.; Yi, H. Effect of Genetically Modified Poplars on Soil Microbial Communities during the Phytoremediation of Waste Mine Tailings. Appl. Environ. Microbiol. **2011**, 77, 7611–7619.

(19) Robert, T.; Mercer, S. M.; Clark, T. J.; Mariampillai, B. E.; Champagne, P.; Cunningham, M. F.; Jessop, P. G. Nitrogen-Containing Polymers as Potent Ionogens for Aqueous Solutions of Switchable Ionic Strength: Application to Separation of Organic Liquids and Clay Particles from Water. Green Chem. **2012**, 14, 3053–3062.

(20) Bantignies, J.; Moulin, C. C. D.; Dexpert, H. Wettability Contrasts in Kaolinite and Illite Clays: Characterization by Infrared and X-Ray Absorption Spectroscopies. Clays Clay Miner. **1997**, 45, 184–193.

(21) Donahue, R. L.; Miller, R. W. Soils: An Introduction to Soils and Plant Growth; 4th ed.; Prentice-Hall: Englewood Cliffs, NJ, **1977**.

(22) Gailhanou, H.; Blanc, P.; Rogez, J.; Mikaelian, G.; Kawaji, H.; Olives, J.; Amouric, M.; Denoyel, R.; Bourrelly, S.; Montouillout, V.; et al. Thermodynamic Properties of Illite, Smectite and Beidellite by Calorimetric Methods: Enthalpies of Formation, Heat Capacities, Entropies and Gibbs Free Energies of Formation. Geochim. Cosmochim. Acta

2012, 89, 279–301.

(23) Xu, W.; Johnston, C. T.; Parker, P.; Agnew, S. F. Infrared Study of Water Sorption on Na-, Li-, Ca-, and Mg-Exchanged (SWy-1 and SAz-1) Montmorillonite. Clays Clay Miner. **2000**, 48, 120–131.

(24) Wang, S.; Liu, Q.; Tan, X.; Xu, C.; Gray, M. R. Study of Asphaltene Adsorption on Kaolinite by X-Ray Photoelectron Spectroscopy and Time-of-Flight Secondary Ion Mass Spectroscopy. Energy & Fuels **2013**, 27, 2465–2473.

(25) Šolc, R.; Gerzabek, M. H.; Lischka, H.; Tunega, D. Wettability of Kaolinite (001) Surfaces - Molecular Dynamic Study. Geoderma **2011**, 169, 47–54.

(26) Penner, T. J.; Foght, J. M. Mature Fine Tailings from Oil Sands Processing Harbour Diverse Methanogenic Communities. Can. J. Microbiol. **2010**, 56, 459–470.

(27) Nikooyeh, K.; Shaw, J. M. On Enthalpies of Solution of Athabasca Pentane Asphaltenes and Asphaltene Fractions. Energy & Fuels **2013**, 27, 66–74.

(28) Andersen, S. I.; Manuel del Rio, J.; Khvostitchenko, D.; Shakir, S.; Lira-galeana, C. Interaction and Solubilization of Water by Petroleum Asphaltenes in Organic Solution. Langmuir **2001**, 17, 307–313.

(29) Maczynski, A.; Shaw, D. G. IUPAC-NIST Solubility Data Series. 81. Hydrocarbons with Water and Seawater-Revised and Updated. Part 5. C7 Hydrocarbons with Water and Heavy Water. J. Phys. Chem. **2005**, 34, 1399–1487.

(30) Glasoe, P. K.; Schults, S. D. Solubility of H2O and D20 in Carbon Tetrachloride , Toluene,

and Cyclohexane at Various Temperatures. J. Chem. Eng. Data **1972**, 17, 66–68.

(31) Stephenson, R. M. Mutual Solubilities: Water-Ketones, Water-Ethers, and Water-Gasolinie-Alcohols. J. Chem. Eng. Data **1992**, 37, 80–95.

(32) Schatzberg, P. Solubilities of Water in Several Normal Alkanes from C7 to C16. J. Phys. Chem. **1963**, 67, 776–779.

(33) Yaws, C. L. Yaws' Handbook of Properties for Aqueous Systems; Knovel: Norwich, NY, **2012**.

(34) Speight, J. G. Enhanced Recovery Methods for Heavy Oil and Tar Sands; Gulf Publishing Company: Houston, TX, **2009**; Vol. 25.

(35) Hooshiar, A.; Uhlik, P.; Liu, Q.; Etsell, T. H.; Ivey, D. G. Clay Minerals in Nonaqueous Extraction of Bitumen from Alberta Oil Sands: Part 1. Nonaqueous Extraction Procedure. Fuel Process. Technol. **2012**, 94, 80–85.

(36) Johnston, C. T. Probing the Nanoscale Architecture of Clay Minerals. Clay Miner. **2010**, 45, 245–279.

(37) Kaminsky, H.; Etsell, T.; Ivey, D. G.; Omotoso, O. Fundamental Particle Size of Clay Minerals in Athabasca Oil Sands Tailings. Clay Sci. **2006**, 12, 217–222.

CHAPTER 4: PROBING THE IMPACT OF ASPHALTENE CONTAMINATION ON KAOLINITE AND ILLITE CLAY BEHAVIORS IN WATER AND ORGANIC SOLVENTS: A CALORIMETRIC STUDY

This chapter has been submitted to Energy & Fuels as Pourmohammadbagher, A.; Shaw, J. M. Probing the impact of asphaltene contamination on kaolinite and illite clay behaviors in water and organic solvents: A calorimetric study.

ABSTRACT: Detailed understanding of the impacts of trace compounds and asphaltene adsorption on the behavior of clays contributes to the development of production processes for heavy oils and bitumen with lower environmental impacts, to the treatment of tailings from mined bitumen, and to the mitigation of impacts from oil spills in natural environments. Probes, such as solution calorimetry are sensitive to species transfer to and from clay surfaces, and outcomes can be interpreted unambiguously, when supplemented with TGA and SEM measurements. In this study, the effects of asphaltene coating on the enthalpy of solution of kaolinite and illite clays in toluene, n-heptane, and deionized water were investigated at 60 °C and atmospheric pressure. Asphaltene coating increases organic compound sorption but does not impact water sorption vis-a-vis uncoated clay particles or water displacement from clay particles by organic liquids as solvents or as trace contaminants in water. Experimental outcomes are interpreted using a quantitative mass and energy balance model framework that isolates terms for solvent and trace contaminant sorption/desorption and surface energy effects. Mechanistic and quantitative insights underlying the stability of asphaltene coated clay dispersions in tailings ponds, and the behaviors of these clays in diverse industrial and natural environments are discussed.

Key words: Clays, kaolinite, illite, asphaltenes, tailings, organic contamination, calorimetry

4.1 INTRODUCTION

Dispersions of oil and asphaltene coated clays arise following terrestrial oil spills, during natural erosion of oil sands deposits as rivers and streams course through them; and during the production of oil sands deposits in the Athabasca region of Canada[1], where mined oil sands ore is treated with hot water and solvent. In the industrial process, coarse solids are gravity separated and bitumen attaches to air bubbles in a flotation step to produce a bitumen rich froth. This froth is further processed to remove water and remaining solids prior to upgrading. The mineral matter rich tailings is transported to tailings ponds where the aqueous slurry comprising sand particles, clays, residual organic liquids, and residual bitumen sediment. Water is recovered and reused in the bitumen extraction process. Larger sand particles in the tailings segregate quickly to form stable deposits. Fine solids, primarily phyllosilicate clays, most commonly kaolinite and illite,[2,3] form a distinctive middle layer known as Mature Fine Tailings (MFT).[4] This material takes years to settle and solidify.[5] MFT pose significant technical and environmental problems linked to tailings toxicity and loss of process water.[9] Reclamation of disturbed contaminated clays in natural environments poses parallel toxicity and mitigation challenges.[10–13] Tailings management is one of the most difficult environmental challenges faced by the oil sands mining sector.[6–8]

The surface properties of clays dictate their aggregation and sorption behaviors in industrial and natural environments. Detailed foreknowledge of surface properties permits the identification of potential risks and mitigation strategies. Clays, such as kaolinite and illite, possess a strong affinity for the adsorption of organic material on their surfaces due to their structure and cation exchange capacity.[14] Adsorption of petroleum compounds on clay surfaces alters their wettability, producing biwettable characteristics[15,16] and causes particles to exhibit some degree of hydrophobicity[17] through surface composition changes, that impact over all surface

wettability, surface energy, and surface charge.[6,7,14,18–20] These clay properties pose containment and reclamation challenges.[6,18,21] Understanding the effect of oil contamination on clay properties is crucial for the development of technologies that, for example, improve the rate of clay settling and compaction.

Asphaltenes, a poorly-defined low-volatility crude oil fraction, are separable from crude oils on the basis of various ASTM and other standard procedures. They comprise polynuclear aromatic compounds; sulphur, nitrogen and oxygen substituted organic compounds; and trace amounts of organo-metallic compounds containing nickel and vanadium, that enable asphaltenes to interact strongly with one another[19,22,23] and with clay minerals.[14,24 25,26] Details of the asphaltene adsorption process including monolayer and multilayer adsorption and the field variables that impact the adsorption process are addressed elsewhere.[27]

In chapter 3 we provided an experimental and theoretical framework for interpreting enthalpy of solution measurements for kaolinite and illite clays. It was shown that organic liquids (toluene and heptane), even trace quantities in water, displace water from clays surfaces. The current study examines the solution behaviors of asphaltene coated kaolinite and illite clays in organic liquids (toluene and n-heptane, as-received and contaminated with trace amount of water) and deionized water (as-received and contaminated with trace amount of toluene and n-heptane). Hydrocarbon contaminants of clays include ill-defined components such as asphaltenes, resins, aromatics, and saturates. These additional constituents add additional complexity to the behaviors of clays and merit attention. In this work, asphaltene sorption is addressed. Asphaltenes are the least volatile constituent of hydrocarbon resources, and hence the most persistent one in natural and disturbed environments. Other types of contaminants may comprise subjects of future studies. Deionized water was also used instead of industrial waste-water to

reduce the number of unknown or uncontrolled variables. Water chemistry, as well, merits separate consideration. The outcomes of this study will contribute to the understanding of the impact that pre-contamination of clays has on their behaviors in industrial and in natural environments.

4.2 EXPERIMENTAL

4.2.1 Materials

HPLC grade toluene (99.9 %, 20 ppm water) and n-heptane (99.4 %, 10 ppm water) were purchased from Fisher Scientific and used as-received . Copper (II) sulfate pentahydrate (99.99 %) was purchased from Sigma-Aldrich and used as-received . Clays, asphaltene coated clays, and asphaltene samples were provided by Prof. Murray Gray at the University of Alberta. Clay samples, described in detail elsewhere,[22] were purchased from Ward's Natural Science (Rochester, NY) and used as-received. Asphaltene preparation and asphaltene coating procedures were described previously.[22] In brief, the Athabasca asphaltenes were derived from the bottoms stream of a deasphalting unit processing bitumen from a steam-assisted gravity drainage (SAGD) operation. The asphaltenes were prepared by: (1) mixing the bitumen sample with n-heptane, (2) filtering the mixture through a 0.22 μm Millipore filter to recover the retentate, (3) mixing the retentate with toluene and filtering for a second time, (4) drying the permeate from step 3 in vacuum oven at 80 °C for 12 hours. Asphaltene adsorption on the clays was conducted at 25 °C with solutions of asphaltene in toluene at a concentration of 5 g/L and a fixed ratio of clays mass/solvent volume, i.e., 40 mg/mL solution. The asphaltene coated clays were filtered through 0.22 μm Millipore filters and rinsed with toluene until the filtrate was colorless. The separated asphaltene coated particles were then placed in a vacuum oven at 80 °C overnight and stored in

sealed containers at room temperature. The thickness of asphaltene coating was estimated to be 11 nm based on XPS depth profile measurements.[22]

4.2.2 FTIR Spectroscopy

Diffuse Reflectance Infrared Fourier Transform (DRIFT) spectra of samples in the mid-infrared region (4000 – 700 cm^{-1}) were collected using a Thermo Nicolet NEXUS 670 FT-IR. A 1.5 mg sample was gently stirred with 300 mg of KBr for 2 min prior to spectrum acquisition using an Avatar Diffuse Reflectance Smart Accessory. A pure KBr background was collected and subtracted from all sample spectra prior to statistical analysis. A total of 256 scans at 4 cm^{-1} resolution were combined to produce each spectrum. All spectra were analyzed using OPUS 6.5 software (Bruker Optics Inc.).

4.2.3 Scanning Electron Microscopy

The structure and surface texture of clays were determined using a Philips 525 M scanning electron microscope (SEM). The samples were sprinkled onto carbon tape with a spatula and pressed lightly to seat. The sample holders were then turned upside down, tapped to remove loose material, and then held in a vacuum at room temperature for 6 hours prior to analysis.

4.2.4 Thermogravimetric Analysis (TGA)

Thermogravimetric analysis (TGA) was performed using a TG-DSC 111 thermoanalyzer (Setaram, France). 30 to 60 mg samples were placed in open crucibles and heated from 20 °C to 150 °C at 5 °C/min in a 20 mL/min stream of dry nitrogen. Baseline measurements with an

empty crucible were used to correct mass loss measurements for the effect of buoyancy with temperature. The accuracy of TGA mass loss (mass fraction) measurements is ± 0.001 based on Copper (II) sulfate pentahydrate dehydration as a reference.

4.2.5 Solution Calorimetry

Solution calorimetry measurements were performed using a precision solution calorimetry module (SolCal) from TA Instruments at 60 °C to simulate the industrial environment.[22] In brief, a sealed ampule containing 30 mg of the sample is placed in 25 mL of a solvent and the whole system is kept in a TAM III thermostat at 60 °C until equilibrium is reached. During the experiment the sample is mixed at 500 rpm using a gold impeller. Two calibrations were performed before and after the ampule breakage. By adjusting the breakage time using the calorimeter software, measurement accuracy was improved from ± 1 J/g to ± 0.5 J/g in the present work. Positive enthalpy of solution values indicate net endothermic behaviors while negative values indicate net exothermic behaviors and a value of zero may mean no interaction or a balance of concurrent exothermic and endothermic interactions. All of the data are reported on a mass basis because many organic fluids of environmental interest, such as “asphaltenes”, comprise complex mixtures that do not possess well-defined mean molar masses.

4.2.6 Interpretative Framework for Calorimetric and Thermogravimetric Data

The framework developed for clays + organic solvents/water (Equation 4.1) was adopted for the present study, assuming that asphaltene desorption from clay surfaces does not occur. This assumption was validated by direct observation in this work, asphaltene coated clays did not discolor water and slightly discolored organic solvents, and is consistent with prior observations

by others.[28] Enthalpies of solution Δh_s comprise contributions from the underlying surface energy Δh_s^0 of the asphaltene coated clay particles, that can be altered by the presence of additional trace contaminants on their surfaces, $\Delta h_{surface,TC}$. When immersed in a solvent, other than sorption/desorption of the solvent onto/from asphaltene coated clay surfaces, $\Delta h_{solvent\ sorption/desorption}$, the additional trace species present on asphaltene coated clay surfaces or in the solvent transfer from one to the other as equilibrium is established, $\Delta h_{TC\ sorption/desorption}$.

$$\Delta h_s = \Delta h_s^0 + \Delta h_{solvent\ sorption/desorption} + \Delta h_{TC\ sorption/desorption} + \Delta h_{surface,TC} \quad (4.1)$$

The evaluation of impacts of individual terms appearing in the solution enthalpy model, equation 4.1, are based on one solution enthalpy measurement, with an uncertainty of ± 0.5 J/g, or on the difference between two measurements, with an uncertainty of ± 1 J/g. The experimental matrix is shown in Figure 4.1. Experiments marked with red dots, permit direct evaluation of Δh_s^0 because there are no solvent sorption/desorption effects. $\Delta h_{solvent\ sorption/desorption}$ values are isolated as a difference between enthalpy of solution measurements marked with red and blue dots and those with red dots. The combined impacts of $\Delta h_{TC\ sorption/desorption} + \Delta h_{surface,TC}$ are obtained similarly as a difference measurement between experiments denoted with red and green dots and those denoted with only red dots.

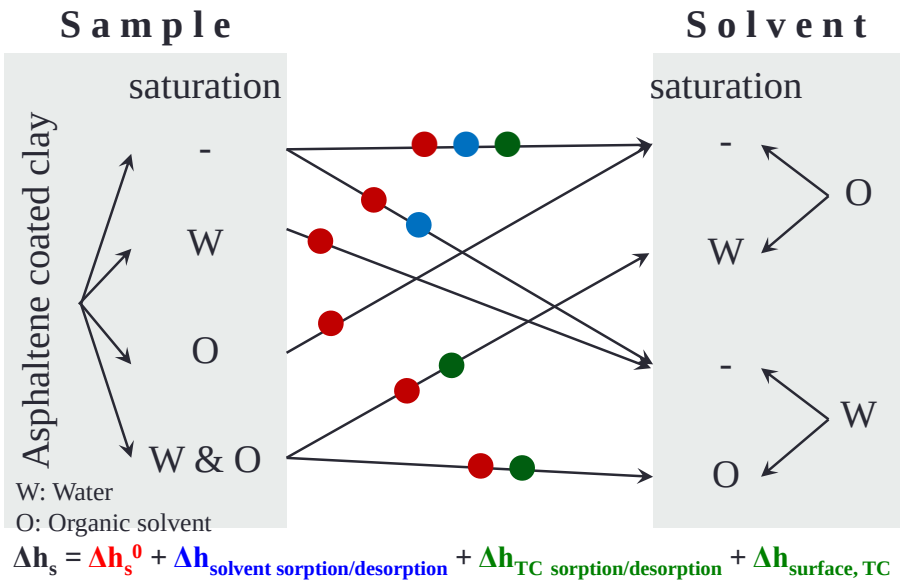

Figure 4.1. *The enthalpy of solution experimental matrix for asphaltene coated clay + solvent pairs required to isolate specific contributions to the enthalpy of solution. The dots are color coded to terms in the enthalpy of solution model (inset) that comprise each measurement.*

Equation 4.1 can be expanded to a linear enthalpy of solution model (equation 4.2), which combines both TGA and calorimetric measurements and literature data for the solubility of trace contaminants in solvents. The development of equation 4.2 is described in chapter 3 in detail and is presented here without proof. The enthalpy of solution comprises contributions from reference enthalpy of solution (Δh_s^0), initial mass fraction of solvent (x_s^I) and trace contaminant (x_{TC}^I), saturation mass fraction of trace contaminant on the surface of clays (x_{TC}^{sat}), composition of trace contaminant in the solvent (y_{TC}), saturation limit of the mass fraction of solvent plus trace contaminant on the surface of clays (γ), enthalpic effect of surface modification due to trace contaminant when the particles are saturated with the contaminant ($\Delta h_{surface,TC}^{sat}$), an empirical coefficient that is obtained by fitting the enthalpy of solution data for each combination of solvent, contaminant, and clay (α), enthalpy of fusion of solvent ($h_{f,s}$), and enthalpy of fusion and solution of trace contaminant ($h_{f,TC}$, $h_{s,TC}$).

$$\Delta h_s = \Delta h_s^0 - (\gamma + \alpha y_{TC} - x_s^I)\left(h_{f,s}\right) + (-\alpha y_{TC} - x_{TC}^I)[\frac{\Delta h_{surface,TC}^{sat}}{x_{TC}^{sat}} - \left(h_{s,TC} + h_{f,TC}\right)] \quad (4.2)$$

Equation 4.2 provides a general framework from which simpler working equations can be identified. The simplest models for the enthalpy of solution of kaolinite and illite clays that capture the relevant chemistry in organic solvents, equation 4.3, and in water, equation 4.4, were also reported in chapter 3 and are reproduced here:

$$\Delta h_s = \Delta h_s^0 - (\gamma + \alpha y_{H_2O} - x_O^I)\left(h_{f,O}\right) + (-\alpha y_{H_2O} - x_{H_2O}^I)[\frac{-1\left(\frac{J}{g}\right)}{x_{H_2O}^{sat}} - \left(h_{s,H_2O} + h_{f,H_2O}\right)] \quad (4.3)$$

$$\Delta h_s = -1\ (\frac{\mathrm{J}}{\mathrm{g}}) - (\gamma + \alpha y_O - x_{H_2O}^I)\left(h_{f,H_2O}\right) + (-\alpha y_O - x_O^I)[\frac{2(\frac{\mathrm{J}}{\mathrm{g}})}{x_O^{sat}} - \left(h_{s,O} + h_{f,O}\right)] \quad (4.4)$$

If asphaltenes do not desorb from clay surfaces, the general form of the enthalpy of solution model for asphaltene coated clays is identical to one derived previously for uncoated clays (equation 4.2). Thus, this study evaluates the generalizability of equation 4.2 and tests the application of the working equations (equations 4.3 and 4.4) for asphaltene coated clays, using the carefully posed experimental matrix, provided in Figure 4.1.

4.3 RESULTS AND DISCUSSION

4.3.1 Detection of Asphaltenes on Clay Surfaces

The FT-IR DRIFT spectra of asphaltenes, and as-received and asphaltene coated kaolinite and illite clays are shown in Figures 4.2a, b, and c, respectively. In the FT-IR spectrum of asphaltenes (Figure 4.2a) peaks at 1375, 1455, 2854, and 2925 cm^{-1} are attributed to aliphatic group vibration bands, peaks at 1704 and 1598 cm^{-1} are attributed to carboxylic groups, and aromatic groups are assigned to the peak at 3055cm^{-1}.[29,30] The spectra of clays (Figures 4.2b and 2c) show Si-O vibration of the tetrahedral layers at 1000 cm^{-1}. For the kaolinite clay (Figure 4.2b) three different OH bands were detected. The inner OH groups located within the layers (3622 cm^{-1}) of the clay structure, the inner surface OH groups located on the surface of octahedral sheets between the layers (3655 and 3670 cm^{-1}), and combinations of inner surface OH groups and outer surface hydroxyl groups (3700 cm^{-1}).[31] For the illite clay (Figure 4.2c) the inner OH groups of the octahedral sheet are detected as a broad peak at 3630 cm^{-1}.[32] By comparing the spectra for as-received and asphaltene coated kaolinite and illite clays, Figures 4.2b and 4.2c, it is clear that the structure of the clays is not impacted by asphaltene adsorption. Further, the low intensity bands at 2854 and 2925 cm^{-1} indicate the presence of asphaltenes on clay surfaces.

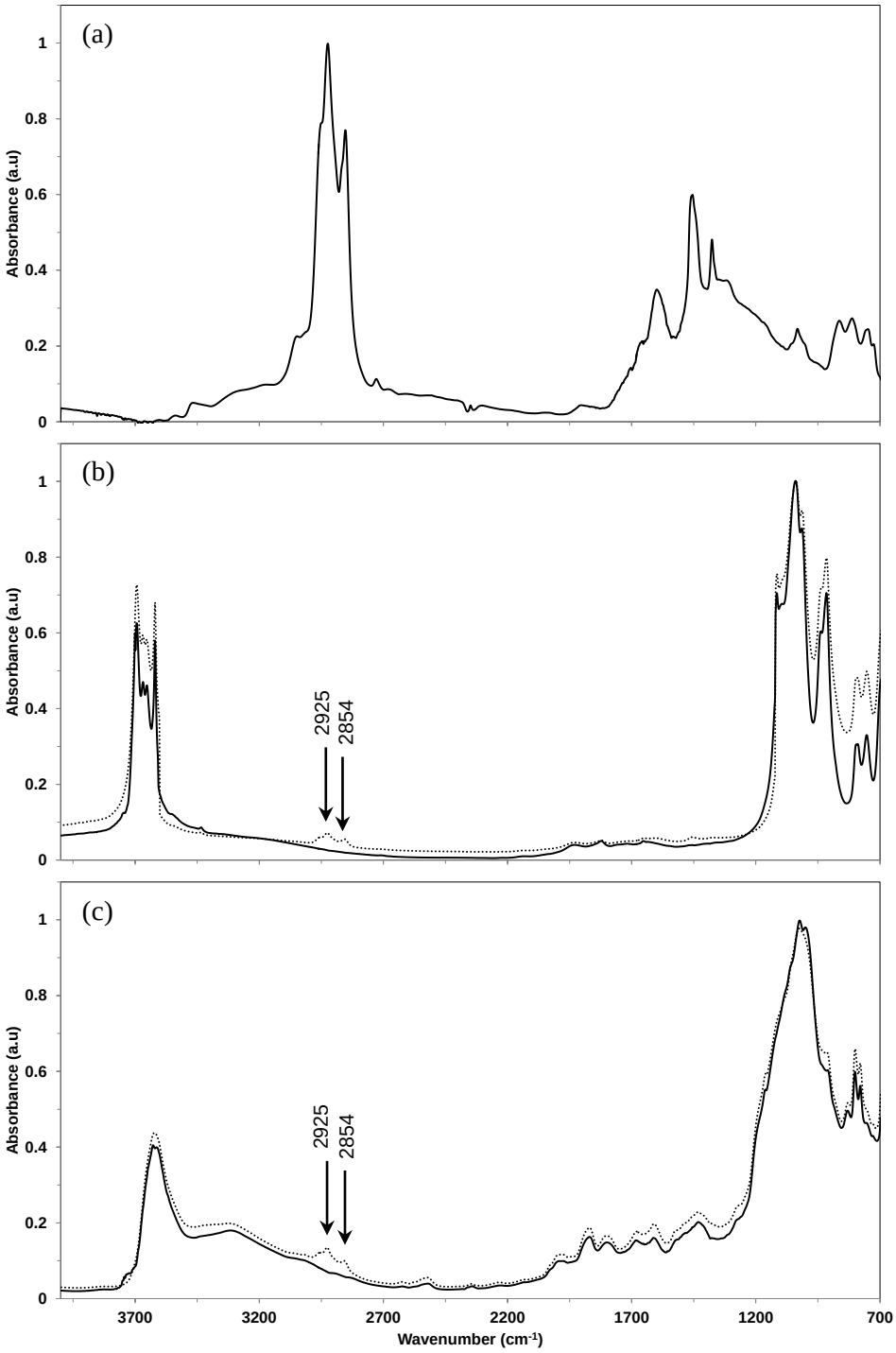

Figure 4.2. *FT-IR DRIFT spectra for: (a) asphaltenes, (b) kaolinite (—) and asphaltene coated kaolinite (...), and (c) illite (—) and asphaltene coated illite (...)*

4.3.2 Observation of As-received and Asphaltene Coated Clay Particles

SEM micrographs of as-received and asphaltene coated kaolinite and illite particles are presented in Figure 4.3. The scale of all four micrographs is the same. The as-received kaolinite particles (Figure 4.3a) are larger than the as-received illite particles (Figure 4.3c), and the asphaltene coated kaolinite (Figure 4.3b) and illite (Figure 4.3d) particles are larger than the corresponding as-received clays. The significant increase in particle size is attributed to particle agglomeration caused by the asphaltene coating.[28] At higher magnification, the coated kaolinite particles, Figure 4.4a, and illite, Figure 4.4b, are clearly agglomerated. The surface texture of the kaolinite, Figure 4.4a, resembles the texture of the asphaltenes, Figure 4.4c, while the illite particle texture, Figure 4.4b, does not, suggesting that there may be more asphaltenes on the coated kaolinite sample than on the coated illite sample, even though this is not evident in the FTIR results reported in Figure 4.2. The validity of this qualitative observation is investigated further using calorimetric measurements in the next section.

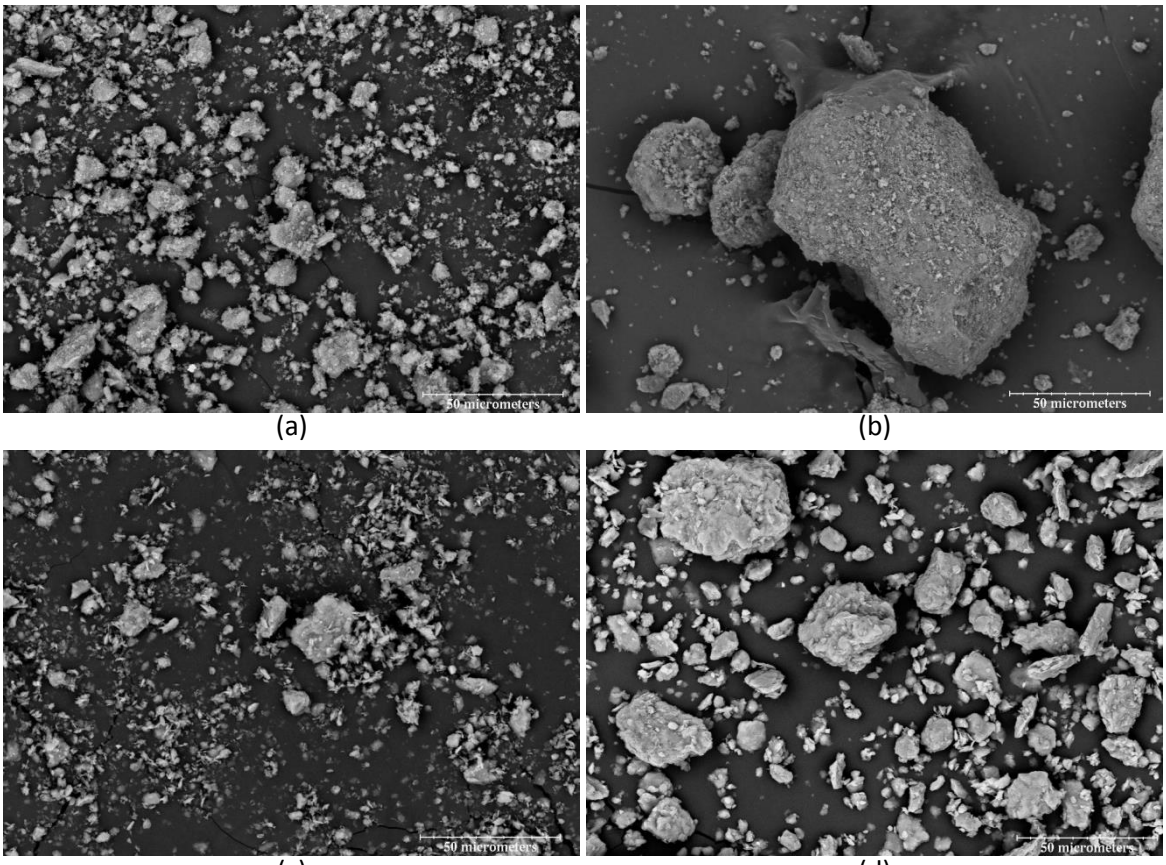

(a) (b)

(c) (d)

Figure 4.3. *Scanning electron microscopy images of: (a) kaolinite, (b) asphaltene coated kaolinite, (c) illite, and (d) asphaltene coated illite.*

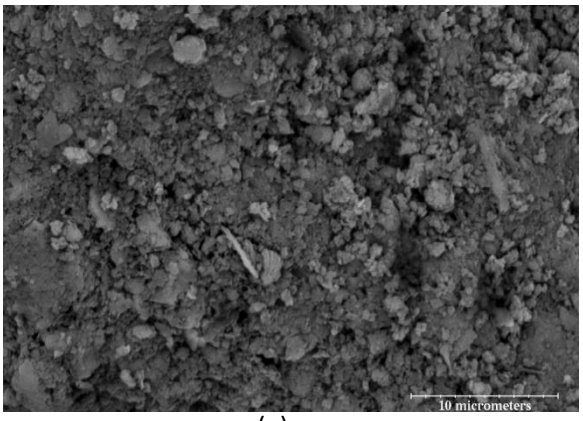

(a)

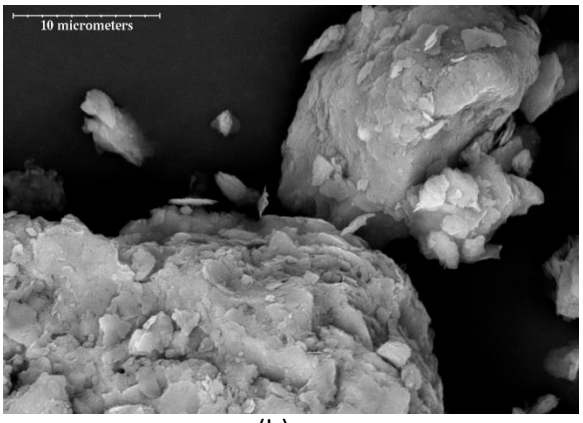

(b)

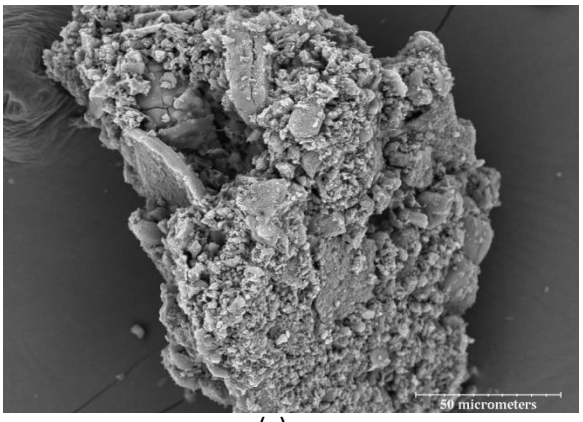

(c)

Figure 4.4. *Scanning electron microscopy images of the surface texture of: (a) asphaltene coated kaolinite, (b) asphaltene coated illite, and (c) asphaltenes.*

4.3.3 Calorimetric Evaluation of the Asphaltene Coating Procedure

Asphaltene coated clay particles were prepared by exposing as-received clay particles to 5 g/L asphaltene + toluene mixtures. The enthalpy of solution for clay particles as a function of asphaltene composition, Figure 4.5, plateaus at less than 0.5 g/L asphaltene for both kaolinite and illite indicating that the surfaces are saturated with asphaltenes. Wang et al.[22] made a similar observation at ~ 0.2 g/L asphaltenes at room temperature. Clearly, both clays are saturated with asphaltenes under the condition of their preparation, and as the exothermic effect is greater for kaolinite (~ -3 J/g) than for illite (~ -1 J/g), more asphaltene sorbs on kaolinite than illite at saturation.

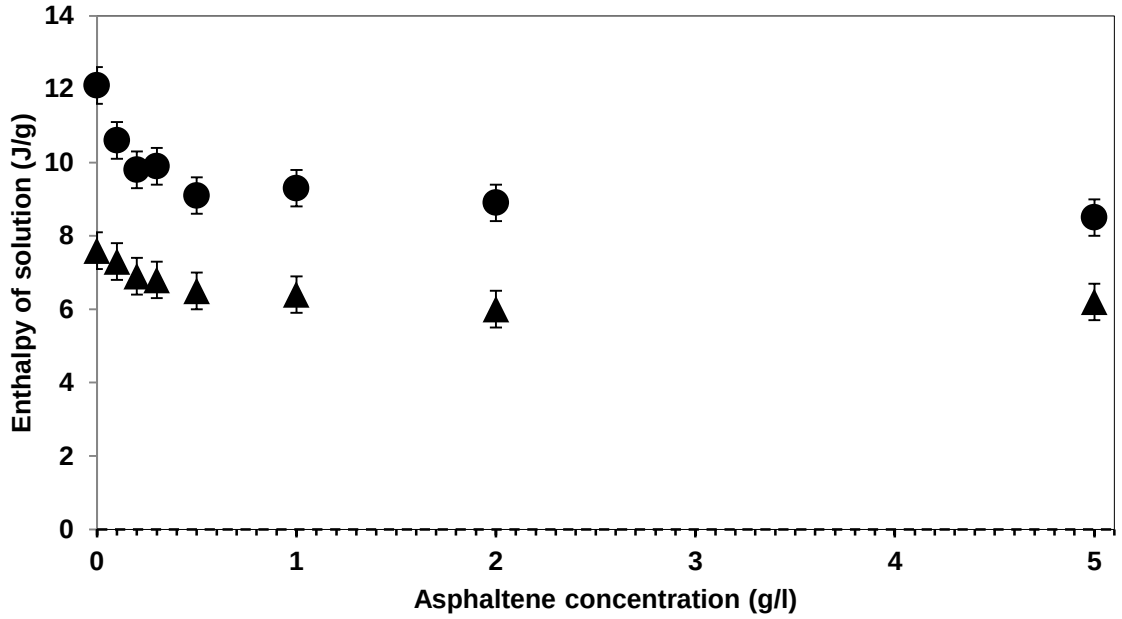

Figure 4.5. *Effect of asphaltene solution concentration on the enthalpy of solution of kaolinite (●) and illite (▲) at 60 °C and atmospheric pressure*

4.3.4 Thermogravimetric Analysis (TGA)

To determine the effect of asphaltene contamination on the tendency of clays to sorb organic liquids, TGA measurements were carried out on as-received and toluene and heptane-saturated clays and asphaltene coated clays. Table 4.1 shows the mass losses associated with asphaltene coated clays and as-received clays on heating from 20 °C to 150 °C at 5 °C/min. Asphaltene coating is expected to cause the surface of clay particles to become more hydrophobic[22] and therefore should decrease the amount of water adsorbed from the ambient environment.[14,20,33] The decrease in moisture sorption arising from asphaltene sorption for both kaolinite and illite clays, falls within the uncertainty of measurements and is not interpretable. By contrast, the capacity of both clays to adsorb organic liquids is maintained or enhanced by the asphaltene coating. Thus, asphaltene contamination amplifies the potential environmental and production problems caused by organic contamination of clays.[6,16]

Table 4.1. *Mass loss (mass fraction) on heating from 20 to 150 °C at 5 °C/min of as-received and asphaltene coated clays saturated at 60 °C with water and organic compounds*

Clay	Mass loss (± 0.001) of particles saturated with			
	As-received	Water	Toluene	n-Heptane
Kaolinite	0.005	0.01	0.009	0.007
Asphaltene coated kaolinite	0.003	0.009	0.013	0.01
Illite	0.003	0.005	0.005	0.004
Asphaltene coated illite	0.002	0.004	0.006	0.005

4.3.5 Enthalpy of Solution of Asphaltene Coated Clays

4.3.5.1 Impact of clay contamination

Enthalpies of solution of asphaltenes, as-received and asphaltene coated kaolinite and illite in toluene, n-heptane, and water at 60 °C and atmospheric pressure are shown in Figure 4.6. The results illustrate the variation in the nature and relative balance of the complex interactions that arise. For the cases surveyed, the range of values is broad, from -5 to more than +20 J/g of solute. As the enthalpy of solution values for the coated clays do not equal or trend toward the values for aphaltenes consistently, surfaces accessible by the organic solvents must be only partially coated with asphaltenes. Partial surface coverage was also found by Wang et al.[22]

The absolute values of the enthalpies of solution are also orders of magnitude larger than those caused by particle aggregation/disaggregation alone (<< ± 0.1 J/g) and must be attributed to adsorption, desorption/dissolution and surface-liquid interaction. For example, hydrogen bondings between water and OH groups on the as-received and asphaltene coated clay particles contribute a significant exotherm that is not observed in the organic liquids or with asphaltene particles on their own. Asphaltene coating of clay particles causes the surface to be more hydrophobic and decreases water sorption. As water sorption is an exothermic process,[22] the solution enthalpies of asphaltene coated clays in water are greater than as-received clays. For kaolinite, the impact is + 2 J/g and for illite the impact is + 1 J/g, values that are near and at the resolution of difference measurements respectively.

The strong repulsive interaction between the clays and coated clays and n-heptane is also evident. The decrease in the enthalpy of solution in toluene and n-heptane arising from coating kaolinite with asphaltenes can be attributed to an increase in toluene/n-heptane sorption on the

surface of clays (an exothermic process), or to a decrease in the repulsive interaction between the surface and these two organic liquids due to the presence of asphaltenes on the surface.

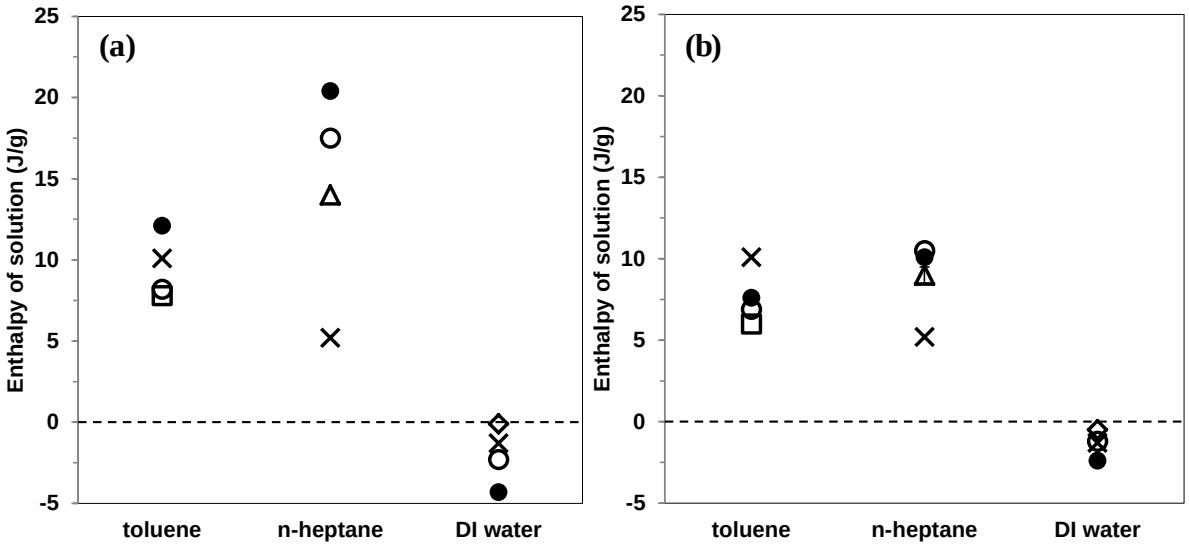

Figure 4.6. *Enthalpy of solution of asphaltenes (✕), as-received clays (●), asphaltene coated clays (○), water-saturated asphaltene coated clays (◇), toluene-saturated asphaltene coated clays (□), and n-heptane-saturated asphaltene coated clays (△) for kaolinite (a) and illite (b) at 60 °C and atmospheric pressure. The enthalpy value uncertainties are the same size as the symbols.*

4.3.5.2 Impact of organic solvent contamination with water

The impact of trace water in toluene and n-heptane on the enthalpy of solution of asphaltene coated clays was investigated systematically. For toluene and n-heptane three water mole fractions were employed. The as-received water content, water-saturated solvent at 25 °C, and water-saturated solvent at 60 °C. Figures 4.7a and b show that the enthalpy of solution for asphaltene coated clays decreases with trace water addition to organic solvents. Trace water addition to solvents reduces the magnitude of the water desorption endotherm, or causes water from the solution to adsorb onto coated clay particle surfaces (an exothermic effect). Asphaltene coated kaolinite is more affected by trace water in organic solvents than asphaltene coated illite.

If asphaltene coated kaolinite has more water on its surface compared to asphaltene coated illite, one would expect that reducing water desorption from the surface of clays would have a greater impact on the enthalpy of solution of asphaltene coated kaolinite than asphaltene coated illite. The solution behaviors of the clays appear uncorrelated with the solution behaviors of asphaltenes on their own, suggesting that the impacts of asphaltenes on clay behaviors are indirect.

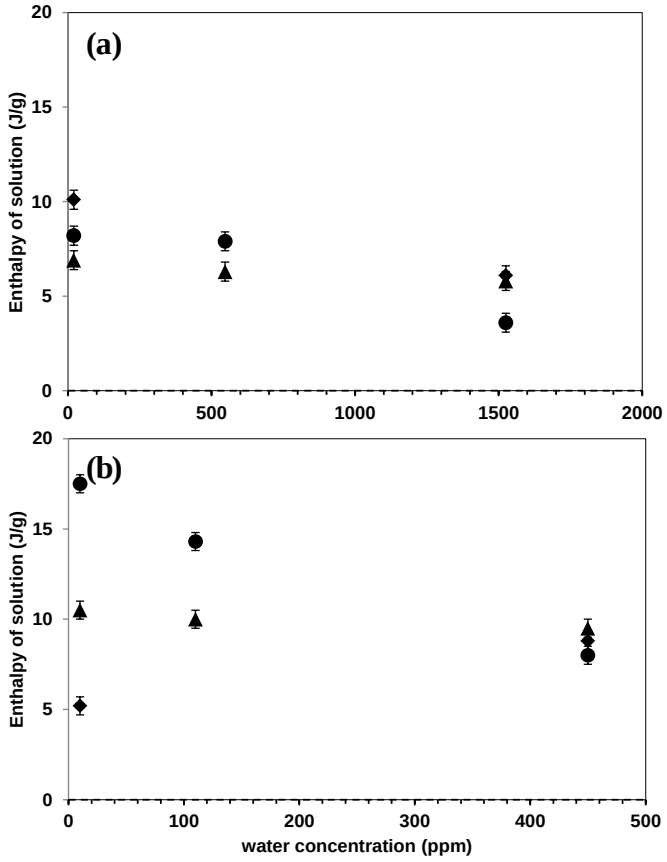

Figure 4.7. *Effect of trace water addition to organic solvents on the enthalpy of solution of asphaltenes (◆), asphaltene coated kaolinite (●) and asphaltene coated illite (▲) in toluene (a) and n-heptane (b) at 60 °C and atmospheric pressure.*

4.3.5.3 Impact of water contamination with organic liquids

The impact of trace contamination of water with toluene and n-heptane on the enthalpy of solution of asphaltenes, as-received and asphaltene coated clays is presented in Figure 4.8. Pre-saturation of water with toluene (740 ppm) and n-heptane (3 ppm) raises the enthalpies of solution for all samples. These trace species displace water from clay surfaces. The net impact on the enthalpy of solution is positive because the sum of the enthalpies for the steps involved, the enthalpy to desorb the water (positive) minus the enthalpy of solution of the organic liquids in water (positive) plus the enthalpy of sorption of organic liquids on clay surfaces (negative), exceeds zero. Asphaltene coating reduces the impact of this adsorption mechanism for kaolinite but does not change it for illite. This outcome is consistent with the work of Fafard[34] who showed that toluene sorbed more strongly than n-heptane on kaolinite.

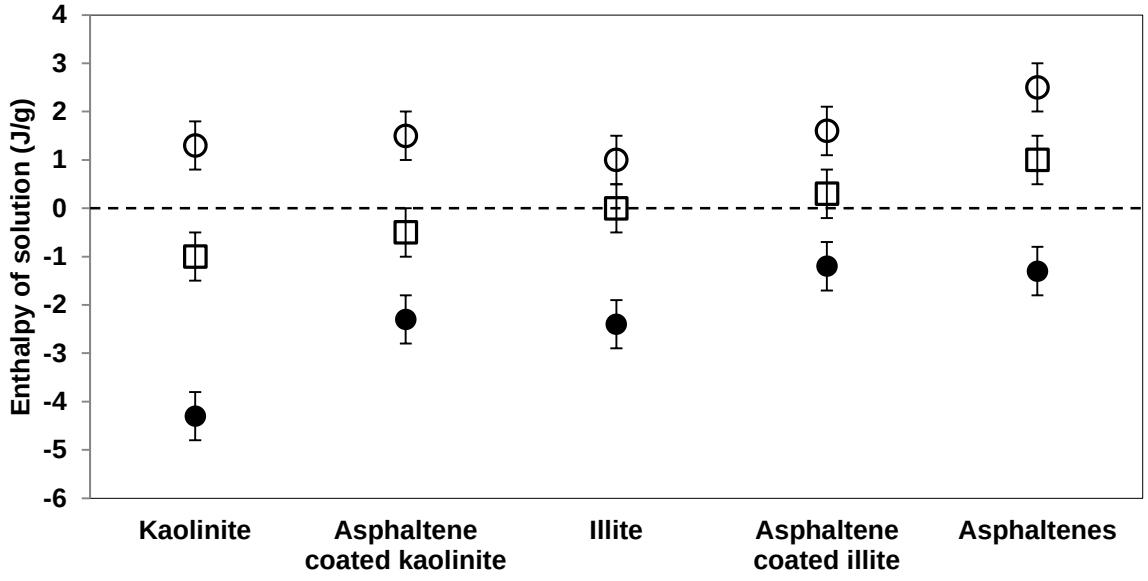

Figure 4.8. *Enthalpy of solution of clays and asphaltene coated clays in: water (●), toluene-saturated water (○), and n-heptane-saturated water (□) at 60 °C and atmospheric pressure.*

4.3.6 Generalizing the Parameters of the Solution Enthalpy Model

By pre-saturating the clays with a solvent and then measuring the enthalpy of solution in the same solvent, the reference enthalpies of solution (Δh_s^0) are obtained. Other terms in equation 4.1, go to zero. Similarly, by pre-saturating clays with both water and organic liquids, the surface energy changes introduced by contaminants, $\Delta h_{surface,TC}^{sat}$ are obtained. These values are reported in Table 4.2 along side values for uncoated clays reported in chapter 3. For asphaltene coated clays in water, the Δh_s^0 values agree with one another within experimental uncertainty and possess a value of 0 J/g, while Δh_s^0 values in toluene and n-heptane are large, positive and variable. $\Delta h_{surface,TC}^{sat}$ values for water, toluene and n-heptane are small and possess an uncertainty of ± 1 J/g. In water, all values are positive and agree within the experimental uncertainty. For trace water contamination in toluene and n-heptane the values are uniformly negative and agree within the experimental uncertainty with an average value of -2 J/g. Δh_s^0 values for asphaltene coated clays and as-received clays remain the same for illite and vary for kaolinite. $\Delta h_{surface,TC}^{sat}$ values for asphaltene coated clays are the same as as-received clays within experimental uncertainty. By inputting these parameter values for asphaltene coated clays into equation 4.2, the surface coverage by solvents and residual water mass fraction on the asphaltene coated clays, Table 4.3, can be inferred from known composition data, either on the surface (saturated compositions) or in the bulk (composition and saturated composition). The reported parameter values were obtained by fitting the enthalpy of solution data for all combinations of solvent, contaminant and clay. It is clear that for both uncoated and asphaltene coated clays, organic solvents such as toluene and n-heptane displace water from clays on immersion in them, and that the trace organic contaminants, such as toluene and n-heptane in water, also displace water from clay surfaces.

Table 4.2. *Measured Δh_s^0 and $\Delta h_{surface,TC}^{sat}$ at 60 ° C and atmospheric pressure for uncoated and asphaltene coated clays*

Solvent	Contaminant	$\Delta h_s^0 \pm 0.5$ J/g				$\Delta h_{surface,TC}^{sat} \pm 1$ J/g			
		Kaolinite		Illite		Kaolinite		Illite	
		uncoated	coated	uncoated	coated	uncoated	coated	uncoated	coated
Toluene	none	9	7.5	6.3	6				
	Water					-1	-1	-2	-1.5
n-Heptane	none	17	14	8.5	9				
	Water					-3	-2	-2	-2
Water	none	-1.5	0	-1	-0.5				
	Toluene					2	1	1	1.5
	n-Heptane					2	1.5	1	1

Table 4.3. *Clay surface coverage by solvents and trace contaminants for uncoated and asphaltene coated kaolinite and illite clays following immersion at 60 ° C and atmospheric pressure.*

Solvent	Contaminant	$\frac{x_S^F}{x_S^F + x_{TC}^F}$				$x_{H_2O}^F$				α			
		Kaolinite		Illite		Kaolinite		Illite		Kaolinite		Illite	
		uncoated	coated	uncoated	coated	uncoated	coated	uncoated	coated	uncoated	coated	uncoated	coated
Toluene	none	1	1	0.7	0.8	0	0	0.002	0.001				
	Water*	0.5	0.4	0.4	0.6	0.005	0.006	0.003	0.002	-3	-4	-0.9	-1.3
Heptane	none	0.9	1	0.9	1	0.001	0	0.001	0				
	Water*	0.4	0.3	0.3	0.6	0.006	0.007	0.004	0.002	-11.8	-15.5	-6.7	-4.5
Water	none	1	1	1	1	0.01	0.01	0.005	0.004				
	Toluene*	0	0	0	0	0	0	0	0	-13.5	-13.5	-6.8	-6.8
	n-Heptane*	0.3	0.3	0.1	0.2	0.003	0.003	0.001	0.001	-2692	-2692	-1731	-1379

* at saturation in the solvent.

4.3.7 Working Equations for the Enthalpy of Solution of Asphaltene Coated Clays

Equations 4.3 and 4.4 provided a simple framework for interpreting enthalpy of solution measurements for uncoated kaolinite and illite clays at 60 °C. The applicability of these equations for asphaltene coated clays was evaluated knowing the reference enthalpy of solution (Δh_s^0) values for asphaltene coated clays from Table 4.2 and the initial mass fractions of solvents and trace contaminants on the asphaltene coated clays surface from TGA measurements (Table 4.1). Figure 4.9 compares the computed and experimental enthalpies of solution for asphaltene coated clays in different solvents. Equations 4.3 and 4.4, developed for uncoated clays, also predict the behavior of asphaltene coated kaolinite and illite clays in organic liquids and water. A common framework for the prediction of properties of uncoated, and asphaltene coated clays facilitates the development and provides key steps toward general and predictive clay behavior models for industrial and natural environment applications. Equations 4.3 and 4.4 provide sound bases for the extension of the modeling framework to include impacts of ionic strength or pH of water or other inadvertent or intentionally introduced modifications that cause clay behaviors to differ from those arising in the natural or industrial environment from which they were originally obtained[35,36] are envisioned.

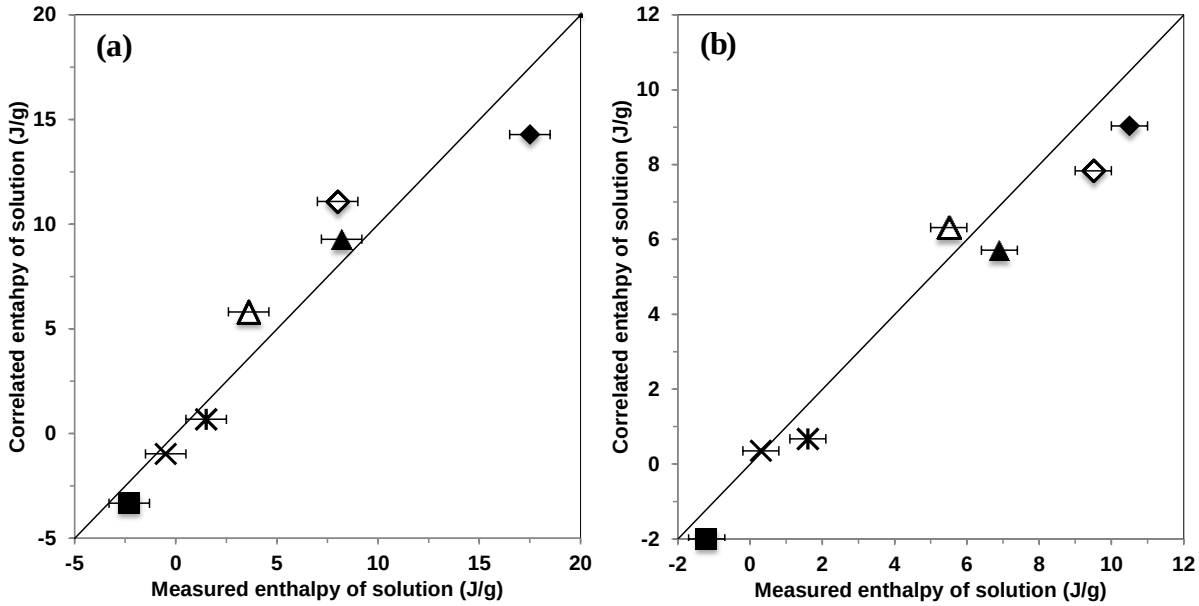

Figure 4.9 *A comparison between measured and correlated enthalpy of solution (equations 4.3 and 4.4) for (a) asphaltene coated kaolinite and (b) asphaltene coated illite in: toluene (◢), water-saturated toluene (△), n-heptane (◆), water-saturated n-heptane (◇), water (■), toluene-saturated water (✳), and n-heptane-saturated water (✕) at 60 °C and atmospheric pressure.*

4.4 ENVIRONMENTAL IMPLICATIONS

The surface properties of clays dictate their aggregation and sorption behaviors in industrial and natural environments. Detailed foreknowledge of surface properties permits the identification of potential risks and mitigation strategies. As these properties are linked to details of the surrounding media, probes such as solution calorimetry, that are sensitive to species transfer to and from clay surfaces can provide both quantitative data and mechanistic insights. Key findings of this work are that kaolinite and illite clays adsorb asphaltenes from asphaltene + toluene mixtures and clay surfaces become saturated with asphaltenes at less than 0.5 g/L asphaltenes but remain only partially coated. Kaolinite sorbs more asphaltenes than illite and consequently, sorbed asphaltenes have a greater impact on the surface properties of kaolinite than illite clays.

Sorbed asphaltenes render the clays less hygroscopic while maintaining or enhancing their capacity to sorb organic liquids. By parsing the roles of individual species and their interactions with other species present, the same quantitative modeling framework that was used previously for uncoated clays[28] was found to be applicable for asphaltene coated clays. This outcome shows that working equations for illite and kaolinite behaviors in organic liquids and water (equation 4.3 and 4.4)[28] predict both uncoated and asphaltene coated clay behaviors. Whether, clays are contaminated with oil or are contaminant free initially, the same behavioral trends are shown to arise. Quantitation of the impacts of temperature, water pH and sparingly soluble ionic species in water (both individually and jointly) are subjects of ongoing interest that are relevant to diverse industrial and natural environments.

ACKNOWLEDGEMENTS

The authors thank Mildred Becerra, Michelle Liu, and Jordon French for their assistance in the laboratory, Jun Zhao for supplying the clay samples, Gayle Hatchard for assistance with SEM tests, and Ni Yang for assistance with FT-IR tests. The authors gratefully acknowledge funding from Alberta Innovates Energy and Environment Solutions, British Petroleum, ConocoPhillips Inc., NEXEN Inc., Shell Canada, Total E & P Canada, VMG Inc., and the Natural Sciences and Engineering Research Council of Canada (NSERC).

NOMENCLATURE

Δh_s - enthalpy of solution (J/g)

Δh_s^0 - reference enthalpy of solution in the absence of sorption or desorption effects (J/g)

$\Delta h_{solvent\ sorption/desorption}$ - enthalpy of sorption/desorption of solvent on/from particles, for both organic liquids and water when they are used as a solvent (J/g)

$\Delta h_{TC\ sorption/desorption}$ - enthalpy of sorption/desorption of trace contaminant on/from particles, for both organic liquids and water when they are used as a contaminant (J/g)

$\Delta h_{surface,TC}$ - enthalpic effect of surface modification due to trace contaminant, for both organic liquids and water when they are used as a contaminant (J/g)

$\Delta h^{sat}_{surface,TC}$ - enthalpic effect of surface modification due to trace contaminant when the particles are saturated with the contaminant, for both organic liquids and water when they are used as a contaminant (J/g)

y_{TC} - composition of trace contaminant in the solvent, for both organic liquids and water when they are used as a contaminant (wt/wt)

y_{H_2O} - composition of water in organic solvent (wt/wt)

y_O - composition of organic liquids in water (wt/wt)

x_s^I and x_s^F - initial and final mass fraction of solvent on the surface of particles respectively, for both organic liquids and water when they are used as a solvent (wt/wt)

x_{TC}^I and x_{TC}^F - initial and final mass fraction of trace contaminant on the surface of particles respectively, for both organic liquids and water when they are used as a contaminant (wt/wt)

$x_{H_2O}^I$ and $x_{H_2O}^F$ - initial and final mass fraction of water on the surface of particles respectively (wt/wt)

x_O^I - initial mass fraction of organic liquids on the surface of particles (wt/wt)

x_{TC}^{sat} - saturation mass fraction of trace contaminant, for both organic liquids and water when they are used as a contaminant

$x_{H_2O}^{sat}$, x_O^{sat} - saturation mass fraction of water and organic liquids at the surface of clay particles (wt/wt)

$h_{s,TC}$ - enthalpy of solution of trace contaminant in the solvent, for both organic liquids and water when they are used as a contaminant (J/g)

h_{s,H_2O} - enthalpy of solution of water in the organic solvent (J/g)

$h_{s,o}$ - enthalpy of solution of organic liquids in the water (J/g)

$h_{f,s}$ - enthalpy of fusion of solvent, for both organic liquids and water when they are used as a solvent (J/g)

$h_{f,TC}$ - enthalpy of fusion of trace contaminant, for both organic liquids and water when they are used as a contaminant (J/g)

h_{f,H_2O}, $h_{f,O}$ - enthalpy of fusion of water and organic liquids (J/g)

α - an empirical coefficient, reported in Table 4.3, that is obtained by fitting the enthalpy of solution data for each combination of solvent contaminant and clay

γ - the saturation limit of the mass fraction of solvent plus contaminant on the surface of clays (wt/wt)

REFERENCES

(1) Kasongo, T.; Zhou, Z.; Xu, Z.; Masliyah, J. Effect of clays and calcium ions on bitumen extraction from Athabasca oil sands using flotation. Can. J. Chem. Eng. **2000**, 78, 674–681.

(2) Kotlyar, L. S.; Deslandes, T.; Sparks, B. D.; Hodama, H.; Schutte, R. Characterization of colloidal solids from Athabasca fine tails. Clays Clay Miner. **1993**, 41, 341–345.

(3) Budziak, C. J.; Vargha-Butler, E. I.; Hancock, R. G. V.; Neumann, A. W. Study of fines in bitumen extracted from oil sands by heat-centrifugation. Fuel **1988**, 67, 1633–1638.

(4) Siddique, T.; Fedorak, P. M.; Foght, J. M. Biodegradation of short-chain n-alkanes in oil sands tailings under methanogenic conditions. Environ. Sci. Technol. **2006**, 40 (17), 5459–5464.

(5) Beier, N.; Wilson, W.; Dunmola, A.; Sego, D. Impact of flocculation-based dewatering on the shear strength of oil sands fine tailings. Can. Geotech. J. **2013**, 50, 1001–1007.

(6) Camps, F. W. Processing Athabasca Tar Sands - Tailings Disposal. Can. J. Chem. Eng. **1977**, 55 (5), 581–591.

(7) Ostergren, J. D.; Brown, G. E.; Parks, G. A.; Tingle, T. N. Quantitative speciation of lead in selected mine tailings from Leadville, CO. Environ. Sci. Technol. **1999**, 33 (10), 1627–1636.

(8) Macur, R. E.; Wheeler, J. T.; Mcdermott, T. R.; Inskeep, W. P. Microbial populations associated with the reduction and enhanced mobilization of arsenic in mine tailings. Environ. Sci. Technol. **2001**, 35 (18), 3676–3682.

(9) Scott, A. C.; MacKinnon, M. D.; Fedorak, P. M. Naphthenic acids in athabasca oil sands tailings waters are less biodegradable than commercial naphthenic acids. Environ. Sci. Technol. **2005**, 39 (21), 8388–8394.

(10) Siddique, T.; Penner, T.; Klassen, J.; Nesbø, C.; Foght, J. M. Microbial communities involved in methane production from hydrocarbons in oil sands tailings. Environ. Sci. Technol. **2012**, 46, 9802–9810.

(11) Kumar, M.; Fogden, A. Patterned wettability of oil and water in porous media. Langmuir **2010**, 26 (6), 4036–4047.

(12) Lebedeva, E. V.; Fogden, A. Adhesion of oil to kaolinite in water. Environ. Sci. Technol. **2010**, 44 (24), 9470–9475.

(13) Hooshiar, A.; Uhlik, P.; Liu, Q.; Etsell, T. H.; Ivey, D. G. Clay minerals in nonaqueous extraction of bitumen from Alberta oil sands: Part 1. Nonaqueous extraction procedure. Fuel Process. Technol. **2012**, 94 (1), 80–85.

(14) Lebedeva, E. V.; Fogden, A. Wettability alteration of kaolinite exposed to crude oil in salt solutions. Colloids Surfaces A Physicochem. Eng. Asp. **2011**, 377 (1-3), 115–122.

(15) Dongbao, F.; Woods, J. R.; Kung, J.; Kingston, D. M.; Kotlyar, L. S.; Sparks, B. D.; Mercier, P. H. J.; McCracken, T.; Ng, S. Residual Organic Matter Associated with Toluene-Extracted Oil Sands Solids and Its Potential Role in Bitumen Recovery via Adsorption onto Clay Minerals. Energy & Fuels **2010**, 24 (4), 2249–2256.

(16) Lebedeva, E. V.; Fogden, A. Adhesion of oil to kaolinite in water. Environ. Sci. Technol. **2010**, 44 (24), 9470–9475.

(17) Liu, J.; Xu, Z.; Masliyah, J. Interaction between Bitumen and Fines in Oil Sands Extraction System. Can. J. Chem. Eng. **2004**, 82, 655–666.

(18) Dudášová, D.; Simon, S.; Hemmingsen, P. V.; Sjöblom, J. Study of asphaltenes adsorption onto different minerals and clays Part 1. Experimental adsorption with UV depletion detection. Colloids Surfaces A Physicochem. Eng. Asp. **2008**, 317, 1–9.

(19) Lebedeva, E. V.; Fogden, A. Nano-scale structure of crude oil deposits on water-wet substrates: Dependence on aqueous phase and organic solvents. Colloids Surfaces A Physicochem. Eng. Asp. **2011**, 380 (1-3), 280–291.

(20) Jada, A.; Debih, H. Hydrophobation of clay particles by asphaltenes adsorption. Compos. Interfaces **2009**, 16 (2-3), 219–235.

(21) Bantignies, J.; Moulin, C. C. D.; Dexpert, H. Wettability contrasts in kaolinite and illite clays: Characterization by infrared and x-ray absorption spectroscopies. Clays Clay Miner. **1997**, 45 (2), 184–193.

(22) Wang, S.; Liu, Q.; Tan, X.; Xu, C.; Gray, M. R. Study of asphaltene adsorption on kaolinite by X-ray photoelectron spectroscopy and time-of-flight secondary ion mass spectroscopy. Energy & Fuels **2013**, 27, 2465–2473.

(23) Nikakhtari, H.; Vagi, L.; Choi, P.; Liu, Q.; Gray, M. R. Solvent screening for non-aqueous extraction of Alberta oil sands. Can. J. Chem. Eng. **2013**, 91 (6), 1153–1160.

(24) Xing, C.; Hilts, R. W.; Shaw, J. M. Sorption of Athabasca Vacuum Residue Constituents on Synthetic Mineral and Process Equipment Surfaces from Mixtures with Pentane. Energy & Fuels **2010**, 24 (4), 2500–2513.

(25) Pernyeszi, T.; De, I. Sorption and elution of asphaltenes from porous silica surfaces. Colloids Surfaces A Physicochem. Eng. Asp. **2001**, 194, 25–39.

(26) Pernyeszi, T.; Patzk, A.; Berkesi, O.; Dekany, I. Asphaltene adsorption on clays and crude oil reservoir rocks. Colloids Surfaces A Physicochem. Eng. Asp. **1998**, 137, 373–384.

(27) Mendoza de la Cruz, J. L.; Castellanos-Ramírez, I. V.; Ortiz-Tapia, A.; Buenrostro-González, E.; Durán-Valencia, C. D. L. a.; López-Ramírez, S. Study of monolayer to multilayer adsorption of asphaltenes on reservoir rock minerals. Colloids Surfaces A Physicochem. Eng. Asp. **2009**, 340 (1-3), 149–154.

(28) Fafard, J.; Lyubimova, O.; Stoyanov, S. R.; Dedzo, G. K.; Gusarov, S.; Kovalenko, A.; Detellier, C. Adsorption of indole on kaolinite in nonaqueous media: Organoclay preparation and characterization, and 3D-RISM-KH molecular theory of solvation investigation. J. Phys. Chem. C **2013**, 117, 18556–18566.

(29) Batina, N.; Reyna-Cordova, A.; Trinidad-Reyes, Y.; Quintana-Garcia, M.; Buenrostro-Gonzalez, E.; Lira-Galeana, C.; Andersen, S. I. Qualitative analysis of thin films of crude oil deposits on the metallic substrate by fourier transform infrared (FTIR) microscopy. Energy & Fuels **2005**, 19 (5), 2001–2005.

(30) Mullins, O. Review of the Molecular Structure and Aggregation of Asphaltenes and Petroleomics. SPE J. **2008**, 13 (1), 48–57.

(31) Ledoux, R. . L.; White, J. L. Infrared study of the OH groups in expanded kaolinite. Science **1964**, 143 (3603), 244–245.

(32) Oinuma, K.; Hayashi, H. Infrared study of mixed-layer clay minerals. Am. Mineral. **1965**,

50, 1213–1227.

(33) Giraldo, J.; Nassar, N. N.; Benjumea, P.; Pereira-almao, P.; Corte, F. B. Modeling and Prediction of Asphaltene Adsorption Isotherms Using Polanyi's Modified Theory. Energy & Fuels **2013**, 27, 2908–2914.

(34) Fafard, J. Adsorption and desorption behaviour of organic molecules on kaolinite particles in non-aqueous media. M.Sc. Thesis, University of Ottawa, ON, 2012.

(35) Johnston, C. T. Probing the nanoscale architecture of clay minerals. Clay Miner. **2010**, 45 (3), 245–279.

(36) Kaminsky, H.; Etsell, T.; Ivey, D. G.; Omotoso, O. Fundamental particle size of clay minerals in athabasca oil sands tailings. Clay Sci. **2006**, 12, 217–222.

CHAPTER 5: PROBING THE ROLE OF WATER CHEMISTRY ON THE BEHAVIOR OF CLAYS IN PROCESS AND NATURAL ENVIRONMENTS USING SOLUTION CALORIMETRY

This chapter has been submitted to Energy & Fuels as Pourmohammadbagher, A.; Shaw, J. M. Probing the role of water chemistry on the behavior of clays in process and natural environments using solution calorimetry.

ABSTRACT: Clays, due to their specific surface area and electrical charge density, are among the most active minerals in aquifers, oil and gas reservoirs, and tailings ponds. Important problems, such as limited yield of oil recovery during petroleum exploration, involve the interaction of process fluids with minerals, which constitute reservoir pore walls. During mine tailings treatment and management, water chemistry impacts the aggregation and settling of clays. Solution calorimetry is a sensitive probe for species transfer to and from clay surfaces, and for the measurement of the effects of water chemistry (temperature, pH, salinity) on clay particle surfaces, in this case kaolinite, illite, and montmorillonite. In this work we show that interactions between clays and surrounding water are temperature independent for all three clay types and that water chemistry has no measurable effect on the surface properties of illite. For kaolinite, water pH does impact surface properties and has a synergistic impact with salinity at high pH. The surface properties of montmorillonite are sensitive to water pH and salinity. These data and observations extend a solution enthalpy modeling framework for clays and contaminated clays in water and liquid hydrocarbons. In the next phases of this work, entropic effects will be addressed so that a quantitative Gibbs free energy modeling framework for the enthalpy of solution of clays can be constructed and linked to clay settlement kinetics.

Key words: Clays, kaolinite, illite, montmorillonite, tailings, salinity, pH, calorimetry

5.1 INTRODUCTION

Clay + water interactions arise in diverse natural and industrial environments such as minerals extraction, coal mining, oil production, construction, and building materials fabrication.[1] The lead example for this work is oil sands production, where approximately one million cubic meters of tailings are discharged into tailings ponds daily.[2] Mature fine tailings (MFT)[3], a mixture of clay, water and soluble organic compounds, require decades to settle and solidify. Mitigation and reclamation of tailings ponds and MFT management have become pressing issues for the oil sands industry.[4–10] Environmental challenges also include impacts of inorganic and organic contaminants of clays (petroleum hydrocarbons[11], salts[12], metals[13,14], naphthenic acids[15], etc.) and emission of biogenic greenhouse gases from tailings ponds (CH_4 and CO_2)[16]. It is critical to understand the behavior of clays in tailings environments and to find new ways to increase the rate of clay settlement.

Clay minerals include 1:1-type and 2:1-type clays. 1:1-type clays comprise stacked tetrahedral sheets (Si–O tetrahedrons) and octahedral sheets (mainly Al–O octahedrons) while 2:1-type clays, comprise octahedral sheets sandwiched between tetrahedral sheets. In oil sands MFT kaolinite is one of the most common 1:1-type clays, and illite and montmorillonite are the most common 2:1-type clays.[17] The degree of flocculation and consequently, the rate of MFT formation, is dependent on factors such as the amount and size of clay particles, the surface contamination of clay particles, and the composition and properties of the liquid in which the clay particles are dispersed.[18,19]

Water chemistry is critical for the settlement of fine clays in aqueous environments. Residual organic matter present in the water or on clay surfaces influences their wettability, producing biwettable characteristics[20] that cause clay particles to exhibit some degree of

hydrophobicity.[21] Dissolved inorganic salts in water also influence the settling and flocculation behavior of fine clays.[22,23] Clays are more dispersed in suspensions containing monovalent cations[24] and are less dispersed in dispersions containing divalent cations. Zeta potential measurements agree with this observation, as lower values were measured for fine clays in the presence of divalent ions such as Ca^{2+} than for Na^{+} and other monovalent cations under otherwise comparable conditions.[23,25]

Solution calorimetry measures the amount of heat that is exchanged during chemical, physical or biological processes. It is sensitive to particle surface properties and to the variation in surface properties of particles arising from changes in the surrounding liquid medium. The effects of clay surface contamination and asphaltene coating on the enthalpy of solution of clays have been studied in chapters 3 and 4. Organic liquids, as solvents or as trace contaminants, displace water from clay surfaces. Adsorption of organic compounds on clay surfaces alters the hydrophilic/hydrophobic balance of clay particles through surface composition changes, that impact surface wettability, surface energy, and surface charge.[26–28] In this study, we build on our prior work and focus on impacts of water chemistry (temperature, pH, and salinity) on the solution behavior of kaolinite, illite, and montmorillonite clays in water. Deeper understanding of interactions between clays and other constituents is expected to lead to improved process and environmental performance of industrial processes, and to facilitate mitigation of impacts in disturbed natural environments where they are present.

5.2 EXPERIMENTAL

5.2.1 Materials

HPLC grade toluene (99.9 %), sodium hydroxide (99.8%), calcium chloride dehydrate (99.9 %), and sodium chloride (99.4 %) were purchased from Fisher Scientific and reagent grade hydrochloric acid (38%) was purchased from Caledon. All of the materials were used as-received . Kaolinite and illite clays, described in detail in chapter 3,[29] were purchased from Ward's Natural Science (Rochester, NY) and used as-received . Na-Montmorillonite clay from Crook Country, Wyoming, USA was purchased from Clay Minerals Society (Chantilly, VA).

5.2.2 Thermogravimetric Analysis (TGA)

Thermogravimetric analysis (TGA) was performed using a TG-DSC 111 thermoanalyzer (Setaram, France). 30 to 60 mg samples were placed in open crucibles and heated from 15 °C to 25, 45, 60, and 80 °C at 5 °C/min in a 20 mL/min stream of dry nitrogen. Baseline measurements with an empty crucible were used to correct mass loss measurements for the effect of buoyancy with temperature. The accuracy of TGA mass loss measurements is ±0.1 wt.% based on Copper (II) sulfate pentahydrate dehydration as a reference.

5.2.3 pH measurements

pH measurements were performed using a FiveEasyPlus^{TM} pH meter (FEP20) from Mettler Toledo with a resolution of 0.01 pH. The measurements were repeated 3 times for each sample and the average data is reported. The uncertainty of the reported pH data is ± 0.04.

5.2.4 Solution Calorimetry

Solution calorimetry measurements were performed using a precision solution calorimetry module (SolCal) from TA Instruments. A detailed explanation of the experimental procedure was presented in chapter 3. In brief, a sealed ampule containing 30 mg of the sample is placed in 25mL of a solvent and the whole system is kept in a TAM III thermostat until equilibrium is reached. During an experiment a sample is mixed at 500 rpm using a gold impeller. Two calibrations are performed - before and after ampule breakage, yielding a low uncertainty (±0.5 J/g). Positive enthalpy of solution values indicate net endothermic behaviors while negative values indicate net exothermic behaviors. A value of zero may mean no interaction or a balance of concurrent exothermic and endothermic interactions.

5.2.5 Interpretative Framework for Calorimetric and Thermogravimetric Data

The generic enthalpy of solution model at pH = 7 ($\Delta h_{s,7}$), equation 5.1, combines both TGA and calorimetric measurements and literature data for the solubility of trace contaminants in solvents, was developed in chapter 3 and can be summarized as:

$$\Delta h_{s,7} = \Delta h_s^0 - (\gamma + \alpha y_{TC} - x_s^I)\left(h_{f,s}\right) + (-\alpha y_{TC} - x_{TC}^I)[\frac{\Delta h_{surface,TC}^{sat}}{x_{TC}^{sat}} - \left(h_{s,TC} + h_{f,TC}\right)] \quad (5.1)$$

In brief, the enthalpy of solution comprises contributions from reference enthalpy of solution (Δh_s^0), initial mass fraction of solvent (x_s^I) and trace contaminant (x_{TC}^I), saturation mass fraction of trace contaminant on the surface of clays (x_{TC}^{sat}), composition of trace contaminant in the solvent (y_{TC}), saturation limit of the mass fraction of solvent plus trace contaminant on the surface of clays (γ), enthalpic effect of surface modification due to trace contaminant when the particles are saturated with the contaminant ($\Delta h_{surface,TC}^{sat}$), an empirical coefficient that is obtained by fitting the enthalpy of solution data for each combination of solvent, contaminant, and clay (α), enthalpy of fusion of solvent ($h_{f,s}$), and enthalpy of fusion and solution of trace contaminant ($h_{f,TC}$, $h_{s,TC}$).

5.3 RESULTS AND DISCUSSION

5.3.1 Labile water content of clays

The TGA measurements were carried out to determine the amount of water that is lost when clay samples are heated from a baseline temperature to specific higher temperatures. The results of these tests guide the interpretation the enthalpy of solution measurements. Table 5.1 shows the mass loss data for kaolinite, illite, and montmorillonite clays when the temperature is increased from 15 °C to 25, 45, 60, and 80 °C (the upper temperature limit of the calorimeter). Substantially more water desorbs from montmorillonite clay than from kaolinite and illite clays.

Table 5.1. *Mass loss (wt.%) of different clays at different temperatures*

Clay	Mass loss (wt.% ± 0.1)			
	15 °C – 25 °C	15 °C – 45 °C	15 °C – 60 °C	15 °C – 80 °C
Kaonilinte	0.0	0.1	0.2	0.3
Illite	0.0	0.0	0.1	0.1
Montmorillonite	0.1	0.4	0.9	2.1

5.3.2 Enthalpy of Solution

5.3.2.1 Effect of water temperature

Enthalpies of solution of kaolinite, illite, and montmorillonite clays in water at temperatures between 15 °C to 80 °C are shown in Figure 5.1. The raw enthalpy of solution values, Figure 5.1a, decrease for all three clays with increasing temperature. However, at higher temperatures during equilibration, a portion of the water sorbed on clay surfaces evaporates into the ampule. Thus, the clays have more surface available for water adsorption once the ampule is broken and the clays are exposed to liquid water. As a result, water adsorption occurs when clays are mixed with liquid water. This causes a negative enthalpic effect evident in the Figure 5.1a. The solution enthalpy outcomes must be compensated for the impact of this artifact explicitly. The maximum mass fractions of water needed to saturate the

vapour in the ampules are calculated to be 0.08, 0.22, 0.43, and 0.97 wt.% of clay samples at 25, 45, 60, and 80 °C, respectively. A comparison between these mass fractions and the values in Table 5.1 shows that not all of the water from the surface of montmorillonite needs to desorb to saturate the ampule. The impact of re-sorption of water following the breakage of the ampule on clays surfaces can be calculated as the enthalpy of water sorption ($\Delta h_{w\,sorption}$) using equation 5.2.

$$\Delta h_{w\,sorption} = -x_w h_{f,w} \tag{5.2}$$

where x_w is the mass fraction and $h_{f,w}$ is the enthalpy of fusion of water. The maximum impacts of this effect, at 80 °C, are -1, -0.3, and -3.2 J/g for kaolinite, illite, and montmorillonite, respectively. These values are in good agreement with observed differences shown in Figure 5.1a (-1.7, -0.8, and -3.7 ± 1 J/g, respectively). Based on corrected values, Figure 5.1b, temperature variation from 15 °C to 80 °C does not have a measurable impact on the enthalpy of solution of clays in water. Thus equation 5.1 can be applied to data from 15 °C to °80 C without modification. When clays are added to pure water, the enthalpy of solution consists of the effect of the first two terms only. Δh_s^0, the effect of surface charge of clays and $(\gamma + \alpha y_{TC} - x_s^I)(h_{f,s})$ the amount of water sorbed on the surface of clay particles, which is directly related to the number of available surface sites for sorption, are both independent of temperature.

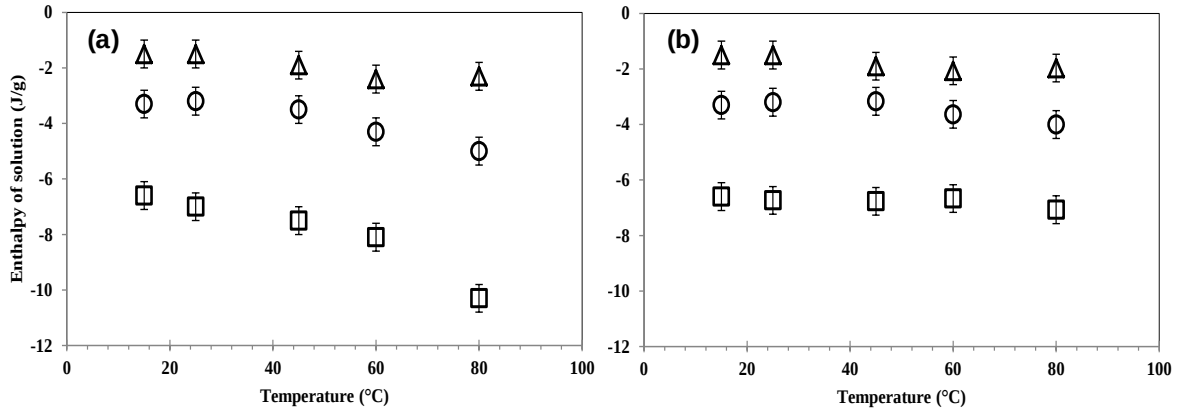

Figure 5.1. *Enthalpies of solution of illite (△), kaolinite (○), and montmorillonite (□) in water as a function of temperature at a fixed clay mass fraction (0.12 g/L), atmospheric pressure, and pH=7: a) raw data, b) corrected for water desorption from clay particles into the ampule prior to measurement.*

5.3.2.2 Effect of water pH

The effect of water pH (initial solution value) on the enthalpy of solution of kaolinite, illite, and montmorillonite clays at 25 °C and atmospheric pressure is shown in Figure 5.2a and b. Variation of the initial pH, using sodium hydroxide and hydrochloric acid, does not change the enthalpy of solution of illite clay in water. By increasing the pH, the enthalpy of solution of kaolinite stays the same from pH ~2 up to pH ~7. Above pH 7 a gradual decrease in the enthalpy of solution occurs up to a pH of ~ 11. The enthalpy of solution plateaus above a pH of 11. This trend in the enthalpy of solution of kaolinite is attributed to changes in the surface charge densities of external silica and alumina surfaces which have a distinct pH dependence.[30] At pH ≤ 6 silica faces are negatively charged and the alumina faces are positively charged. At pH ≥ 8, both the silica and alumina faces are negatively charged. For montmorillonite clay, the enthalpy of solution decreases from -5 J/g at pH 2.5 to -14 J/g at pH 13.5, a trend also noted by Tombacz et al.[31]

pH measurements were performed before adding clays ($pH_{initial}$) and after adding clays and mixing for two hours (pH_{final}). Figure 5.3 shows the difference between the final and initial pH ($\triangle pH = pH_{final} - pH_{initial}$) as a function of initial water pH. At low pH, the impact of clay addition on the pH value is negligible for all three clay types. At high pH, pH values decrease for all three clay types. The results are in agreement with Yukselen and Kaya study.[25] They found that the pH of the kaolinite clay solution decreases with time by 0.7 pH units after 120 min when the initial pH is very high and remains constant at low pH values and proposed that reaction between Si^{4+} (equation 5.3) and Al^{3+} (equation 5.4) cations on the surfaces of the octahedral and tetrahedral layers of clays with water causes the decrease in the solution pH:

$$Si^{4+} + 4OH^- \Leftrightarrow Si(OH)_4 \quad (5.3)$$

$$Al^{3+} + 3OH^- \Leftrightarrow Al(OH)_3 \quad (5.4)$$

Clays are complex aluminosilicates that include iron, and magnesium,[32] and the extents of reaction among cations on clay surfaces and OH^- are unknown. Therefore the effect of pH on the enthalpy of solution is quantified by fitting the enthalpy of solution data. The enthalpy of solution of any clay at any pH ($\Delta h_{s,pH}$) is obtained based on the enthalpy of solution of the same clay at pH=7 ($\Delta h_{s,7}$ from equation 5.1) using equation 5.5:

$$\Delta h_{s,pH} = \Delta h_{s,7} + A[pH - 7] \quad (5.5)$$

A is a clay dependent empirical coefficient obtained by fitting the enthalpy of solution data as a function of pH (Figure 5.2b) for each clay. The value of A (J/g) is zero for illite. Kaolinite and montmorillonite share a common A value of -0.54 J/g.

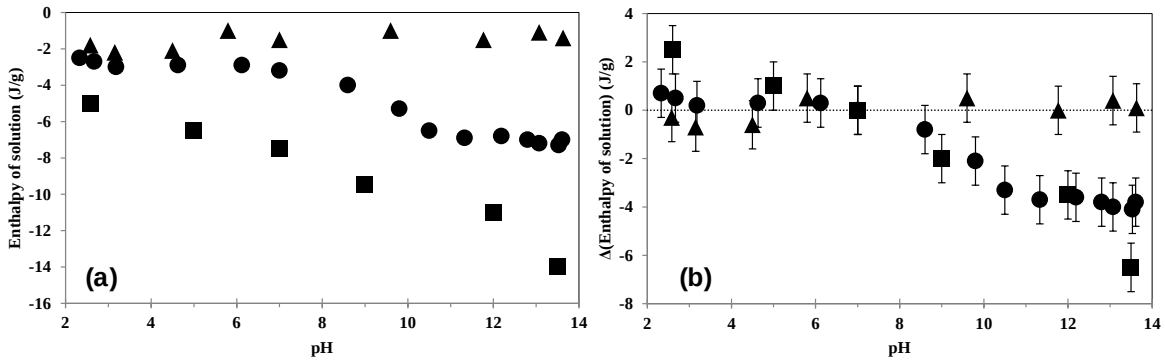

Figure 5.2. *(a) Enthalpy of solution of clays in water as a function of water pH, (b) The difference between enthalpy of solution at a specific pH value and enthalpy of solution at pH=7 for kaolinite (●), illite (▲), and montmorillonite (■) at clay concentration of 0.12 g/L, 25 °C and atmospheric pressure*

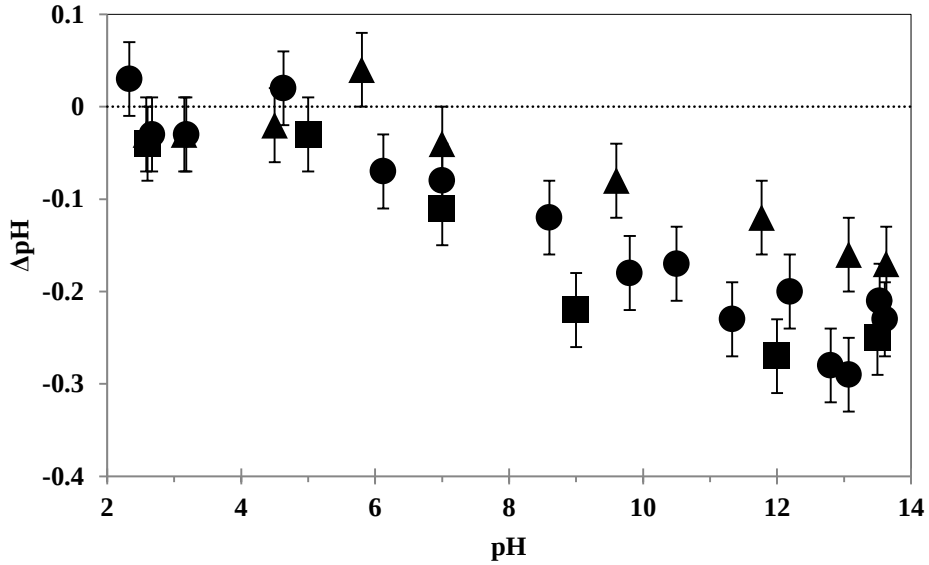

Figure 5.3. *Difference between the final and the initial pH (△pH= pH_{final} - $pH_{initial}$) as a function of initial water pH for kaolinite (●), illite (▲), and montmorillonite (■) at a fixed clay mass fraction (0.12 g/L)*

5.3.2.3 Effect of water salinity at pH=7

Salts can act as a shield and decrease the repulsive forces between clay particle surfaces. By adding Na^+ and Ca^{2+} ions to the water, the balance of repulsive forces that exist and van der Waals attraction between clay particles can change. The effect of salts and salts concentration on the enthalpy of solution of clays in water at 25 °C and atmospheric pressure is shown in Figure 5.4 for kaolinite (5.4a), illite (5.4b), and montmorillonite clays (5.4c). Na^+ has no effect on the enthalpy of solution of kaolinite (Figure 5.4a), while Ca^{2+} has a -2 J/g impact with a plateau at very low concentration (< 1 mM). Neither Na^+ nor Ca^{2+} impact the enthalpy of solution of illite (Figure 5.4b). For montmorillonite (Figure 5.4c), Na^+ and Ca^{2+} induce a -1 and -2 J/g impact respectively that plateaus at ~ 3mM. The decrease in the enthalpy of solution of clays when Ca^{2+} and Na^+ ions are added can be the result of surface charge neutralization by sorption of ions on clay surfaces or double layer compression. Hydration of sorbed ions can also attribute to a decrease in the enthalpy of solution. The effect of salinity on the enthalpy of solution at pH 7 is not significant and salinity per se is not included to the enthalpy of solution model.

5.3.2.4 Joint effect of water salinity and pH

The joint impact of pH and water salinity on the enthalpy of solution of clays was investigated at 25 °C and atmospheric pressure. The pH of solutions was adjusted to specific values, and three concentrations of Na^+ and Ca^{2+} cations (5, 50, and 100 mM) were added to the solutions in the form of chloride salts. The clay samples were then mixed with these solutions and the enthalpy of solution was evaluated. The results are presented in Figures 5.5a, b, and c for kaolinite, illite, and montmorillonite, respectively. At low pH, water salinity

has little impact on the enthalpy of solution for all three clays. At high pH, the enthalpy of solution decreases with increasing salt concentration. Since the Al faces of clay structures have positive charge in acidic and negative charge in basic solutions,[30] Na^+ and Ca^{2+} cations are expected to have greater impacts in basic solutions. pH and salt content jointly impact the behavior of clays in the order illite < kaolinite < montmorillonite. Nasser et al.[22] made a parallel observation for kaolinite. They found that at low pH, kaolinite flocculation was independent of salt concentration and at high pH, particles dispersed at low salt concentrations and flocculated at higher salt concentrations.

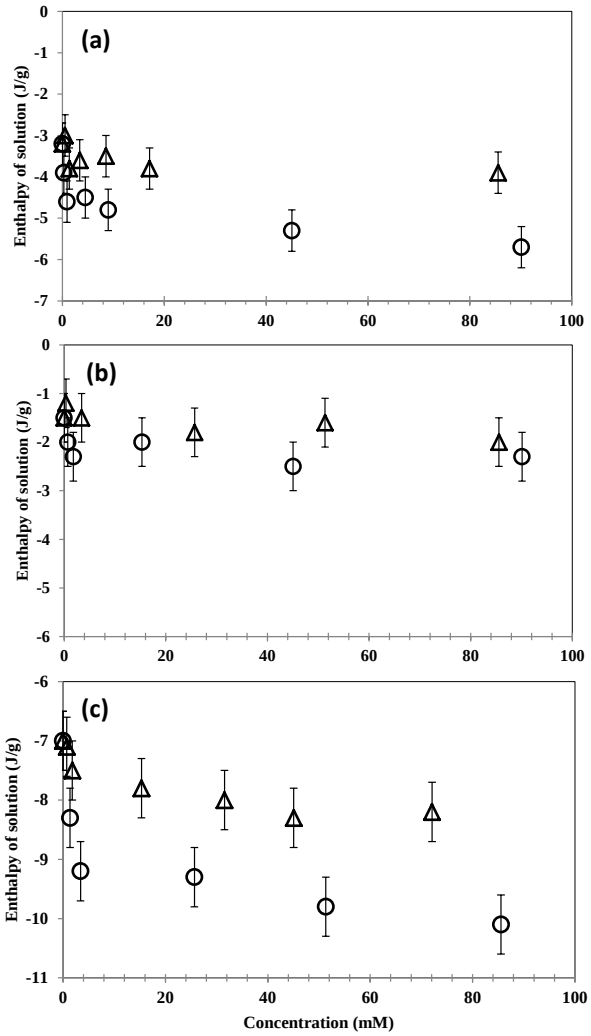

Figure 5.4. *Enthalpy of solution of kaolinite (a), illite (b), and montmorillonite (c) in water as a function of dissolved salt concentration for Na^+ (△) and Ca^{2+} (○) at clay concentration of 0.12 g/L, 25 °C, atmospheric pressure, and pH=7.*

Our results are also consistent with observations of the joint impacts of pH and electrolyte content on montmorillonite clay behaviors in solution.[31] The three clays present qualitatively and quantitatively different responses to joint variation of salinity and pH. While it is clear from experimental data that the joint impact is significant, quantitative modeling of the effect requires further detailed study. It is a subject for future work.

5.4 CONCLUSIONS

Quantitation of the impacts of temperature, pH and sparingly soluble ionic species on the behaviors of clays in water are relevant to diverse industrial and natural environments. In tailings lacking the right water chemistry, the electric charge on clay surfaces is sufficient to establish a repulsion force greater than van der Waals attraction force. This prevents fine clay particles from approaching one another. Adjustment of process water pH or interactions with other ions reduces the surface charge. This reduces the repulsion force between particles allowing them to approach one another and permitting aggregation to occur.

Table 5.2 summarizes the effects of water chemistry (temperature, pH, monovalent and divalent cations) on the enthalpy of solutions of kaolinite, illite, and montmorillonite clays. Interactions between clays and surrounding water are temperature independent for kaolinite, illite, and montmorillonite clays showing that Δh_s^0 (the effect of surface charge of clays) and $(\gamma + \alpha y_{TC} - x_s^I)(h_{f,s})$ (the amount of water sorbed on the surface of clay particles) in equation 5.1 are temperature independent. Thus, the quantitative modeling framework, equation 5.1, is applicable at pH = 7 over a broad range of temperatures.

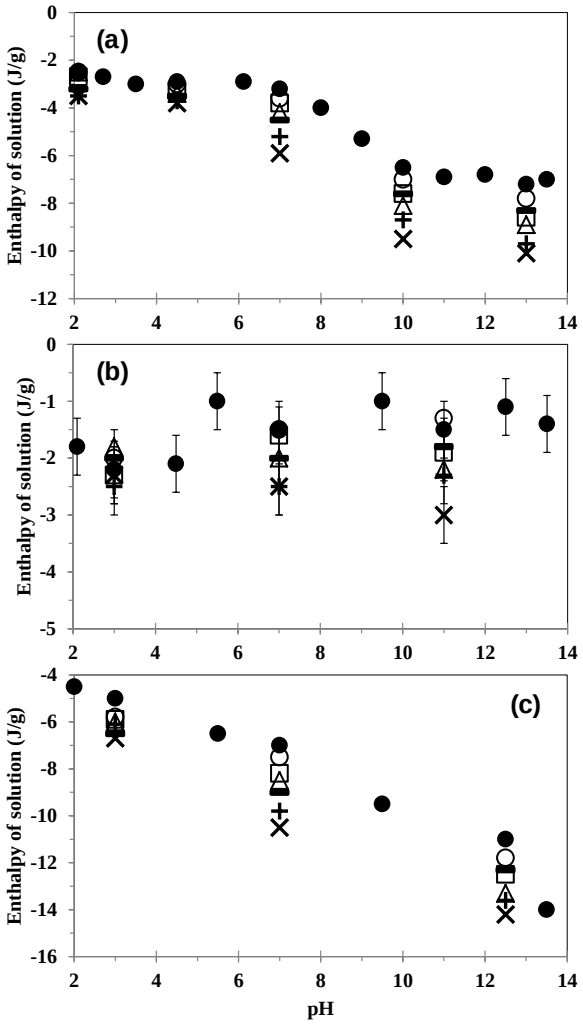

Figure 5.5. *Joint impact of water salinity and pH on the enthalpy of solution of kaolinite (a), illite (b), and montmorillonite (c) in water as a function of water pH at clay concentration of 0.12 g/L, 25 °C and atmospheric pressure. Salt concentration: no salt (●), 5mM Na^+ (○), 50mM Na^+ (□), 100mM Na^+ (△), 5mM Ca^{2+} (-), 50mM Ca^{2+} (+), and 100mM Ca^{2+} (×) is a parameter.*

pH, monovalent and divalent cations have almost no effect on the enthalpy of solution of illite clay, while the enthalpy of solution of montmorillonite clay is strongly related to these aspects of water chemistry. Impacts on kaolinite clay are in between. Monovalent ions have

less impact than divalent ions especially in basic solutions. These quantitative and qualitative outcomes were used to augment modeling framework for clays to include the impact of pH on the enthalpy of solution. In the next phases of this work, entropic effects will be addressed so that a quantitative Gibbs free energy modeling framework for the enthalpy of solution of clays can be constructed and linked to clay settlement kinetics.

Table 5.2. *A summary of the impacts of water chemistry on the enthalpy of solution of clays*

Clay	Temperature	pH	Monovalent cation (Na^+)	Divalent cation (Ca^{2+})
Kaolinite	–	M	L	L (acidic environment) M (basic environment)
Illite	–	–	–	–
Montmorillonite	–	H	L	L (acidic environment) H (basic environment)

–: no effect, L: little impact, M: medium impact, H: high impact

ACKNOWLEDGEMENTS

The authors thank Mildred Becerra, Michelle Liu, and Jordon French for their assistance in the laboratory; Jun Zhao for supplying the clay samples; Gayle Hatchard for assistance with SEM analysis; and Ni Yang for assistance with FT-IR measurements. The authors gratefully acknowledge financial support from the sponsors of the NSERC Industrial Research Chair in Petroleum Thermodynamics: the Natural Sciences and Engineering Research Council of Canada (NSERC), Alberta Innovates Energy and Environment Solutions, BP Canada, ConocoPhillips Canada Resources Corp., Nexen Energy ULC, Shell Canada Ltd., Total E&P Canada Ltd., and the Virtual Materials Group.

REFERENCES

(1) Gillott, J. E. Some Clay-Related Problems in Engineering Geology in North America. Clay Miner. **1986**, 21 (3), 261–278.

(2) Beier, N.; Wilson, W.; Dunmola, A.; Sego, D. Impact of flocculation-based dewatering on the shear strength of oil sands fine tailings. Can. Geotech. J. **2013**, 50, 1001–1007.

(3) An, D.; Brown, D.; Chatterjee, I.; Dong, X.; Ramos-Padron, E.; Wilson, S.; Bordenave, S.; Caffrey, S. M.; Gieg, L. M.; … Voordouw, G. Microbial community and potential functional gene diversity involved in anaerobic hydrocarbon degradation and methanogenesis in an oil sands tailings pond. Genome **2013**, 56 (10), 612–618.

(4) Kasongo, T.; Zhou, Z.; Xu, Z.; Masliyah, J. Effect of clays and calcium ions on bitumen extraction from Athabasca oil sands using flotation. Can. J. Chem. Eng. **2000**, 78, 674–681.

(5) Saada, A.; Papirer, E.; Balard, H.; Siffert, B. Determination of the Surface Properties of Illites and Kaolinites by Inverse Gas Chromatography. J. Colloid Interface Sci. **1995**, 175, 212–218.

(6) Gailhanou, H.; van Miltenburg, J. C.; Rogez, J.; Olives, J.; Amouric, M.; Gaucher, E. C.; Blanc, P. Thermodynamic properties of anhydrous smectite MX-80, illite IMt-2 and mixed-layer illite-smectite ISCz-1 as determined by calorimetric methods. Part I: Heat capacities, heat contents and entropies. Geochim. Cosmochim. Acta **2007**, 71 (22), 5463–5473.

(7) Konan, K. L.; Peyratout, C.; Smith, a.; Bonnet, J. P.; Magnoux, P.; Ayrault, P. Surface modifications of illite in concentrated lime solutions investigated by pyridine adsorption. J. Colloid Interface Sci. **2012**, 382 (1), 17–21.

(8) Kumar, M.; Fogden, A. Patterned wettability of oil and water in porous media. Langmuir **2010**, 26 (6), 4036–4047.

(9) Bantignies, J.; Moulin, C. C. D.; Dexpert, H. Wettability contrasts in kaolinite and illite clays: Characterization by infrared and x-ray absorption spectroscopies. Clays Clay Miner. **1997**, 45 (2), 184–193.

(10) Dudášová, D.; Simon, S.; Hemmingsen, P. V.; Sjöblom, J. Study of asphaltenes adsorption onto different minerals and clays Part 1. Experimental adsorption with UV depletion detection. Colloids Surfaces A Physicochem. Eng. Asp. **2008**, 317, 1–9.

(11) Siddique, T.; Fedorak, P. M.; Foght, J. M. Biodegradation of short-chain n-alkanes in oil sands tailings under methanogenic conditions. Environ. Sci. Technol. **2006**, 40 (17), 5459–5464.

(12) Sun, D.; Zhou, X.; Luo, W.; Liu, Z.; Shi, Z.; Zhang, X. Study on the settlement experiment of iron tailings. Appl. Mech. Mater. **2013**, 281, 511–516.

(13) Ostergren, J. D.; Brown, G. E.; Parks, G. A.; Tingle, T. N. Quantitative speciation of lead in selected mine tailings from Leadville, CO. Environ. Sci. Technol. **1999**, 33 (10), 1627–1636.

(14) Macur, R. E.; Wheeler, J. T.; Mcdermott, T. R.; Inskeep, W. P. Microbial populations

associated with the reduction and enhanced mobilization of arsenic in mine tailings. Environ. Sci. Technol. **2001**, 35 (18), 3676–3682.

(15) Scott, A. C.; MacKinnon, M. D.; Fedorak, P. M. Naphthenic acids in athabasca oil sands tailings waters are less biodegradable than commercial naphthenic acids. Environ. Sci. Technol. **2005**, 39 (21), 8388–8394.

(16) Siddique, T.; Penner, T.; Klassen, J.; Nesbø, C.; Foght, J. M. Microbial communities involved in methane production from hydrocarbons in oil sands tailings. Environ. Sci. Technol. **2012**, 46, 9802–9810.

(17) Kaminsky, H. A. W.; Etsell, T. H.; Ivey, D. G.; Omotoso, O. Distribution of clay minerals in the process streams produced by the extraction of bitumen from Athabasca oil sands. Can. J. Chem. Eng. **2009**, 87 (1), 85–93.

(18) Kotlyar, L. S.; Sparks, B. D.; Schutte, R.; Woods, J. R. Understanding of fundamentals: Key to process modification for tailings reduction. J. Environ. Sci. Heal. **1993**, 28 (10), 2215–2224.

(19) Kotlyar, L. S.; Sparks, B. D.; Lepage, Y.; Woods, J. R. Effect of particle size on the flocculation behaviour of ultra-fine clays in salt solutions. Clay Miner. **1998**, 33, 103–107.

(20) Dongbao, F.; Woods, J. R.; Kung, J.; Kingston, D. M.; Kotlyar, L. S.; Sparks, B. D.; Mercier, P. H. J.; McCracken, T.; Ng, S. Residual Organic Matter Associated with Toluene-Extracted Oil Sands Solids and Its Potential Role in Bitumen Recovery via Adsorption onto Clay Minerals. Energy & Fuels **2010**, 24 (4), 2249–2256.

(21) Liu, J.; Xu, Z.; Masliyah, J. Interaction between Bitumen and Fines in Oil Sands Extraction System. Can. J. Chem. Eng. **2004**, 82, 655–666.

(22) Nasser, M. S.; James, A. E. The effect of electrolyte concentration and ph on the flocculation and rheological behaviour of kaolinite suspensions. J. Eng. Sci. Technol. **2009**, 4 (4), 430–446.

(23) Chorom, M.; Rengasamy, P. Dispersion and zeta potential of pure clays as related to net particle charge under varying pH, electrolyte concentration and cation type. Eur. J. Soil Sci. **1995**, 46, 657–665.

(24) Marchuk, A.; Rengasamy, P. Clay behaviour in suspension is related to the ionicity of clay-cation bonds. Appl. Clay Sci. **2011**, 53 (4), 754–759.

(25) Yukselen, Y.; Kaya, A. Zeta potential of kaolinite in the presence of alkali, alkaline earth and hydrolyzable metal ions. Water. Air. Soil Pollut. **2003**, 145, 155–168.

(26) Lebedeva, E. V.; Fogden, A. Wettability alteration of kaolinite exposed to crude oil in salt solutions. Colloids Surfaces A Physicochem. Eng. Asp. **2011**, 377 (1-3), 115–122.

(27) Lebedeva, E. V.; Fogden, A. Nano-scale structure of crude oil deposits on water-wet substrates: Dependence on aqueous phase and organic solvents. Colloids Surfaces A Physicochem. Eng. Asp. **2011**, 380 (1-3), 280–291.

(28) Jada, A.; Debih, H. Hydrophobation of clay particles by asphaltenes adsorption. Compos. Interfaces **2009**, 16 (2-3), 219–235.

(29) Wang, S.; Liu, Q.; Tan, X.; Xu, C.; Gray, M. R. Study of asphaltene adsorption on

kaolinite by X-ray photoelectron spectroscopy and time-of-flight secondary ion mass spectroscopy. Energy & Fuels **2013**, 27, 2465–2473.

(30) Gupta, V.; Hampton, M. a.; Stokes, J. R.; Nguyen, A. V.; Miller, J. D. Particle interactions in kaolinite suspensions and corresponding aggregate structures. J. Colloid Interface Sci. **2011**, 359 (1), 95–103.

(31) Tombácz, E.; Szekeres, M. Colloidal behavior of aqueous montmorillonite suspensions: the specific role of pH in the presence of indifferent electrolytes. Appl. Clay Sci. **2004**, 27 (1-2), 75–94.

(32) Gailhanou, H.; Blanc, P.; Rogez, J.; Mikaelian, G.; Kawaji, H.; Olives, J.; Amouric, M.; Denoyel, R.; Bourrelly, S.; … Gaucher, E. C. Thermodynamic properties of illite, smectite and beidellite by calorimetric methods: Enthalpies of formation, heat capacities, entropies and Gibbs free energies of formation. Geochim. Cosmochim. Acta **2012**, 89, 279–301.

CHAPTER 6: CONCLUSIONS AND RECOMMENDATIONS

6.1 CONCLUSIONS

An experimental and theoretical interpretative framework for performing and parsing enthalpy of solution measurements and for determining and validating the signs and magnitudes of the energetics of specific clay surface−liquid interactions is presented. The effect of different surface and/or solvent contamination on the behavior of kaolinite, illite, and montmorillonite clays was investigated. Experimental outcomes were interpreted using a quantitative mass and energy balance modeling framework and a generic model was developed for prediction of the enthalpic behavior of clays in water and organic liquids.

Trace and sparingly soluble organic liquids in water can displace sorbed water from clay particle surfaces. This displacement can lead to a change in the sign of the enthalpy of solution for clay particles in contaminated water from net negative to net positive values. This one outcome impacts the development of predictive models for how oil spills or contaminated water plumes spread in clay rich environments; and illustrates how easily surface properties of clays can be altered through handling or treatment intended to “clean” or “purify” samples. This outcome also calls in to question the efficacy and the appropriateness of organic liquid injection based enhanced oil recovery processes. Significant solvent loss can be expected if clays are present in formations.

Sorbed asphaltenes render clays less hydroscopic while maintaining or enhancing their capacity to sorb organic liquids. Whether, clays are contaminated with oil or are contaminant free initially, the same behavioral trends are shown to arise. Kaolinite sorbs more asphaltenes

on its surface than illite and consequently, sorbed asphaltenes have a greater impact on the surface properties of kaolinite than illite clays.

Clay reactions with water were shown to be independent temperature. Water chemistry has almost no effect on the behavior of illite clays. However, montmorillonite clay behavior is directly impacted by water chemistry. Monovalent ions have negligible effect on all of the clay types but divalent ions have more effect especially in a basic environment.

These findings provided a basis for an enthalpy of solution behavioral model for clays in organic liquids and water that correlates and predicts behaviors of both uncoated and asphaltene coated clays. Since solution enthalpies are temperature independent, the quantitative modeling framework elaborated at 60 °C and a pH of 7, is shown to be equally applicable at 15 °C – 80 °C. A correlation was also developed to address the effect of pH on the enthalpy of solution model. This model will be used in developing a quantitative Gibbs free energy modeling framework that can be linked to clay settlement kinetics.

6.2 FUTURE WORK

- Parsing the entropy effects of individual species and combining the results with this work to construct a quantitative Gibbs free energy modeling framework for clay behaviors in liquids.
- Predicting the effect of measurable variables (Temperature, pH, organic contamination, oil spills contamination, ion type and concentration) on the settling rates of clays using the Gibbs free energy modeling framework.

- Providing tailings remediation and reclamation guidelines that reduce environmental risks and operating costs for industrial processes.

APPENDIX A. SUPPORTING INFORMATION OF CHAPTER 3

The supporting material includes Table S3.1 concerning physicochemical properties of solvents, Table S3.2 concerning enthalpy of fusion and dissolution data, and Tables S3.3 – S3.8 comprising data appearing in Chapter 3.

Table S3.1. *Physicochemical properties of toluene, n-heptane and pyridine**

Chemical	Toluene	n-Heptane	Pyridine
Formula	C_7H_8	C_7H_{16}	C_5H_5N
Molecular Weight (g/mol)	92.1384	100.2019	79.0999
Density at 60 °C (g/mL)	0.82923	0.64941	0.942539
Normal boiling point (°C)	110.6	98.38	115.55

*NIST Chemistry WebBook, NIST Standard Reference Database Number 69. http://webbook.nist.gov/chemistry/ (accessed July 5, 2015).

Table S3.2. *Enthalpy of fusion and solution (J/g) for organic liquids and water*

Enthalpy (J/g)	Toluene	n-Heptane	Pyridine	Water
h_f	72[1]	140[2]	104[3]	333[4]
$h_{s,water}$	390*	340*	-60*	–
$h_{s,toluene}$	–	–	–	60 ± 1*
$h_{s,heptane}$	–	–	–	56 ± 1*
$h_{s,pyridine}$				-45 ± 1*

* measured in this work

Table S3.3. *Tabular enthalpy of solution (J/g) data for Figures 3.3 (uncertainty: ± 1J/g)*

Particle	Toluene	n-Heptane	Pyridine
Kaolinite	12.1	20.4	-0.2
Water saturated kaolinite	8.3	11.2	-0.7
Toluene saturated kaolinite	9	–	–
n-Heptane saturated kaolinte	–	17	–
Pyridine saturated kaolinite	–	–	-1
Illite	7.6	10.1	2
Water saturated illite	6.5	7.5	1.3
Toluene saturated illite	6.3	–	–
n-Heptane saturated illite	–	8.5	–
Pyridine saturated illite	–	–	0.5

Table S3.4. *Tabular enthalpy of solution (J/g) data for Figure 3.4a (uncertainty: ± 1J/g)*

Particle	Water concentration in toluene (ppm)		
	20	547	1525
Kaolinite	12.1	10.8	9.5
Illite	7.6	7.1	6.5

Table S3.5. *Tabular enthalpy of solution (J/g) data for Figure 3.4b (uncertainty: ± 1J/g)*

Particle	Water concentration in n-heptane (ppm)		
	10	110	450
Kaolinite	20.4	19.4	15.1
Illite	10.1	9.1	7.5

Table S3.6. *Tabular enthalpy of solution (J/g) data for Figure 3.4c (uncertainty: ± 1J/g)*

Particle	Water concentration in pyridine (ppm)			
	200	910	2050	5010
Kaolinite	-0.2	-0.1	-0.8	-1.2
Illite	2	2.5	1.2	0.9

Table S3.7. *Tabular enthalpy of solution (J/g) data for Figure 3.5 (uncertainty: ± 1J/g)*

Particle	Water	Toluene saturated water	n-Heptane saturated water
Kaolinite	-4.3	1.3	-1
Water saturated kaolinite	-1.5	1.5	0.5
Illite	-2.4	1	0
Water saturated illite	-1	1.2	0.3

Table S3.8. *Tabular enthalpy of solution (J/g) data for Figure 3.6 (uncertainty: ± 1J/g)*

Particle	Water saturated toluene	Water saturated n-heptane	Toluene saturated water	n-Heptane saturated water
Water and toluene saturated kaolinite	7.8	–	0	–
Water and toluene saturated illite	4.4		0.2	–
Water and n-heptane saturated kaolinite	–	14	–	0.2
Water and n-heptane saturated illite	–	6.2	–	0

REFERENCES:

(1) Scott, D. W.; Guthrie, G. B.; Messerly, J. F.; Todd, S. S.; Berg, W. T.; Hossenlopp, I. A.; McCullough, J. P. Toluene: thermodynamic properties, molecular vibrations, and internal rotation. J. Phys. Chem. **1962**, 911–914.

(2) Huffman, H. M.; Gross, M. E.; Scott, D. W.; McCullough, I. P. Low temperature thermodynamic properties of six isomeric heptanes. J. Phys. Chem. **1961**, 495–503.

(3) Domalski, E. S.; Hearing, E. D. Heat Capacities and Entropies of Organic Compounds in the Condensed Phase. Volume III. J. Phys. Chem. Ref. Data **1996**, 25 (1), 1–525.

(4) Lemmon, E. W.; Harvey, A. H. Fluid Properties. In CRC Handbook of Chemistry and Physics; Haynes, W. M., Ed.; CRC Press: Boca Raton, Florida, 2014; pp 146–155.

APPENDIX B. SUPPORTING INFORMATION OF CHAPTER 4

The supporting materials include Tables S4.1 – S4.5 comprising data appearing in chapter 4.

Table S4.1. *Tabular enthalpy of solution (J/g) data for Figures 4.5 (uncertainty: ± 0.5 J/g)*

Asphaltene concentration in toluene (g/l)	Enthalpy of solution (J/g)	
	Kaolinite	Illite
0	12.1	7.6
0.1	10.6	7.3
0.2	9.8	6.9
0.3	9.9	6.8
0.5	9.1	6.5
1	9.3	6.4
2	8.9	6
5	8.5	6.2

Table S4.2. *Tabular enthalpy of solution (J/g) data for Figure 4.6 (uncertainty: ± 0.5 J/g)*

Particle	Toluene	n-Heptane	DI Water
Kaolinite	12.1	20.4	-4.3
Asphaltene coated kaolinite	8.2	17.5	-2.3
Water-saturated asphaltene coated kaolinite	–	–	-0.1
Toluene-saturated asphaltene coated kaolinite	7.8	–	–
n-Heptane-saturated asphaltene coated kaolinite	14	–	–
illite	7.6	10.1	-2.4
Asphaltene coated illite	6.9	10.5	-1.2
Water-saturated asphaltene coated illite	–	–	0.5
Toluene-saturated asphaltene coated illite	6	–	–
n-Heptane-saturated asphaltene coated illite	–	9	–
Asphaltenes	10.1	5.2	-1.3

Table S4.3. *Tabular enthalpy of solution (J/g) data for Figure 4.7a (uncertainty: ± 0.5 J/g)*

Particle	Water concentration in Toluene (ppm)		
	20	547	1525
Asphaltene	10.1	–	6.1
Asphaltene coated kaolinite	8.2	7.9	3.6
Asphaltene coated illite	6.9	6.3	5.8

Table S4.4. *Tabular enthalpy of solution (J/g) data for Figure 4.7b (uncertainty: ± 0.5 J/g)*

Particle	Water concentration in n-Heptane (ppm)		
	10	110	450
Asphaltene	5.2	–	8.8
Asphaltene coated kaolinite	17.5	14.3	8
Asphaltene coated illite	10.5	10	9.5

Table S4.5. *Tabular enthalpy of solution (J/g) data for Figure 4.8 (uncertainty: ± 0.5 J/g)*

Particle	Water	Toluene - saturated water	n-Heptane - saturated water
Kaolinite	-4.3	1.3	-1
Asphaltene coated kaolinite	-2.3	1.5	-0.5
Illite	-2.4	1	0
Asphaltene coated illite	-1.2	1.6	0.3
Asphaltenes	-1.3	2.5	1

APPENDIX C. SUPPORTING INFORMATION OF CHAPTER 5

The supporting material includes Tables S5.1 – S5.11 comprising data appearing in chapter 5.

Table S5.1. *Tabular enthalpy of solution (J/g) data for Figures 5.1a (uncertainty: ± 0.5 J/g)*

Temperature (°C)	Enthalpy of solution (J/g)		
	Kaolinite	Illite	Montmorillonite
15	-3.3	-1.5	-6.6
25	-3.2	-1.5	-7
45	-3.5	-1.9	-7.5
60	-4.3	-2.4	-8.1
80	-5	-2.3	-10.3

Table S5.2. *Tabular enthalpy of solution (J/g) data for Figures 5.1b (uncertainty: ± 0.5 J/g)*

Temperature (°C)	Enthalpy of solution (J/g)		
	Kaolinite	Illite	Montmorillonite
15	-3.3	-1.5	-6.6
25	-3.2	-1.5	-6.7
45	-3.2	-1.9	-6.8
60	-3.6	-2	-6.7
80	-4	-2	-7

Table S5.3. *Tabular enthalpy of solution (J/g) data for Figure 5.2a (uncertainty: ± 0.5 J/g)*

Kaolinite		Illite		Montmorillonite	
pH	Enthalpy of solution (J/g)	pH	Enthalpy of solution (J/g)	pH	Enthalpy of solution (J/g)
2.33	-2.5	2.58	-1.8	2.6	-5
2.67	-2.7	3.15	-2.2	5	-6.5
3.18	-3	4.50	-2.1	7	-7.5
4.63	-2.9	5.8	-1	9	-9.5
6.12	-2.9	7	-1.5	12	-11
7.00	-3.2	9.60	-1	13.5	-14
8.60	-4	11.77	-1.5		
9.80	-5.3	13.07	-1.1		
10.50	-6.5	13.63	-1.4		
11.33	-6.9				
12.19	-6.8				
12.8	-7				
13.07	-7.2				
13.53	-7.3				
13.61	-7				

Table S5.4. *Tabular ∆(enthalpy of solution) of solution (J/g) data for Figure 5.2b (uncertainty: ± 1 J/g)*

Kaolinite		Illite		Montmorillonite	
pH	Enthalpy of solution (J/g)	pH	Enthalpy of solution (J/g)	pH	Enthalpy of solution (J/g)
2.33	0.7	2.58	-0.3	2.6	2.5
2.67	0.5	3.15	-0.7	5	1
3.18	0.2	4.50	-0.6	7	0
4.63	0.3	5.8	0.5	9	-2
6.12	0.3	7	0	12	-3.5
7.00	0	9.60	0.5	13.5	-6.5
8.60	-0.8	11.77	0		
9.80	-2.1	13.07	0.4		
10.50	-3.3	13.63	0.1		
11.33	-3.7				
12.19	-3.6				
12.8	-3.8				
13.07	-4				
13.53	-4.1				
13.61	-3.8				

Table S5.5. *Tabular ⊿pH data for Figure 5.3 (uncertainty: ± 0.04)*

Kaolinite		Illite		Montmorillonite	
pH	△pH	pH	△pH	pH	△pH
2.33	0.03	2.58	-0.03	2.6	-0.04
2.67	-0.03	3.15	-0.03	5	-0.03
3.18	-0.03	4.50	-0.02	7	-0.11
4.63	0.02	5.8	0.04	9	-0.22
6.12	-0.07	7	-0.04	12	-0.27
7.00	-0.08	9.60	-0.08	13.5	-0.25
8.60	-0.12	11.77	-0.12		
9.80	-0.18	13.07	-0.16		
10.50	-0.17	13.63	-0.17		
11.33	-0.23				
12.19	-0.2				
12.8	-0.28				
13.07	-0.29				
13.53	-0.21				
13.61	-0.23				

Table S5.6. *Tabular enthalpy of solution (J/g) data for Figure 5.4a (uncertainty: ± 0.5 J/g)*

Na^+		Ca^{2+}	
Concentration (mM)	Enthalpy of solution (J/g)	Concentration (mM)	Enthalpy of solution (J/g)
0.0	-3.2	0.0	-3.2
0.5	-3	0.3	-3.9
1.4	-3.8	0.9	-4.6
3.4	-3.6	4.5	-4.5
8.6	-3.5	9.0	-4.8
17.1	-3.8	45.1	-5.3
85.6	-3.9	90.1	-5.7

Table S5.7. *Tabular enthalpy of solution (J/g) data for Figure 5.4b (uncertainty: ± 0.5 J/g)*

Na^+		Ca^{2+}	
Concentration (mM)	Enthalpy of solution (J/g)	Concentration (mM)	Enthalpy of solution (J/g)
0.0	-1.5	0.0	-1.5
0.3	-1.2	0.7	-2
3.4	-1.5	1.8	-2.3
25.7	-1.8	15.3	-2
51.3	-1.6	45.1	-2.5
85.6	-2	90.1	-2.3

Table S5.8. *Tabular enthalpy of solution (J/g) data for Figure 5.4c (uncertainty: ± 0.5 J/g)*

Na^+		Ca^{2+}	
Concentration (mM)	Enthalpy of solution (J/g)	Concentration (mM)	Enthalpy of solution (J/g)
0.0	-7	0.0	-7
0.7	-7.1	1.4	-8.3
1.8	-7.5	3.4	-9.2
15.3	-7.8	25.7	-9.3
31.5	-8	51.3	-9.8
45.1	-8.3	85.6	-10.1
72.1	-8.2		

Table S5.9. *Tabular enthalpy of solution (J/g) data for Figure 5.5a (uncertainty: ± 0.5 J/g)*

	Enthalpy of solution (J/g)						
pH	no salt	Ca^{2+} 5mM	Ca^{2+} 50mM	Ca^{2+} 100mM	Na^{+} 5mM	Na^{+} 50mM	Na^{+} 100mM
2.1	-2.5	-3.2	-3.5	-3.5	-2.5	-2.7	-2.5
2.7	-2.7						
3.5	-3						
4.5	-2.9	-3.5	-3.7	-3.8	-3	-3.3	-3.4
6.12	-2.9						
7	-3.2	-4.5	-5.2	-5.9	-3.6	-3.8	-4.2
8	-4						
9	-5.3						
10	-6.5	-7.6	-8.7	-9.5	-7	-7.6	-8.1
11	-6.9						
12	-6.8						
13	-7.2	-8.3	-9.7	-10.1	-7.8	-8.6	-8.9
13.5	-7						

Table S5.10. *Tabular enthalpy of solution (J/g) data for Figure 5.5b (uncertainty: ± 0.5 J/g)*

	Enthalpy of solution (J/g)						
pH	no salt	Ca^{2+} 5mM	Ca^{2+} 50mM	Ca^{2+} 100mM	Na^{+} 5mM	Na^{+} 50mM	Na^{+} 100mM
2.1	-1.8						
3	-2.2	-2	-2.5	-2.3	-2	-2.3	-1.8
4.5	-2.1						
5.5	-1						
7	-1.5	-2	-2.5	-2.5	-1.5	-1.6	-2
9.5	-1						
11	-1.5	-1.8	-2.3	-3	-1.3	-1.9	-2.2
12.5	-1.1						
13.5	-1.4						

Table S5.11. *Tabular enthalpy of solution (J/g) data for Figure 5.5c (uncertainty: ± 0.5 J/g)*

	Enthalpy of solution (J/g)						
pH	no salt	Ca^{2+} 5mM	Ca^{2+} 50mM	Ca^{2+} 100mM	Na^{+} 5mM	Na^{+} 50mM	Na^{+} 100mM
2	-4.5						
3	-5	-6.5	-6.1	-6.7	-5.8	-5.9	-6
5.5	-6.5						
7	-7	-9	-9.8	-10.5	-7.5	-8.2	-8.5
9.5	-9.5						
12.5	-11	-12.3	-13.6	-14.2	-11.8	-12.5	-13.3
13.5	-14						